A NUMERICAL STUDY OF THERMO-HYDRODYNAMIC LUBRICATION OF TILTED PAD SLIDER BEARINGS

A Thesis Submitted

in Partial Fulfillment of the Requirements

for the Degree of

Doctor of Philosophy

by

PENTYALA SRINIVASA RAO

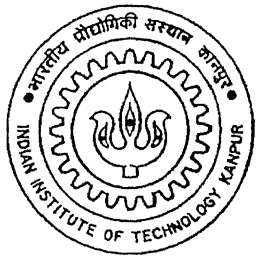

to the

DEPARTMENT OF MATHEMATICS

INDIAN INSTITUTE OF TECHNOLOGY KANPUR

June, 2000

Certificate

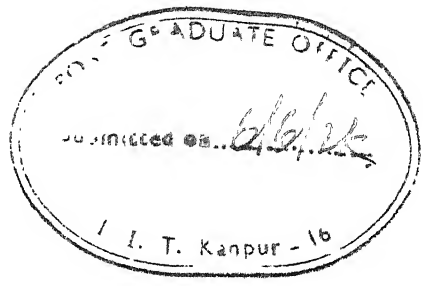

It is certified that the work contained in the thesis entitled "**A NUMERICAL STUDY OF THERMOHYDRODYNAMIC LUBRICATION OF TILTED PAD SLIDER BEARINGS**", by *"Pentyala Srinivasa Rao"*, has been carried out under our supervision and that this work has not been submitted elsewhere for a degree.

Prawal Sinha

Dr. Prawal Sinha
Professor
Department of Mathematics
Indian Institute of Technology
Kanpur - 208016, INDIA.

B.V. Rathish Kumar

Dr. B.V. Rathish Kumar
Assistant Professor
Department of Mathematics
Indian Institute of Technology
Kanpur - 208016, INDIA.

June, 2000

Dedicated With Love
To My Parents
Sri. Pentyala Veeraiah
Smt. Pentyala Kamalamma

Acknowledgements

It is my privilege to work with Professor Prawal Sinha and Professor B.V.Rathish Kumar, Department of Mathematics, IIT, Kanpur. I sincerely record my gratitude for their invaluable guidance and constant encouragement throughout the preparation of this thesis work. The amount of freedom I have enjoyed during my research work with them is inexpressible.

I am deeply indebted to Professor J.B. Shukla for his critical comments and suggestions during my research work. I am thankful to the faculty, Department of Mathematics for their constant encouragement and suggestions at various stages like the comprehensive examination, state of the art seminar, open seminar etc. My special thanks to Professor V. Raghavendra for his comments and suggestions during the series of special lectures on mathematical theory of finite elements. I am also thankful to Professor Peeyush Chandra, Professor Punyatma Singh, Professor M.K. Kadalbajoo, Professor Kundu, Dr. D. Bhahugu-na, Dr. A.K. Lal for their concern showed for the progress of my work.

I thank all my friends, especially Indrajith, Kali, Hari kishan, Appaji, Murthy for being co-operative and also for making every moment of my stay in the campus, enjoyable.

To my parents, sister, I am indebted for the sacrifice they have made for the sake of my education. I am grateful to my uncle (late) Sri. Cherukumalli Venkateswarlu and his parents who have been a constant source of inspiration and encouragement throughout my education, my heart felt gratitude to them.

Lastly, but not least, I am very much grateful to my wife Shobha whose love and encouragement accelerated the thesis work during the final stages.

Financial assistance for this research work from IIT, Kanpur is gratefully acknowledged.

June, 2000. P. Srinivasa Rao

Abstract

A numerical study of thermohydrodynamic lubrication of a slider bearing has been made. The partial differential equations governing the conservation of mass, momentum and energy equations coupled with temperature dependent density and viscosity are solved using Streamline Upwind Petrov-Galerkin Finite Element Method (SUPGFEM) to yield various bearing characteristics. The influence of the solid pad under various thermal boundary conditions in conjunction with thermal boosting on the load carrying capacity and frictional drag force of a slider bearing, at different inlet pressures and for various values of inclination parameter have been analyzed. The results depicted through plots and contours indicate that a boundary layer and re-circulation zones are noticed in the temperature field. Subsequently the influence of heat conduction both in the stationary pad as well as the moving slider on bearing performance have been analyzed. SUPGFEM is effective not only in precluding the numerical oscillations arising in the flow field, but also in achieving convergent solution. Although various temperature boundary conditions are prescribed on the pad and slider, the study reveals that the computed load carrying capacity remains unaffected. This is due to the fact that the thermal flux across fluid-solid interface changes marginally only. However, when compared with the case of no conduction the load decreases.

Further, apart from heat conduction in pad, the effect of fluid inertia on bearing characteristics has also been analyzed. The results reveal that fluid inertia has a profound effect on bearing characteristics and its inclusion enhances the load carrying capacity of a slider bearing with a reduction in the frictional drag force.

Synopsis

Name of the student: **Pentyala Srinivasa Rao**

Roll Number: **9420862**

Degree for which submitted: **Ph.D.**

Department: **Mathematics**

Thesis Title: **A Numerical Study of Thermohydrodynamic Lubrication of Tilted Pad Slider Bearings**

Thesis supervisors: **Professor Prawal Sinha** and **Professor B. V. Rathish Kumar**

Month and year of thesis submission: **June, 2000**

The thesis is devoted to the study of thermal and inertia effects on the lubrication characteristics of a slider bearing. The coupled partial differential equations governing the mass, momentum and energy equations of a Newtonian fluid together with temperature dependent viscosity and density are solved using the Streamline Upwind Petrov-Galerkin Finite Element Method (SUPGFEM) to yield various bearing characteristics. The influence of thermal boosting, various thermal flux boundary conditions, viscosity temperature coefficient and for different values of k (parameter governing inclination of the pad) on load carrying capacity, drag force, temperature distribution and on flow field have been analyzed.

The thesis consists of seven Chapters. Chapter 1 gives a General Introduction, wherein a brief history of lubrication and various bearing geometries has been presented. It also provides a chronological development made in the area of thermal and inertia effects in lubrication. This Chapter provides a motivation for the work reported in the subsequent Chapters of this thesis.

In Chapter 2, the Streamline Upwind Petrov-Galerkin Finite Element Method has been discussed. It provides a clear description of Finite Element Numerical Technique and its applicability for fluid flows. It also presents advantages of FEM in comparison with other numerical techniques like Finite Difference Method, Spectral Element Method etc. This Chapter also deals with the various weight functions used in the Variational formulation/Weak formulation and shape functions for the bilinear rectangular elements used in SUPGFEM. It also describes the implementation of the SUPGFEM.

Chapter 3 deals with the investigation of the influence of various temperature boundary prescriptions and thermal boosting on bearing characteristics. For the numerical simulation of hydrodynamic lubrication, we have used Bubnov-Galerkin FEM for a Generalized Reynolds equation and SUPGFEM for energy equation in the lubricant film. The study in this Chapter reveals that the consideration of (a) Lubricants with low values of viscosity temperature coefficient (β^+) (b) Non zero inlet pressure and (c) T_i^+ (inlet temperature) $<$ T_s^+ (slider temperature) $<$ T_p^+ (pad temperature) or $T_i^+ < T_s^+$ with non zero flux on the pad constitutes a desirable set-up for enhancing the load carrying capacity of a slider bearing with a reduction in the frictional drag force. An attempt has also been made for analyzing the load generation in a parallel slider bearing ($k = 1$).

Lubrication under high load and high speed is common in engineering practice today. In the thin film that separates the two rubbing surfaces a large amount of heat may be generated. The heat generated in the fluid may escape through conduction in the bearing surfaces. In Chapter 4, we have investigated the hydrodynamic lubrication of finite width slider bearing taking not only the temperature variation in the fluid film but also the heat conduction in the stationary pad. Influence of thermal boosting, different values of inclination of the pad and several practical thermal boundary prescriptions on load carrying capacity and frictional drag force have been analyzed. SUPGFEM have been used to preclude the numerical oscillations arising in the fluid flow.

In Chapter 4, we allowed heat conduction only in the stationary surface. But in practice heat may escape through the slider also which is moving in the direction of sliding. Hence, In Chapter 5, we have included the heat conduction in the pad as well as in the moving slider. The system of governing equations which now include two heat conduction equations apart from the Generalized Reynolds equation and energy equation are solved simultaneously using SUPGFEM. The results indicate that this method is effective not only in precluding the numerical oscillations in the flow field but also obtaining a convergent solution. Load carrying capacity of slider bearing can be thermally boosted by setting slider at temperature lower than that of incoming lubricant. In this study we have chosen different boundary settings for pad and slider conduction. These boundary conditions do alter the temperature field in the pad. However, the thermal flux across the fluid-solid interface changes marginally only. Consequently the load carrying capacity of the slider bearing remains unaffected. It is to be noted that the isothermal pad employed in the present study has been set at temperature similar to that of inlet flow.

In Chapter 6, we have included the effect of fluid inertia along with the thermal effects. The system of nonlinear partial differential equations governing the conservation of mass, momentum and energy with viscosity and density depending on the temperature has been solved. From the results, it is observed that fluid inertial effects are significant when the Reynolds number exceeds 5×10^4. Inclusion of fluid inertia enhances the load capacity of a slider bearing for various values of k and at various inlet pressures. Also, the investigation on the influence of viscosity temperature coefficient (β^+) on the load carrying capacity at various inlet pressures has been made. The dependency of load carrying capacity on β^+ for $p_i^+ = 0, 0.5, 1$ shows that, for small inlet pressures, load generation in slider bearing decreases with increasing β^+, but at high inlet pressures this reduction in load generation becomes marginal. It can also be noted that for fixed T^+, $\mu^+(T^+)$ increases with decreasing β^+ and thus the effective viscosity of the lubricant increases and this leads to a higher load capacity.

Chapter 7 deals with the combined influence of fluid inertia and heat conduction in the pad. In this Chapter, load carrying capacity for various thermal boundary conditions are shown in the form of Tables. The computed load carrying capacity have been compared with the results obtained for no conduction in the pad. The results show that for higher tilt (decreasing k) load capacities are high for the case with no conduction. Whereas for lower tilt (increasing k) the load carrying capacities are low for the case with conduction. This could be due to an increase in the lubricant temperature which may not have been able to escape as the conduction in the pad was not allowed. Also the nonlinear model (with inertia) has an upper hand as compared with the linearized model (with no inertia) in the computed load capacities for various values of k.

Contents

List of Symbols

B	Length of the bearing.
c	Specific heat of the lubricant.
E_c	Eckert number.
h	Film thickness.
h_1	Thickness of the pad.
h_{11}	Thickness of the slider.
h_i	Inlet film thickness.
h_o	Outlet film thickness.
H	Heat transfer coefficient.
$k = \frac{h_o}{h_i}$	Inclination of pad.
k or k_f	Thermal conductivity of the lubricant.
K_s	Thermal conductivity of the slider.
$\vec{n}$	Outward unit normal vector.
p_i	Inlet pressure.
p_o	Outlet pressure.
P_e	Peclet number.
P_r	Prandtl number.

$R_e = \frac{\rho_a U B}{\mu_a}$	Reynolds number.
$R_e^* = \frac{\rho_a U B}{\mu_a}(\frac{h_0}{B})^2$	Modified Reynolds number.
s	Shear strain.
T	Lubricant temperature
T_i	Inlet lubricant temperature.
T_p	Temperature of the pad.
T_s	Temperature of the slider.
u	Fluid velocity along the sliding direction.
U	Velocity of the moving surface.
v	Fluid velocity perpendicular to the sliding direction.
x	Coordinate along the direction of sliding motion.
y	Coordinate perpendicular to the direction of sliding motion.
x'	Pad coordinate along the sliding direction .
y'	Pad coordinate perpendicular to the sliding direction .
x''	Slider coordinate along the sliding direction .
y''	Slider coordinate perpendicular to the sliding direction .
β	Viscosity temperature coefficient.
τ	Shear stress.
ρ	Density of the lubricant .
ρ_0	Inlet density.

μ Dynamic viscosity of the lubricant .

μ_0 Inlet viscosity.

λ Density temperature coefficient.

η Absolute viscosity of the lubricant .

Symbols with superscript "+" indicate nondemensional quantities.

Symbols with subscript "a" indicate ambient condition.

List of Figures

List of Tables

Chapter 1

General Introduction

1.1 Lubrication

Lubrication is the science and technology of interacting surfaces in relative motion and of the practices thereto. It is simply the use of a material to improve the smoothness of movement of one surface over another surface. The material which is used to achieve this is called lubricant and the process is called "Lubrication." The most common lubricants are oils and greases but other kinds of liquid substances as well as solids and gases are also used as lubricants. Among the solid lubricants graphite, borax, mica, white lead, waxes etc. are found to be used in deep drawing, extrusion and light rolling operations in metal industries, and many modern engineering mechanics, especially in the field of nuclear power, aviation and ballistic missiles. Gases are finding increasing usage in gas-cycle machinery, gyros, where precision and constancy of torque are critical; in food and textile processing machinery, where cleanliness and absence of contaminants are critical; and in high speed dental drills. Lubricants in general help in reducing or controlling friction. However a reduction is not always desirable. There may be situations in which it is more important to maintain steady friction than to obtain the lowest possible friction. Some examples are, the control of chatter in a machine tool slide ways or grinding operation, control of strip movement in metal rolling and elimination of brake sequel or clutch judder in a car. In

addition to controlling friction, lubricants are usually expected to reduce wear and often to prevent overheating and corrosion. In some cases, lubricants are also used as a cooling agent by carrying away heat which is generated in bearings. For example, the chief requirement of the lubricants in forging are cooling the dies and lubrication of the die-workpiece interface in order to minimize metal pick-up, reduce wear and facilitate plastic flow of metal.

1.1.1 Historical Perspective of Lubrication

The understanding of the hydrodynamic lubrication began with the classical experiment of Tower [1] , in which the existence of a film was detected from measurements of pressure within the lubricant, and of Petroff [2, 3, 4, 5] , who reached the same conclusion from frictional measurements. Tower [6] demonstrated that a loaded, oil lubricated journal bearing is subject to local pressures substantially higher than its mean pressure. Tower's [1, 6] experiments to study friction in railroad journal bearings, eventually led to the development of the theory of hydrodynamic lubrication. The work was closely followed by Reynolds [7] and he used linearized form of the equations of motion for laminar flow of a Newtonian fluid with constant viscosity, between rigid surfaces and derived a second order differential equation for the pressure in the narrow converging gap between bearing surfaces. This pressure enables a load to be transmitted between the surfaces with extremely low friction, since the surfaces are completely separated by a fluid film. In such a situation the physical properties of the lubricant, notably the dynamic viscosity, dictate the behavior. The equation describing the pressure in two dimensional hydrodynamic bearings is given by

$$\frac{\partial}{\partial x}\left(\frac{h^3}{\eta}\frac{\partial p}{\partial x}\right) = 6\,U_0\,\frac{\partial h}{\partial x} \tag{1.1}$$

where x is the coordinate in the sliding direction, p is the pressure, η is the viscosity, h is the film thickness and U_0 is the effective sliding velocity. The work of Reynolds received immediate acceptance by the engineering community, but there were great difficulties encountered when attempting to solve the Reynolds equation. As numerical solutions of the Reynolds

equation became a common place, more and more investigators began to ask the question i.e. Does the Reynolds pressure equation account for the physics of the problem adequately?. In fact the extension of classical theory was found to be wanting much earlier. Martin [8] found that it cannot satisfactorily explain the existence of continuous hydrodynamic film in highly stressed contacts, such as those found in gears. With the increasing demands of various sophisticated engineering equipments containing bearings, such as metal industries, die industries and many other application, the extension of Reynolds classical theory became necessary, to predict the bearing operations accurately.

1.1.2 Bearings and their Characteristics

A bearing is a support or a guide that locates one machine component with respect to others in such a way that prescribed relative motion can occur while the forces associated with machine operation are transmitted smoothly and efficiently. Bearings can be classified in several ways: according to the basic mode of operation (rubbing, hydrodynamic, hydrostatic, or rolling element), according to the direction and nature of the applied load (thrust or journal), or according to geometric form (tapered or stepped parallel surface or tilted pad). Various types of bearings are shown in Figures 1.1 - 1.5.

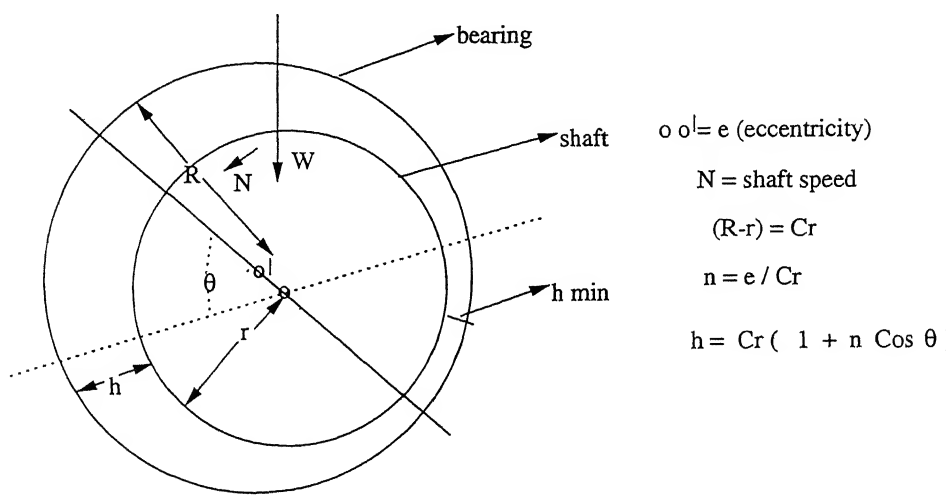

Figure 1.1: Journal bearing

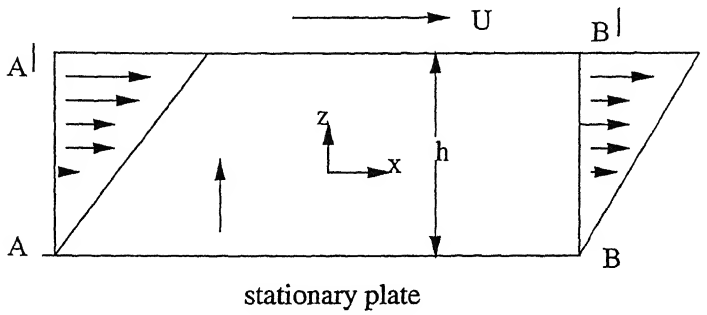

Figure 1.2: Parallel surface slider bearing

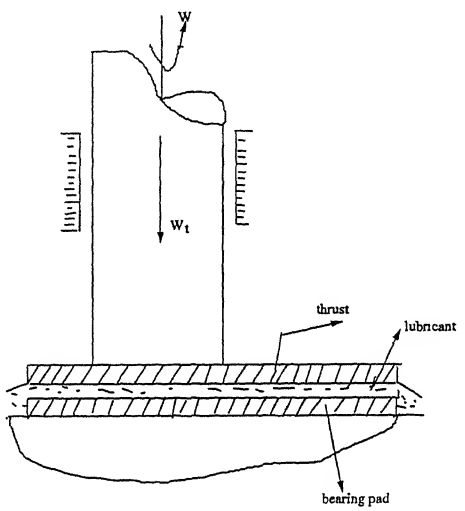

Figure 1.3: Thrust bearing geometry

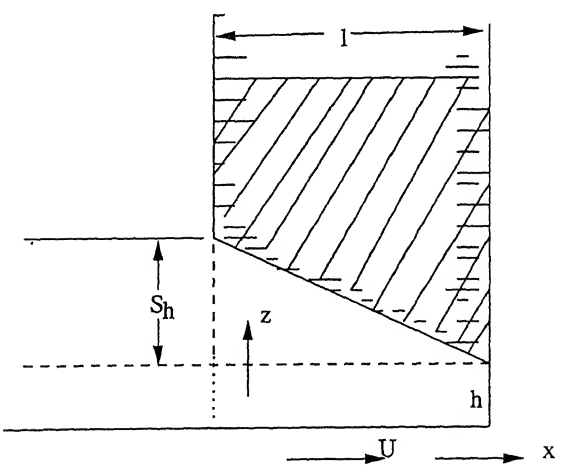

Figure 1.4: Fixed-incline (tilted pad) slider bearing

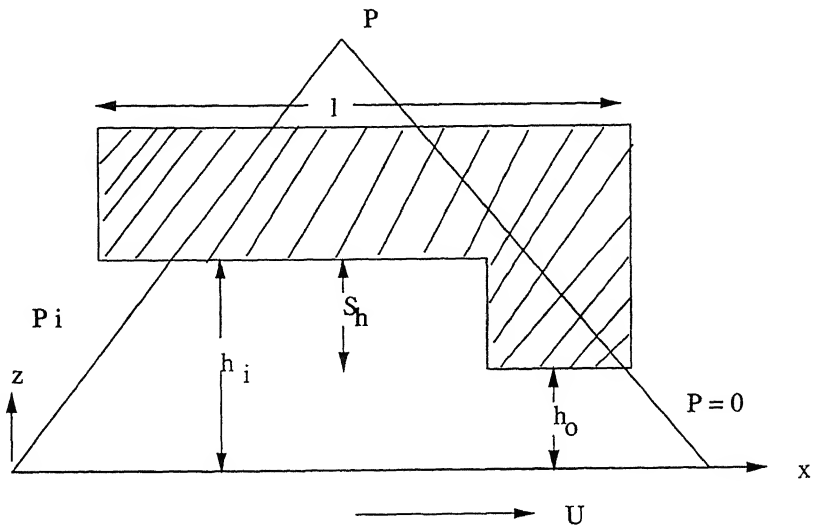

Figure 1.5: Parallel step slider bearing

The basic function of any bearing, irrespective of its configuration or working principle is to restrain unwanted relative movement between the two machine parts while offering the least resistance to the desired relative movement. The other characteristics of a bearing include:

- Load carrying capacity
- Stiffness
- Flow rate of supporting fluid
- Resistance to sliding
- Power required to operate
- Heating.

Design is a creative process aimed at finding a solution to a particular problem. In all forms of design a particular problem may have, many different solutions, mainly because design requirements can be interpreted in many ways. For example, it may be desirable to produce:

- The cheapest solution
- The bearing with ease and with variable material

- The most reliable
- The one that takes up the smallest space
- The one that is lightest in weight
- The best from any of a whole variety of possible stand points.

Therefore, the process of selection and design usually involves these steps.

- Selecting a suitable type of bearing
- Estimating a bearing size that is likely to be satisfactory
- Analyzing bearing performance to see if it meets the requirements
- And then modifying the design and the dimensions until the performance is near to whichever optimum is considered the most important.

1.1.3 Lubrication Regimes

In general the bearings operate under one of the following modes of lubrication.

- Hydrodynamic/Hydrostatic lubrication
- Boundary lubrication
- Mixed lubrication.

In hydrodynamic lubrication, moving surface(s) of the bearing are completely separated by a layer of fluid film of thickness of the order 10^{-7}m - 10^{-5}m and the pressure in the film is generated by hydrodynamic action. Such bearings are called hydrodynamically lubricated bearings. In hydrodynamic lubrication the films are generally thick so that opposing solid surfaces are prevented from coming into contact. This condition is often referred to as "The ideal form of lubrication", since it provides low friction and high resistance to wear. The lubrication of the solid surfaces is governed by the bulk physical properties of the lubricant, notably the viscosity, and the frictional characteristics arise purely from the shearing of the viscous lubricant. For a normal load to be supported by a bearing, positive-pressure profiles

must be developed over the bearing length. For a positive pressure to be developed in a slider bearing (see Figure 1.6 (a)) the lubricant film thickness must be decreasing in the sliding direction. In a squeeze film bearing (see Figure 1.6 (b)) the bearing surfaces approach each other with a normal velocity (squeeze velocity) U_a. The squeeze mechanism of pressure generation provides a valuable cushioning effect when the bearing surfaces approach each other. Positive pressures will be generated only when the film thickness is diminishing.

In some situations, load on the bearing is too high and the relative velocity of the bearing surfaces is too low to generate sufficient hydrodynamic pressure in the oil film. In such cases, an external pressure source may be used to supply oil under a high pressure to prevent metal - to - metal contact between bearing surfaces. Such mode of lubrication is called externally pressurized or hydrostatic. In an externally pressurized bearing (see Figure 1.6 (c)) the pressure across the bearing supports the load.

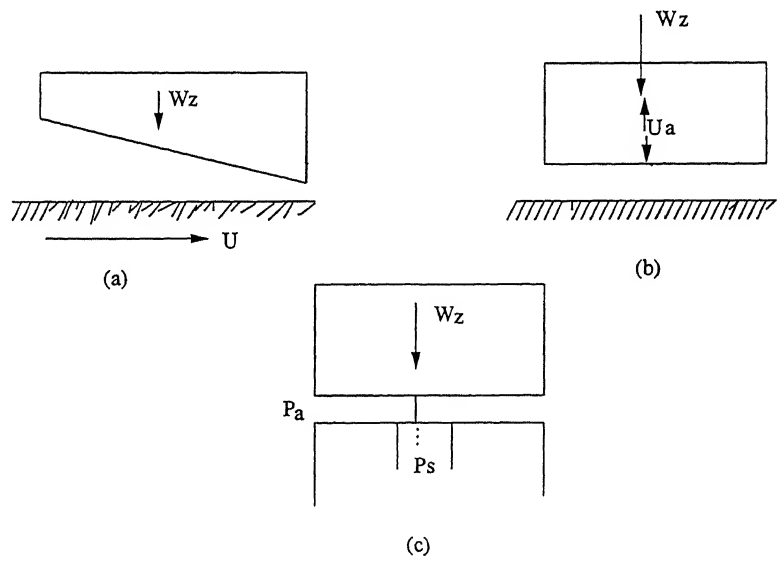

Figure 1.6: Mechanism of pressure development for hydrodynamic lubrication (a) Slider bearing (b) Squeeze film bearing (c) Externally pressurized bearing

In case of boundary lubrication the solid surfaces are not separated by a thick lubricant film, fluid film effects are negligible and there is considerable asperity contact. The frictional characteristics are determined by the properties of the solids and the lubricant film at the

common interfaces. The surface films vary in thickness from 1nm to 10nm depending on the molecular size. In boundary lubrication, although the friction is much higher than in the hydrodynamic regime, it is still much lower than for unlubricated surfaces. The contact mechanism is governed by the physical and chemical properties of thin surface films of molecular proportions. The properties of the bulk lubricant are of minor importance, and the friction coefficient is essentially independent of fluid viscosity. Figure 1.7 illustrates the film conditions in fluid film and boundary lubrication. The surface asperities in this Figure are greatly distorted for purposes of illustration. To scale, real surfaces would appear as gently rolling hills rather than the sharp peaks. The surface asperities are not in contact for fluid film lubrication but are in contact for boundary lubrication.

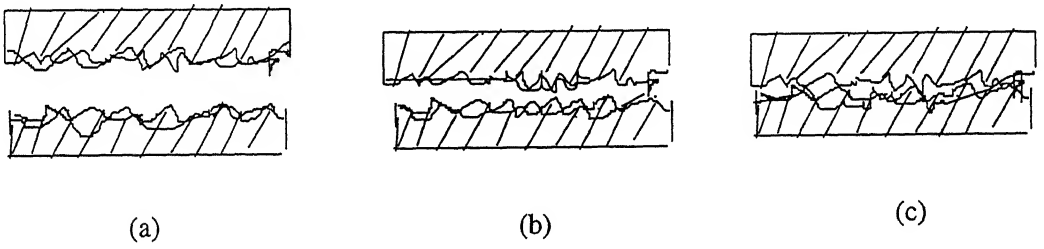

Figure 1.7: Film conditions of lubrication regime (a) Fluid film lubricated-surfaces separated by bulk lubrication film (b) Partial lubrication-both bulk and boundary lubrication play a role (c) Boundary lubrication-performance depends essentially on boundary film

Mixed lubrication is a situation between hydrodynamic and boundary lubrication. The fluid film between the two moving surfaces is thin enough and the surface asperities begin to interfere in the hydrodynamic process. The load is partly supported by asperity contacts and partly by fluid film. Figures 1.8 and 1.9 shows the friction coefficient and wear rate respectively for various types of lubrication regimes.

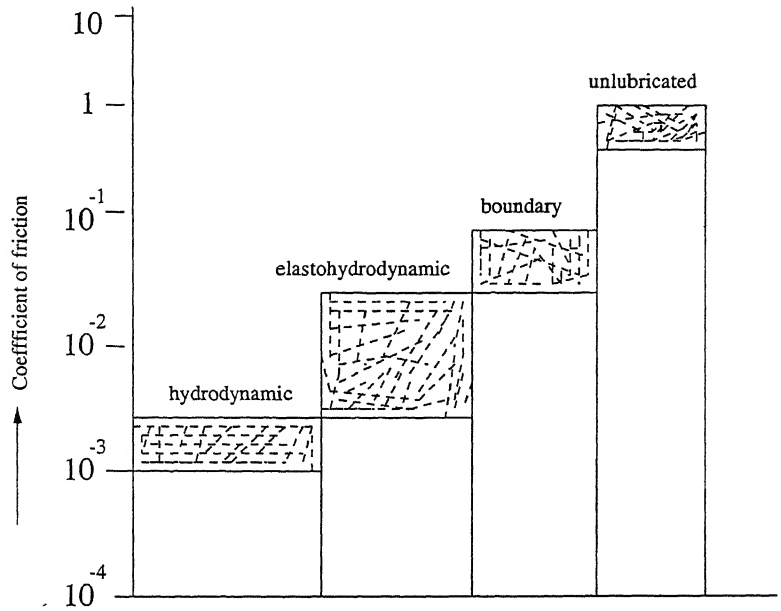

Figure 1.8: Bar diagram showing friction coefficient for various lubrication regimes

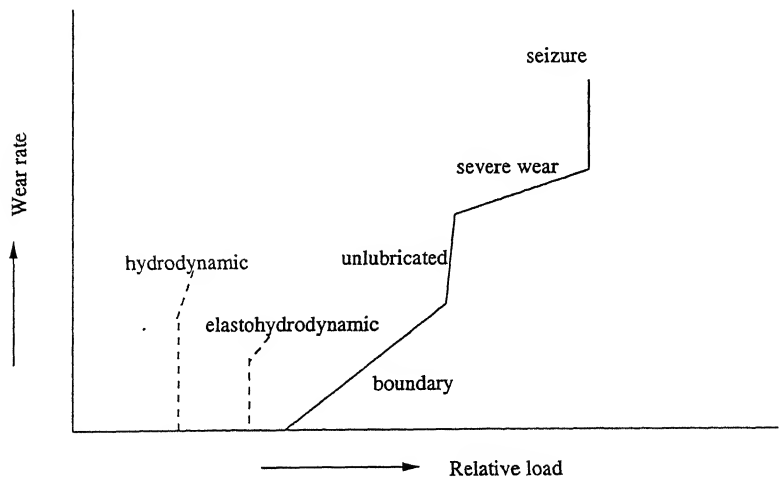

Figure 1.9: Wear rate for various lubricating regimes

1.2 Extension of Classical Lubrication Theory

There were at least six areas in which the extension of classical theory seemed desirable. Each of these areas is concerned with the relaxation of one or more constraints of the classical theory and leads to studies of:

- Thermohydrodynamic effects
- Inertia effects
- Compressibility effects
- Elastohydrodynamic effects
- Turbulence effects
- Non-Newtonian effects.

This thesis is mainly concerned with the first two effects. Hence, in the subsequent Chapters emphasis is given to the related investigations only.

1.2.1 Thermohydrodynamic Effects

In recent years, there has been a growing demand for bearings which can sustain higher load and are at relatively higher speeds. A large amount of heat is generated in such bearings. This necessitates the need for fundamental understanding of the thermal conditions in the bearings. Under normal operating conditions most lubricants undergo an increase in temperature due to viscous dissipation which in turn may significantly influence the viscosity and load carrying capacity of the bearing. Two parameters which are generally responsible for bearing failure are

- Maximum bearing temperature
- Minimum film thickness.

In view of this, the actual temperature distribution at every point needs to be estimated. This can be obtained through the simultaneous solution of equations of continuity, momentum and energy conservation. One of the difficulties encountered in dealing with energy conservation stems from the fact that there are no exact analytical expressions for the viscosity as a function of temperature and pressure. This is because viscosity variation occurs mainly due to

- Heat generation by viscous shear
- Heat transfer to and from the surface.

In many applications, increase in temperature across the bearing, although not negligible, remains small. The classical isothermal theory in this case might still be applied as a first approximation, provided that calculations are based on an "effective" or "operating" viscosity. In large bearings and/or under severe running conditions, thermal effects may be significant (ref: Pinkus, [31], page: 4) and prediction of bearing performance may no longer be possible when based on the assumption of a uniform effective viscosity. Thus, numerical emperical relations of $\mu = \mu(T)$ has been developed and the one, which is extensively used is given by $\mu = \mu_0 \quad \exp\,[-\beta(T - T_0)]$; where μ_0 is the viscosity at temperature T_0 and β is a constant, called the viscosity temperature exponent. In view of these aspects, the thermohydrodynamic model can be defined as "A model which predicts bearing performance based on realistic thermal boundary conditions on the stationary and moving surfaces and includes a pointwise variation of the fluid viscosity with temperature". The study of thermohydrodynamic model involves simultaneous solution of energy balance, the conservation equations of mass and momentum which can be achieved by an iterative numerical process.

The early applications of energy equation to lubrication theory were by Christopherson [9] and by Cameron and Wood [10] . The hydrodynamic theory of film lubrication was investigated by Cope [11], who systematically derived the governing equations of fluid film lubrication with thermal effects. Assuming that oil carries away the entire frictional heat, he

derived a simplified energy equation in which the variation of viscosity across the film was neglected. Hunter and Zienkiewicz [12] showed that in certain circumstances, the viscosity variation across the lubricant film was responsible for generation of an applicable load and, therefore, should not be neglected. Dowson [13] presented a Generalized Reynolds equation and considered the energy equation by taking the variation of viscosity both along and across the lubricant film. Several other researchers who studied the thermal effects include Huebner [14], Ezzat and Rhode [15], Khonsari [16], Gethin [17], Gero and Ettles [18], Schumack [19] etc.

A review of major contributions on thermal effects in various geometries of bearings is done by Khonsari [16]. He has presented an extensive literature survey on heat effects in various type of bearings. Summary, given by Khonsari regarding the advances made in analyzing the thermal effects in bearings, conclude:

- Thermal effects are important as they influence bearing performance significantly
- Viscosity variation as a function of temperature must be considered in bearing design
- The effect of temperature on viscosity is more pronounced than the effect of elastic distortions due to temperature and pressure
- Under most operating conditions, the heat conduction along the direction of motion is small and can be neglected. However, when back flow of oil, is produced the conduction term along the direction of motion must also be retained in the energy equation
- Cooling the slider is generally advantageous because it can increase the load carrying capacity and reduces the friction which is one of the most interesting aspect for the designers.

1.2.2 Inertia Effects

The performance of a typical bearing is significantly affected by inertia effects that are generated within the lubricant. This complex mechanism stems from the convective nature

of the flow field, and are driven by a combination of high operating speeds, low viscosity of the lubricant, large external pressures, and the complexity of the bearing geometry. For the bearing recess region, convection effects will lead to a non-linear pressure distribution. It was found that in typical hydrodynamically lubricated thrust and journal bearings the inertia effects are negligible as compared to the viscous effects. However, inertia effects can sometimes be important. Two examples are given in Myllerup and Hamrock [20], the first example is for any surface feature resulting in a film geometry where $\frac{dh}{dx} \approx$ Order (1) or $\frac{d^2h}{dx^2} \approx$ Order (1) where $h = h(x)$ is film thickness. The singularity arising from the curvature is less severe than the one arising from the film gradient, but in both cases using the Reynolds equation will not allow a proper matching between the fluid regions. The second example where the Reynolds equation will not describe what occurs in the lubricant conjunction is when a solid particle is within the conjunction. In these cases, it is necessary to consider the convective inertia. Inertia effects were studied by Tichy [21] , Talmage et al. [22], Prasad et al. [23] etc. All these studies concluded that inertia effects are more significant when the Reynolds number is not small and bearing performance is influenced by the mass effect of the lubricant and high operating speeds.

1.2.3 Compressibility Effects

When the fluid (lubricant) is compressible (e.g. Gases), compressibility effects have to be considered. Gas lubricated film bearings have commanded considerable attention in recent years because they possess characters that make their usage advantageous in many bearing application. They are analogous to the hydrodynamic oil-lubricated bearings except that the fluid is compressible. Further more, since air is 1000 times less viscous than even the thinnest mineral oils, the viscous resistance is very much less. However, the distance of nearest approach between the bearing surfaces is correspondingly smaller so that special precautions must be taken in manufacturing the bearing. Gross [24], Houpert and Hamrock [25] etc. have given an extensive study about the compressibility effects.

1.2.4 Elastohydrodynamic Effects

In recent years a number of practical bearings have employed layered elastic solids as mating surfaces. Also to avoid wear and seizure and to make the supply of the lubricant easier, thin layer of softer material, such as stiffer plastics, are sometimes coated on the bearing surface. In such situations, neglecting the surface deformation will not predict the film profile and pressure distribution accurately. This has led to the substantial interest in the elastohydrodynamic lubrication of such bearings and it is imperative to consider the deformation of bearing solids.

When the surfaces are no longer rigid, elastohydrodynamic effects become significant. The viscosity must be considered to be pressure dependent. Elastohydrodynamic lubrication can be defined as the study of lubricating film between elastically deformable solids. At one end of the scale, it covers highly stressed lubricated machine elements like ball and roller bearings and gears and at the other it includes the performance of soft rubber seals and bearings with soft liners. Hamrock and Dowson [26, 27, 28] Ghosh and Hamrock [29] etc. have given extensive explanation on elastohydrodynamic lubrication.

1.2.5 Turbulence Effects

It is well known that the motion of fluids may occur in 'irregular fluctuations', resulting in whirls and/or eddying. Such motions are called turbulent flows. When the Reynolds number ($R_e = \frac{\rho UB}{\mu}$) is increased (outside its range for laminar flow), the boundary layers around solid bodies change from laminar to turbulent. Such a transition is influenced by geometries, pressure gradients, suction, compressibility, and heat transfer. It is mandatory to consider fluid inertia along with the turbulence. This would indeed carry the governing equations for fluid film lubrication beyond the customary postulates of lubrication theory. Extensive study have been considered by Venkateswarlu and Rodkiewicz [30], Pinkus [31] etc.

1.2.6 Non-Newtonian Effects

For most fluid film lubrication analysis the lubricant is assumed to behave in a Newtonian manner. This implies that the shear stress τ is linearly related to the shear strain s. i.e $s = \frac{\tau}{\eta}$. Where η is the absolute viscosity or proportionality constant. It may vary with both pressure and temperature. However, in many situations the lubricant may experience rapid and extremely large pressure variations, large temperature changes, and particularly in sliding contacts, high shear rates, this implies that the lubrication shear stress is still a function of the shear rate but that the relationship may no longer be linear. Such class of fluids are called non-newtonian fluids. Shukla and Isa [32] , Prasad et al. [23] have given an extensive study. Hirst and Moore [33] presented an experimental investigation of the dependence of shear stress and shear strain rate and proposed a Eyring type of relationship. Several other non-notonian models have been proposed, such as Power law fluids (Prasad et al. [23]), Bingham fluids (Caldewell and Babbitt [34]), Viscoplastic fluids (Sheu et al. [35]) etc.

1.3 Review of the Literature

It was Fogg [36] who first published his experimental findings suggesting that a pressure film is generated, in a slider bearing, as a result of thermal expansion of the fluid passage through the bearing. Subsequently, this phenomena received considerable attention under various titles, like "thermal wedge", "viscosity wedge", or "density wedge". In the Fogg experiment radial grooves were made as sharp as possible in the direction of rotation of the moving collar and the direction of rotation of moving collar could be reversed. It was concluded that a parallel surface without a rounded inlet edge was capable of sustaining considerable loads which was attributed to the thermal expansion of the fluid. This appears to be plausible except that Fogg [36] recognized only one contributing factor while there must have been, at least, two factors generating lifting force. The other factor is the pressure build-up in

the fore-region (Rodkiewicz et al. [37]). This must have resulted in an above ambient inlet pressure, leading to a non-zero load carrying capacity.

Osterle et al. [38] specialized their governing equations to the infinitely wide parallel-surface slider bearing ($k = 1$), according to presentation of Cope [11]. Inertia forces were neglected, pressure was assumed constant across the fluid film thickness and viscous force was represented by the dominant term in the momentum equation. However, the density and viscosity were not assumed to vary exponentially with temperature and in the energy equation the conduction terms were disregarded. Lewicki [39] introduced the concept of pressure build-up in the inflow zone of a square-faced slider. In his incompressible flow analysis with constant viscosity the stream function approach is used within the inflow zone, and within the lubricating film, pressure is assumed to vary linearly.

The effect of prescribed thermal gradients was also studied for journal bearings as well as for slider bearings by Hagg [40], Tipei and Nica [41]. Zienkiewicz [42] analyzed an infinitely long parallel slider bearing allowing for temperature variations across the film. Cameron and Wood [10] considered "the thermal wedge", and Cameron [43] "viscosity wedge" in a thrust bearing. Basically their problem formulation is similar to that of Osterle et al. [38]. They also disregard the conduction terms in the energy equation. Hunter and Zienkiewicz [12] performed analysis for the one-dimensional slider bearings. In this analysis the thermal boundary conditions at the fluid-solid interface were assumed a priori. Dowson and Hudson [44] re-examined the same problem allowing for the heat transfer to the bearing solids. The effect of thermal distortions of the bearing solids was considered by Hahn and Kettleborough [45] in an analysis of the one dimensional slider bearing. They concluded that while thermal distortions are responsible for the load carrying capacity exhibited by parallel surface slider; they have little effect on the performance of inclined sliders. Also Hahn and Kettleborough [46] presented an iterative method of calculating the steady-state pressure and temperature distributions for infinitely wide slider bearings. The viscosity was a function of

temperature and pressure, and the density a function of temperature.

Lebeck [47, 48] have experimentally investigated the thermal influence on load carrying capacity of parallel slider bearings. Rohde and Kong [49] investigated the thermal influence on bearing characteristics using the finite difference numerical technique. The effect of fluid inertia on bearing characteristics has been analyzed by Hill et al. [50], Artiles et al. [51]. In these investigations, it is concluded that inclusion of inertia has a profound effect on bearing characteristics. Yang and Rodkiewicz [52] also investigated the influence of thermal effects in tilted pad slider bearings.

Another important factor which influences bearing characteristics in case of high speed bearing lubricated with low viscosity fluid and subjected to a squeezing motion is the fluid inertia (Hashimoto and Wada [53], Elkouh [54]). This effect is important even in case of laminar flow where an increase in hydrodynamic film thickness may also some times compel one to consider this effect. Dowson et al. [55] conducted a wide range of experiments on a cylindrical-plane bearing. It was observed that for a moderately large Reynolds number, the experimental data deviated substantially (due to fluid inertia) from the theoretical values predicted by classical Reynolds equation using the Coyne-Elrod film rupture conditions. You and Lu [56] presented a theoretical analysis of a cylindrical-plane bearing and journal bearing. They have shown that the lubricant inertia has a profound effect even at moderate values of the Reynolds number.

Some recent work in this direction is by Talmage et al. [22], Zhang and Rodkiewicz [57] who considered the influence of fluid inertia on bearing characteristics using a CFD technique called Pseudo spectral finite difference method. Their work was mainly on scheme development which could simultaneously solve the complete Navier-Stokes equations, the continuity equation and the energy equation. This method can accommodate arbitrary inlet and exit boundary conditions as in a coupled analysis. But the approach requires greater effort and computational resources. And in all these studies the compressibility work term

was ignored.

Recently, Rodkiewicz and Sinha [58], Schumack [19] have numerically analyzed the problem of thermohydrodynamic lubrication with Dirichlet boundary prescription on the pad and slider. But the actual slider bearing configuration would require zero or non zero flux boundary prescriptions. Gero and Ettles [18] has attempted the same problem but his study was focussed on scheme development. Further, he has dealt with either constant viscosity or density or linearized viscosity with constant density. The influence of thermal boosting, which amounts to considering slider, pad and inflow lubricant at different temperatures, on load carrying capacity, drag force etc. of the lubricant in thermohydrodynamic slider bearing context has not been investigated.

In view of the above comments, a thorough investigation has been made in this thesis to analyze the bearing characteristics in a slider bearing lubrication. Also particular emphasis has been made for the parallel surface slider bearing lubrication.

1.4 Outline of the Dissertation

The main objective of the present study is to simulate the load carrying mechanism in slider bearings using the Streamline Upwind Petrov-Galerkin Finite Element Method (SUPGFEM), because the applicability of FEM alone is limited in cases where the governing equations are highly non-linear, such as those found in the lubrication theory with thermal effects.

The thesis consists of seven Chapters, where Chapter 1 is the General Introduction, which provides a brief history of lubrication and outline of various lubricating regimes. It also presents a chronological developments made in the area of thermal and inertia effects. This Chapter highlights the motivation for the work reported in the subsequent Chapters.

In Chapter 2, we have discussed various forms of obtaining a approximate numerical solution for a differential equation. Special attention has been made for the methodology "Streamline Upwind Petrov-Galerkin Finite Element Method", its applicability for fluid

flows and various steps involved in the implementation of the method has been discussed extensively.

Chapter 3 describes the mechanism of tilted pad slider bearings and influence of various temperature boundary conditions on bearing characteristics. It also deals with the influence of various inlet pressures, different values of k, β^+, various slider and pad temperature settings on the velocity distribution, temperature distribution, load carrying capacity and frictional drag force. Thorough discussion of iso-u velocities and isotherms have also been provided.

In Chapter 4, we have investigated the hydrodynamic lubrication of finite width slider bearing considering not only the temperature variation in the fluid film but also the conduction. Influence of thermal boosting for various values of k and several practical temperature boundary conditions on load carrying capacity and frictional drag force has been discussed. SUPGFEM is found to be very effective in precluding the numerical oscillations arising in the fluid flow.

In Chapter 4, we have included only heat conduction in the stationary pad. But in practice the heat generated in the fluid may escape either through conduction in the pad or slider or both. So in Chapter 5, we have analyzed the performance of slider bearing considering heat conduction in both the bearing surfaces (slider and pad). SUPG weight functions are found to be advantageous in obtaining a convergent solution. In this Chapter, pad and slider are set at various boundary conditions. These boundary conditions do not have a significant variation in their respective computed load capacity, because the variation in the temperature flux gradients is negligibly small.

In Chapter 6, the influence of convective inertia has been included. The nonlinear partial differential equations governing the conservation of mass, momentum and energy with temperature dependent density and viscosity are solved using SUPGFEM to yield various bearing characteristics. Also we have investigated the influence of viscosity temperature

coefficient (β^+) on load carrying capacity. In this Chapter, we have discussed iso-u velocity contours and isotherms for various values of T_s^+, T_p^+, T_i^+.

Chapter 7, deals with the combined influence of convective inertia and heat conduction in the stationary pad. In this Chapter, a comparison has been made for the effective load carrying capacity values with conduction in the pad and no conduction in the pad.

Chapter 2

Streamline Upwind Petrov-Galerkin Finite Element Method

2.1 Introduction

While searching for a quantitative description of physical phenomena, the engineer or the physicist establishes generally a system of ordinary or partial differential equations valid in a certain region (or domain) and imposes on this system, suitable boundary and/or initial conditions. At this stage the mathematical model is complete, and for practical applications "merely" a solution for a particular set of numerical data is needed. Here, however, come the major difficulties, as only the very simplest forms of equations, within geometrically trial boundaries, are capable of being solved exactly with available mathematical methods. Ordinary differential equations with constant coefficients are one of the few examples for which standard solution procedures are available and even here, with a large number of dependent variables, considerable difficulties are encountered.

To overcome such difficulties and to enlist the aid of the most powerful tools developed on computer based techniques, it is necessary to recast the problem in a purely algebraic form, involving only the basic arithmetic operations. To achieve this, various form of the continuum problem defined by the differential equations can be used. In such a discretization

the infinite set of numbers representing the unknown function or functions is replaced by a finite number of unknown parameters, and this process, in general, requires some form of approximation.

Of the various forms of discretization which are possible, one of the simplest is the finite difference process. In the finite difference approximation of a differential equation, the derivatives are replaced by difference quotients (or the function is expanded in a Taylor's series) that involve the value of the solution at discrete mesh points of the domain. The resulting algebraic equations are solved, after imposing the boundary conditions, for the values of the solution at the mesh points. So the finite difference model of a problem gives a pointwise approximation to the governing equations. The model is improved (formed by writing difference equations for an array of grid points) as more points are used. With finite difference technique, we can treat some fairly difficult problems; but, for example, when we encounter irregular geometries or unequal specification of boundary conditions, we find that finite difference technique becomes hard to use. And also it is not economical either in terms of computer storage or CPU time.

For instance, in the solution process of the incompressible lubrication problems for bearings of complex geometry, the finite difference method is inherently hampered by many limitations. In the technique for each problem of interest, a preferred coordinate system is found so that lubricant boundaries are described by constant coordinate lines, or a loss in accuracy of the solution is accepted. In addition, when abrupt variations of the field properties, such as film thickness, occur, auxiliary conditions, such as continuity, are generally invoked.

Thus, the need for a general yet flexible method that will adequately treat diverse problems, within a single framework of numerical procedures is clearly apparent. One such procedure is finite element method (FEM). Unlike the finite difference method, which envisions the solution region as an array of grid points, the finite element method envisions the

solution region as built up of many small, interconnected subregions or elements. A finite element model of a problem gives a piecewise approximation to the governing equations. The basic premises of the finite element method is that a solution region can be analytically modeled or approximated by replacing it with an assemblage of discrete elements. Since these elements can be put together in a variety of ways, they can be used to represent exceedingly complex shapes. As an example of how finite difference and finite element model might be used to represent a complex geometric shape. Consider the turbine blade cross section shown in Figure 2.1.

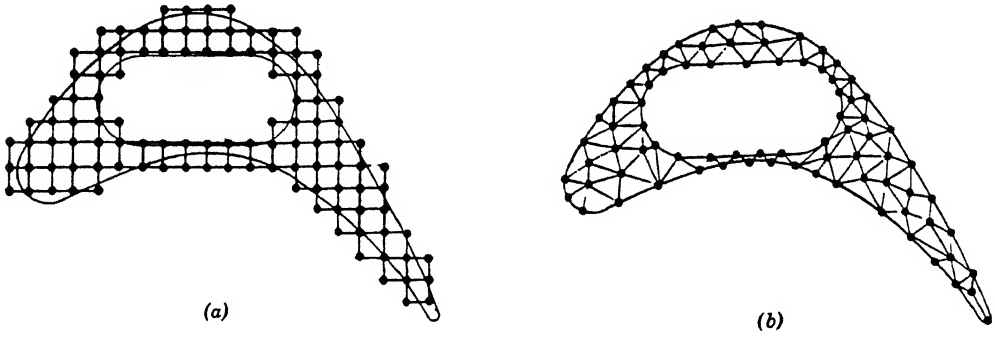

Figure 2.1: Finite difference and finite element discretization of a turbine blade profile (a) Typical finite difference model. (b) Typical finite element model.

For this device, we may want to find the distribution of displacements and stresses for a given force loading. A uniform finite difference mesh would reasonably cover the blade (the solution region), but the boundaries must be approximated by a series of horizontal and vertical lines. On the other hand, the finite element model (using the simplest two-dimensional-the triangle) gives a better approximation to the region and requires fewer nodes. Also, a better approximation to the boundary shape results because the curved boundary is

represented by a series of straight lines. And the grid need not be structured. Due to this unstructured form very complex geometries can be handled with ease. This is clearly the most important advantage of finite element method and is not shared by the familiar finite difference method, which needs a structured grid.

The first essential characteristic of the finite element method (FEM) is that the solution of the discrete problem is assumed a priori to have a prescribed form. The solution has to be in a function space, which is built by varying function values in a given way, for instance linearly or quadratically, between values in nodal points. The nodal points or nodes, are typical points of the elements such as vertices, mid side points or mid-element points, etc. Due to this choice, the representation of the solution is strongly linked to the geometric representation of the domain.

The second essential characteristic is that FEM does not look for a solution of the partial differential equation (PDE) itself, but looks for a solution of some integral form of PDE. In the most general form, this integral formulation is obtained from a weighted residual formulation. By this formulation the method acquires the ability to naturally incorporate differential type boundary conditions. This property constitutes the most important advantage of the FEM and is not shared by any other method (e.g. Finite Difference Method, Finite Volume Method, Spectral Element Method).

The combination of the representation of the solution in a given function space, with the integral formulation treating rigorously the boundary conditions, gives to the method an extremely strong and rigorous mathematical foundation. This allows, for instance, a precise definition of accuracy. The concept of accuracy is very loosely defined in FDM where it often depends upon strongly on the analytic regularity of the solution.

The third essential characteristic of the FEM is the modular way in which the discretization is obtained. The discrete equations are constructed from the contribution on element level which afterwards are assembled to get an over all study of a particular problem.

2.2 Finite Element Method

The finite element method is a type of a scheme which is used to reduce a field problem described by an extremum principle to one in which there are a finite number of unknowns. The method uses many localized functions, termed interpolation functions, each valid only for a small subregion of the domain of interest. Thus the overall state of the unknown field variable is represented piecewise, with continuity of the variable across the boundaries of the subregions or elements being assured by suitable requirements placed on the choice of the interpolation polynomials. Clearly, discretizing the region of the field problem into a smaller regions does not by itself reduce the problem as the continuum to a problem of a finite number of unknowns; within each subregion a continuum problem still exists. However, this is where the finite element method makes the most significant assumption that leads to its success in solving continuum problems. It assumes that the state of the field variable within the subregion or element is completely described by values of the unknown variable at a finite number of points.

The method is a valuable tool in the solution of many engineering problems. In situations where the governing equations are known, but complicated geometry or boundary conditions render analytical solutions difficult or impossible to obtain, the finite element method is often employed. The finite element method makes use of spatial discretization and a weighted residual formulation to arrive at a system of matrix equations. Solution of the matrix equations yields an approximate solution to the original boundary value problem. The most common weighted residual formulation has been the Galerkin method, in which weighting and interpolation functions are from the same class of functions. The Galerkin method, when applied to most structures or heat conduction problems, leads to symmetric stiffness matrices. In this case, it can be shown that the solution possesses 'the best approximation' property. That is, the difference between the finite element and the exact solution is minimized with respect to a certain norm. The success of the Galerkin finite element method in structural

applications is largely due to the 'best approximation' result.

Compared to other numerical techniques, the finite element method possesses numerous advantages. In addition to complete generality with regard to geometry and field property variations, prescription of boundary conditions in terms of pressure or flow, cyclic conditions, present no special difficulties. In the limit, the method can be shown to converge to the exact solution; Thus any degree of accuracy can be obtained. Moreover, the system of equations generated by the method produces a symmetric, banded, definite matrix which can be solved directly with minimal requirements of computer storage and time. The method is characterized by three features.

- The domain of the problem is represented by a collection of simple subdomains, called finite elements. The collection of finite elements is called the finite element mesh
- Over each finite element, the physical process is approximated by functions of desired type (polynomials or otherwise), and algebraic equations relating physical quantities at selective points, called nodes of the element are developed
- The element equations are assembled using continuity and/or "balance" of physical quantities.

In the finite element method, in general, we seek an approximate solution u to a differential equation in the form

$$u \approx \sum_{j=1}^{n} u_j \psi_j$$

where u_j are the values of u at the element nodes, ψ_j are the interpolation functions. Direct substitution of such approximation into the governing differential equations may not always result, (for an arbitrary choice of the data of the problem) in a necessary and sufficient number of equations for the undetermined coefficients u_j. Therefore, a procedure where by a necessary and sufficient number of equations can be obtained is needed. One such procedure is provided by a weighted-integral form of the governing differential equation.

2.2.1 Historical Perspective of FEM

Historically, the finite element method originates from structural mechanics. The first effort to use FEM via piecewise continuous function defined over triangular domains appear in the applied mathematics literature with the work of Courant [59]. Motivated by Euler [60], Courant used an assembly of triangular elements and the principle of minimum potential energy to study the St. Vennat torsion problem. After Courant's work, nearly a decade passed before these discretization ideas were used again. The work of Weinberger [61, 62], Poly [63, 64], Hersch [65] who focussed his attention on boundary eigen values, were a period of renewed interest.

As the popularity of the FEM began to grow in the engineering and physics communities, more applied mathematicians became interested in giving the method a firm mathematical foundation. Although the FEM has its inception in the late 1950's as method for solving structural problems, it was not until 1963 that it got recognized as a general method that can deal with problems of the elastic continuum. Finally, Zienkiewicz and Cheung [66] recognized that the method is one of an even more general nature, applicable to all field problems which can be formulated as extremum or stationary value problems.

Evaluation of the FEM has brought into existence a great body of literature including a text book by Zienkiewicz [67]. Although a major portion of the literature in the early 1970's deals with static and dynamic structural analysis, there has been a continuous steady increase in the number of applications in other fields. Unquestionably, the FEM is now a well-established and accepted engineering analysis tool.

2.3 Variational Methods

Often continuum problems have different but equivalent formulations-a differential equation and a Variational formulation. In the differential formulation, the problem is to integrate a differential equation or a system of differential equations subject to given boundary con-

ditions. The two problems are equivalent because the functions that satisfy the differential equations and their boundary conditions also extremize or make stationary the functionals. This equivalence is apparent form the calculation of variations, which shows that the functionals are extremized or made stationary only when one or more Euler equations and their boundary conditions are satisfied. And these equations are precisely the governing differential equations of the problem. The classical Variational formulation of a continuum problem often has several advantages over the differential formulation from the standpoint of obtaining an approximate solution. First, the functional, which may actually represent some physical quantity in the problem, contains lower order derivatives than the differential operator, and consequently the approximate solution can be sought in a larger class of functions. Second, the problem may possess reciprocal Variational formulations, that is, one functional to be minimized and another functional of a different form to be maximized. In such cases we have a means for finding upper and lower bounds on the functional, and this capability may have significant engineering value. Third, the Variational formulation allows us to treat very complicated boundary conditions as natural boundary conditions. Fourth, form a purely mathematical standpoint the Variational formulation is helpful because with the calculus of variations it can sometimes be used to prove the existence of a solution.

Historically, Variational methods are among the oldest means of obtaining solutions to problems in physics and engineering. One general method for obtaining approximate solutions to problems expressed in Variational form is known as the Rayleigh-Ritz method. Another one is the method of weighted residuals.

2.3.1 Rayleigh-Ritz Method

The Rayleigh-Ritz method consists of assuming the form of the unknown solution in terms of known functions (trial functions) with unknown adjustable parameters. From the family of trial functions we select the function which satisfies the functional theory. The procedure is to substitute the trial functions into the functional and thereby express the functional

in terms of the adjustable parameters. The function is then differentiated with respect to each parameter, and the resulting equations are set equal to zero. If there are 'n' unknown parameters, there will be 'n' simultaneous equations to be solved for these parameters. By this means the approximate solution is chosen from the family of assumed solutions.

The procedure does nothing more than to give us the "best" solution from the family of assumed solutions. Clearly, then the accuracy of the approximate solution depends on the choice of trial functions. We require that the trial functions be defined over the whole solution domain and that they satisfy at least some and usually all of the boundary conditions. Consider, as an example the following simple one dimensional boundary value problem (bvp), consisting of the differential equation

$$\frac{d}{dx}(\lambda\frac{du}{dx}) = f(x) \quad \text{on} \quad 0 \leq x \leq X \tag{2.1}$$

$$u(0) = u_0 \tag{2.2}$$

$$\lambda\frac{du}{dx}(X) = q \tag{2.3}$$

More generally, the differential equation is denoted by

$$a(\hat{u}) = f \tag{2.4}$$

Let us denote the domain by Ω and the boundary by $\partial\Omega$. The boundary condition given by equation (2.2) is usually called 'Dirichlet boundary condition'. In the sequel, the part of the boundary where Dirichlet boundary has to be applied is denoted by $\partial\Omega_0$

$$b_0(u) = g_0 \tag{2.5}$$

The derivative boundary condition given by equation (2.3) is called 'Neumann boundary condition'. In the sequel, it is denoted by $\partial\Omega_1$.

$$b_1(u) = g_1 \tag{2.6}$$

The bvp given by equations (2.1) - (2.3) are said to be in its strong form, requiring the satisfaction of the differential equation (2.1) in all points of the domain $\partial\Omega$, the satisfaction

of the Dirichlet boundary condition given by equation (2.2) on $\partial\Omega_0$ and the satisfaction of Neumann boundary condition equation given by equation (2.3) on $\partial\Omega_1$. In general the method is described below for a linear Variational problem.

Consider the Variational problem of finding the solution u such that

$$B(w,u) = l(w) \tag{2.7}$$

for all sufficiently differentiable functions w satisfying the homogeneous form of any specified essential boundary condition on u. When the functional B is bilinear and symmetric and when l is linear, the problem in equation (2.7) is equivalent to minimization of the quadratic functional

$$I(u) = \frac{1}{2}B(u,u) - l(u) \tag{2.8}$$

In the Rayleigh-Ritz method, we select an approximate solution to equation (2.8) in the form of a finite series

$$u_N = \sum_{j=1}^{N} c_j\phi_j + \phi_0 \tag{2.9}$$

where the constants c_j, called the Ritz coefficients, are chosen such that the equation (2.7) holds for $w = \phi_i$ (i = 1,2,$\cdots$,N); i.e. equation (2.7) holds for N different choices of w, so that N independent algebraic equations in c_j are obtained. The i^{th} algebraic equation is obtained by substituting ϕ_i for w:

$$B(\phi_i, \sum_{j=1}^{N} c_j\phi_j + \phi_0) = l(\phi_i) \ (i = 1,2,\cdots,N)$$

If B is bilinear, the summation and the constants c_j can be taken outside the operator. We have

$$\sum_{j=1}^{N} B(\phi_i,\phi_j)c_j = l(\phi_i) - B(\phi_i,\phi_0) \qquad \text{or}$$

$$\sum_{j=1}^{N} B_{ij}c_j = F_i, \quad B_{ij} = B(\phi_i,\phi_j), \quad F_i = l(\phi_i) - B(\phi_i,\phi_0) \tag{2.10}$$

which represents the i^{th} algebraic equation in a system of N linear algebraic equations in

N constants c_j. The columns (or rows) of the matrix $B_{ij} = B(\phi_i, \phi_j)$ must be linearly independent in order that the coefficient matrix given by equation (2.10) can be inverted. The requirements on ϕ_j and ϕ_0 are as follows.

In the approximation u_N in equation (2.9), we note that u_N must satisfy the specified essential boundary conditions of the problem; any specified natural boundary conditions are already included in the Variational problem in equation (2.7). The particular form of u_N in equation (2.9) facilitates satisfaction of specified boundary conditions. If we were to use the form

$$u_N = \sum_{j=1}^{N} c_j \phi_j(x)$$

then it would not be easy to satisfy non-homogeneous boundary conditions. For example, suppose that u_N is required to satisfy the conditions $u_N(x_0) = u_0$ at a boundary point $x = x_0$:

$$\sum_{j=1}^{N} c_j \phi_j(x_0) = u_0$$

Since c_j are unknown parameters to be determined, it is easy to change $\phi_j(x)$ such that this relation holds. If $u_0 = 0$ then any ϕ_j such that $\phi_j(x) = 0$ would meet the requirement. By writing the approximate solution u_N in the form of equation (2.9), a sum of homogeneous and non-homogeneous parts, the non-homogeneous essential boundary conditions can be satisfied by ϕ_0, $\phi_0(x_0) = u_0$, and ϕ_j are required to satisfy the homogeneous form of the same boundary condition, $\phi_j(x_0) = 0$. In this way u_N satisfy the specified boundary conditions:

$$u_N(x_0) = \sum_{j=1}^{N} c_j \phi_j(x_0) + \phi_0(x_0)$$

$$= 0 + u_0$$

If all specified essential boundary conditions are homogeneous (i.e the specified value u_0 is zero), then $\phi_0(x_0)$ is taken to be zero and ϕ_j must still satisfy the same conditions, $\phi_j = 0$. Since ϕ_i satisfy the homogeneous essential boundary conditions, the choice $w = \phi_i$

is consistent with the requirement of a weight function. The approximate function ϕ_i satisfy the following conditions. (i) ϕ_i should be such that $B(\phi_i, \phi_j)$ is well defined and non zero (ii) ϕ_i must satisfy at least the homogeneous form of essential boundary conditions of the problem. The only role that ϕ_0 plays is to satisfy the specified non-homogeneous essential boundary conditions of the problem.

Further if the bilinear form is symmetric, the Rayleigh-Ritz method can be viewed as one that seeks a solution of the form given by equation (2.9) in which the parameters are determined by minimizing the quadratic functional corresponding to the symmetric bilinear form. If B is not symmetric, we do not have a quadratic functional.

2.3.2 The Method of Weighted Residuals

The first basic ingredient of the finite element method is that an approximate solution is sought which belongs to some finite dimension function space. In the weighted-residual method, the solution u is approximated, in much the same way as in the Rayleigh-Ritz method, by the expression:

$$\hat{u} = \psi + \sum_{k=1}^{N} \phi_k u_k \tag{2.11}$$

except that the requirement on ψ and ϕ_k for the weighted-residual method are more stringent than those for the Rayleigh-Ritz method, ψ is a function which satisfies the boundary conditions given in equations (2.2) and (2.3) and ϕ_k are functions that satisfy the boundary conditions of the same form but with right hand side equal to zero. For the given problem, the construction space ϕ_k are generally called basic functions or shape functions. Since the dimension of the function space $\phi = \{\phi_k : \quad k = 1, 2, \cdots, N\}$ is finite and it yields a set of algebraic equations of the form:

$$K\ U = F \tag{2.12}$$

where U is a vector consisting of elements $(u_1, u_2, \cdots, u_l)$, K is the coefficient matrix and F is a force vector. In general equation (2.11) can not satisfy the differential equation (2.1) at each point of the domain. This means that the approximate solution $\hat{u}$ can not be identical with the exact solution u. Of course, the shape functions should be chosen so that by enriching the function space ϕ, i.e. letting N grow, the approximation obtained by equation (2.11) becomes better. This means that the approximate solution converges to the exact solution. This is called the completeness requirement of the function space.

Since a function $\hat{u}$ given by equation (2.11) can not satisfy the differential equation (2.1), upon substitution of $\hat{u}$ into equation (2.4), a residual is left:

$$r_\Omega = a(\hat{u}) - f \quad \text{in} \quad \Omega \tag{2.13}$$

An approximate solution of the bvp is now obtained by finding a way to make this residual small in some sense. In the finite element method this is done by requiring that an approximate number of weighted integral of the residual over Ω be zero:

$$\int_\Omega w_l \, r_\Omega \, d\Omega = 0; \qquad l = 1, 2, \cdots, N \tag{2.14}$$

where $W = \{w_l; l = 1, 2, \cdots, N\}$ is a set of weighting functions. Obviously, the convergence requirement now also implies a requirement of completeness of the space of weighting functions, i.e. equation (2.14) should imply $r_\Omega \to 0$ for $N \to \infty$.

Clearly with satisfaction of the completeness, for $N \to \infty$, the weighted-residual formulation given by equation (2.14) for a function of the form equation (2.11) is completely equivalent to the strong formulation of the bvp defined by equations (2.1) - (2.3). An approximate solution then is obtained for N being finite.

2.3.3 Galerkin Formulation

Among the possible choices for the set of weighting functions the following ones are the most obvious. The weighting functions can be chosen to be Dirac-Delta functions in N points.

This choice boils down to making the residual equal to zero in a number of chosen points. This method is called the point-collation method. Obviously, it has much in common with the finite difference philosophy.

A second possible choice of weighting functions is given by

$$w_l = \begin{cases} 1 & \text{for } x_l \leq x \leq x_{l+1} \\ 0 & \text{for } x < x_l \text{ or } x > x_{l+1} \end{cases}$$

The weighted residual statements, given in equation (2.14), now require the integral of the residual to be zero on N sub-domains. This method is called the sub-domain collocation method.

The most popular choice for the weighting functions in the FEM is that the shape functions themselves are the weighting functions: $w_l = \phi_l$. This method is called the Galerkin method. Its meaning is that the the residual is made to be orthogonal to the space of the shape functions.

To illustrate the Galerkin method, consider the bvp (2.1), with constant λ. Then:

$$\psi = u_o + \frac{q}{\lambda} x$$

Consider, a Fourier-Sine expansion of u:

$$\hat{u} = \psi + \sum_{k=1}^{N} u_k \, sin\frac{\pi k' x}{X}$$

where $k' = k - \frac{1}{2}$ Then:

$$r_\Omega = -\lambda \sum_{k=1}^{N} u_k \left(\frac{\pi k'}{X}\right)^2 sin\frac{\pi k' x}{X} - f$$

The Galerkin method then gives

$$\lambda \sum_{k=1}^{N} u_k \left(\frac{\pi k'}{X}\right)^2 \int_0^X sin\frac{\pi k' x}{X} \, sin\frac{\pi l' x}{X} \, dx = -\int_0^X sin\frac{\pi l' x}{X} \, f \, dx$$

Then noting that:

$$\int_0^X sin\frac{\pi k' x}{X} \, sin\frac{\pi l' x}{X} \, dx = \frac{X}{2} \quad \text{for } k' = l'$$
$$= 0 \quad \text{for } k' \neq l'$$

we find:

$$u_l = -\frac{2X}{\lambda\pi^2 l'^2}\int_0^X f\, sin\frac{\pi l' x}{X}\, dx$$

In some situations, modification of the standard choice are necessary. The standard choice is denoted by $Bubnov-Galerkin$ method. When modified weighting functions are used, the method is denoted by the term $Petrov-Galerkin$ method. i.e. $w_l \neq \phi_l$. To illustrate the $Bubnov-Galerkin$ and $Petrov-Galerin$ methods, the following example is considered.

$$-\frac{d^2u}{dx^2} - u + x^2 = 0, \quad u(0) = 0, \quad u'(1) = 1$$

For a weighted residual method, ϕ_0 and ϕ_i should satisfy the following boundary conditions (bcs).

$$\phi_0(0) = 0,\ \phi_0'(1) = 1 \text{ (satisfy actual bcs)}$$

$$\phi_i(0) = 0,\ \phi_i'(1) = 0 \text{ (satisfy homogeneous form of a specified bcs)}$$

For a choice of algebraic equations, we assume $\phi_0(x) = a + bx$ and use the two constants on ϕ_0 to determine the constants a and b. We obtain $\phi_0(x) = x$. Since there are two homogeneous conditions, we must assume at least a three parameter polynomial to obtain a nonzero function $\phi_1 = a + bx + cx^2$. Using the constants on ϕ_i, we obtain

$$\phi_1 = -\,c\,x(2-x)$$

The constant c can be set equal to unity because it will be absorbed into any one of the parameters, we can assume one of the forms $\phi_2 = a + bx + dx^3$ or $\phi_2 = a + cx^2 + dx^3$. With $d \neq 0$, ϕ_2 does not contain all order terms in either case, but the approximate solution is complete because $\{\phi_1,\ \phi_2\}$ contains all terms up to degree three. For the first choice of ϕ_2, we obtain

$$\phi_2 = x^2(1 - \frac{2}{3}x)$$

The residual in the approximation of the equation is

$$R = -(0 + \sum_{i=1}^{2} c_i \frac{d^2\phi_i}{dx^2}) - (\phi_0 + \sum_{i=1}^{2} c_i\phi_i) + x^2$$

$$= c_1(2 - 2x + x^2) + c_2(-2 + 4x - x^2 + \frac{2}{3}x^2) - x + x^2$$

In the *Bubnov – Galerkin* method, $\psi_i = \phi_i$, we have

$$\int_0^1 x(2-x)\ R\ dx = 0, \quad \int_0^1 x^2(1 - \frac{2}{3}x)R\ dx = 0$$

or

$$u = 1.2894x - 0.139x^2 - 0.00325x^3$$

In the *Petrov–Galerkin* method, $\psi_i \neq \phi_i$. Let the weighting functions be $\psi_1 = x$, $\psi_2 = x^2$, we have

$$\int_0^1 xR\ dx = 0, \quad \int_0^1 x^2R\ dx = 0$$

or

$$u = 1.302053x - 0.173021x^2 - 0.014663x^3$$

2.3.4 Weak Formulation

In many problems, it is not practical to construct a function which satisfies the boundary conditions in order to arrive at an expression for the approximate solution consisting of set of algebraic equation $K\ U = F$ as discussed in section (2.3.2). More generally , an approximate solution can be expressed as

$$\hat{u} = \sum_{k=1}^{N} \phi_k u_k \tag{2.15}$$

now the approximate solution not only has a residual with respect to the field equation (2.4), but also with respect to the boundary equations (2.5) and (2.6).

$$r_0 = b_0(\hat{u}) - g_0 \tag{2.16}$$

$$r_1 = b_1(\hat{u}) - g_1 \tag{2.17}$$

A weighted residual statement is now to be of the form

$$\int_{\Omega} w_l r_\Omega \, d\Omega + \int_{\partial\Omega_0} w_l^0 r_0 \, d\partial\Omega + \int_{\partial\Omega_1} w_l^1 r_1 \, d\partial\Omega = 0 \tag{2.18}$$

This complicates the formulation since additional weighting functions on the boundaries are now to be chosen. Since the number of degrees of freedom of the approximate solution, equation (2.15) is N, an equal number of independent weighting functions w_l can be chosen, while w_l^0 and w_l^1 are to be dependent on w_l. In practice very often, there is a natural way to chose the dependent weighting functions. For the bvp equations (2.1) - (2.3), above equation (2.18) becomes

$$\int_0^X w_l \, [\, \frac{d}{dx} (\lambda \frac{d\hat{u}}{dx}) - f \,] \, dx + w_l^0 \, [\, \hat{u}(0) - u_0 \,] + w_l^1 \, [\, \lambda \frac{d\hat{u}}{dx}(X) - q \,] \tag{2.19}$$

Of course, for this problem the weighting functions at the boundary reduce to weighting factors w_l^0 and w_l^1. By integration by parts on the first term, this becomes

$$w_l \lambda \frac{d\hat{u}}{dx}|_0^X - \int_0^X \lambda \frac{dw_l}{dx} \frac{d\hat{u}}{dx} \, dx - \int_0^X w_l f \, dx + w_l^0 \, [\, (\hat{u}(0) - u_0 \,] + w_l^1 \, [\, \lambda \frac{d\hat{u}}{dx}(X) - q \,] = 0 \tag{2.20}$$

The weighted residual statement is simplified considerably by choosing the weighting factors on the Neumann boundary as

$$w_l^1 = - w_l(X)$$

The weighted residual statement then becomes

$$- \int_0^X \lambda \frac{dw_l}{dx} \frac{d\hat{u}}{dx} \, dx - w_l(0) \lambda \frac{d\hat{u}}{dx}(0) - \int_0^X w_l \, f \, dx + w_l^0 \, [\, \hat{u}(0) - u_0 \,] + w_l(X) \, q = 0 \tag{2.21}$$

Furthermore, if the Dirichlet boundary condition can be imposed on the approximate solution, the weighting functions and the weighting factors can be chosen to be zero at the Dirichlet boundary, so that the residual statement further simplifies to

$$- \int_0^X \lambda \frac{dw_l}{dx} \frac{d\hat{u}}{dx} \, dx - \int_0^X w_l \, f \, dx + w_l(X) \, q = 0 \tag{2.22}$$

subject to the Dirichlet boundary conditions

$$\hat{u}(0) = u_0$$

$$w_l(0) = 0$$

The weighted residual statement in the form of equation (2.22) is called the *weak formulation*. Clearly, the *weak formulation* given in equation (2.22) along with the Dirichlet boundary conditions is not completely equivalent to the strong formulation even as $N \rightarrow \infty$. By the construction of the *weak formulation*, any solution of the strong formulation satisfies the *weak formulation*. The converse, however, is not true. The *weak formulation* allows solutions which have a lower degree of regularity than required for strong formulation. This is the origin of the terms weak and strong. For instance for the bvp equations (2.1) - (2.3), the solution must have a continuous first derivatives. We express this by saying that the degree of the regularity is to be C^1. Whereas, the corresponding *weak formulation*, only requires continuity of the function value itself; the necessary degree of regularity here is C^0. This means that functions with discontinuous first derivatives are allowed in the *weak formulation*.

Further, in the *weak formulation* the Neumann boundary condition need not be imposed in an explicit way to the solution. Boundary conditions of this type enter through the integration by parts in a natural way into the formulation. Therefore, these boundary conditions are called *natural boundary conditions*. Also, the boundary conditions which have to be imposed explicitly in the *weak formulation* are called as *essential boundary conditions*.

2.3.5 Shape Functions

A second basic ingredient of the finite element method is the piecewise manner in which the shape and weighting functions are constructed. The domain Ω is subdivided into non-overlapping subdomains Ω_e, called "elements simplified geometrical form". In general, the

integral in the *weak formulation* can be split into a sum of integrals over elements.

$$\int_{\Omega} (F)\, d\Omega = \sum_{e} \int_{\Omega_e} (F)\, d\Omega$$

Then, obviously, in the piecewise contributions to the integrals, it is computationally advantageous to have as many zero contributions as possible. This is achieved when the shape functions and the weighting functions associated to some index are only non-zero in the smallest possible number of the elements associated to this index. Shape and weighting functions which are only non-zero in a small set of elements are said to have a compact support. In the finite element method, shape and weighting functions with *compact support* are constructed from an *interpolation problem* over the domain. For instance, a function u which is obtained through linear *interpolation* between function values defined in the grid points of the grid can be written as

$$\hat{u} = \sum_{k=0}^{L} \phi_k u_k \tag{2.23}$$

The shape functions ϕ_k in this expression look like a hat form. For a function representation based on an interpolation, the values u_k in the equation (2.23) have the meaning of function values in the gird points. Obviously, other interpolation schemes are possible. For instance, the function $\hat{u}$ could be obtained by piecewise constant interpolation or the interpolation could be piecewise quadratic.

In all these cases, the values of u_k represent function values in some points associated to the elements. In the finite element technique, these points are called nodes. As a simple example, we first consider the bvp (2.1) - (2.3) with piecewise linear shape functions and a standard Galerkin *weak formulation*. The approximate solution is then represented by

$$\hat{u} = \sum_{k=0}^{L} \phi_k u_k = \sum_{e} \sum_{j=1}^{2} \phi_j^e u_j \tag{2.24}$$

In equation (2.24) the sum over the nodes is rearranged as a double sum, first over the elements and then over the nodes belonging to the element. The shape function, ϕ_k, associated with the nodes, are called the global shape functions. On the element level, the shape

functions ϕ_j^e are called local shape functions or element shape functions. The linear shape functions are shown in Figure 2.2: (a).

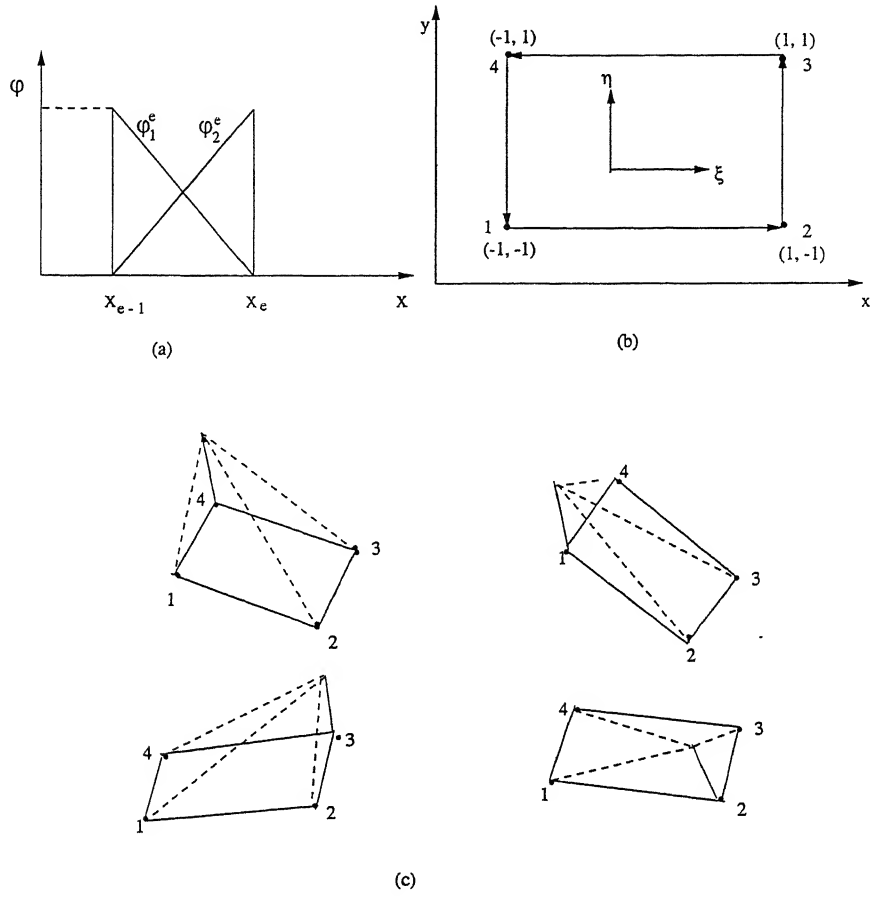

Figure 2.2: (a) Linear one dimensional elements (b) Bilinear rectangular elements and (c) Its shape functions in normalized coordinates.

For the linear shape functions:

$$\phi_1^e = \frac{x_e - x}{\Delta x_e}, \qquad \phi_2^e = \frac{x - x_{e-1}}{\Delta x_e}$$

Hence:

$$\frac{d\phi_1^e}{dx} = \frac{-1}{\Delta x_e}, \qquad \frac{d\phi_2^e}{dx} = \frac{1}{\Delta x_e}$$

The Galerkin *weak formulation* given in equation (2.22) is

$$\int_0^X \lambda \frac{dw_l}{dx} \frac{d\hat{u}}{dx} dx = - \int_0^X w_l f dx + w_l(X) q \tag{2.25}$$

Although by the piecewise shape representation the approximate solution can not satisfy the strong form of the boundary value problem in any point of the domain, the solution obtained from the *weakformulation* represents a valid approximation of the problem.

A rectangular bilinear element is a four noded serendipity class of element. A typical bilinear element in local coordinates (ξ, η) is shown in Figure 2.2: (b). The linear variables in ξ and η directions along the edges are defined by $\xi_0 = \xi\ \xi_i,\ \xi_i = 1$ or -1 and $\eta_0 = \eta\ \eta_i,\ \eta_i = 1$ or -1. The linear nodal shape functions in ξ and η directions at the nodal points $\xi = 1$ or -1, $\eta = 1$ or -1 are defined by

$$\frac{(1+\xi\xi_0)}{2} \quad \text{and} \quad \frac{(1+\eta\eta_0)}{2}$$

respectively. Now for the bilinear element the nodal shape functions can be derived by taking the product of the two linear shape functions associated with that node. The bilinear nodal shape function associated with node i (Shown in Figure 2.2: (c)) are given by

$$\phi_i = \frac{(1+\xi\xi_0)(1+\eta\eta_0)}{4}, \quad i = 1, 2, 3, 4$$

The element is termed bilinear because of the product of ξ and η in addition to the linear terms in the expression. The form given for ϕ_i automatically satisfies the usual requirement. i.e. the value at node i is unity and at all other nodes of the element is zero.

2.4 Upwind Finite Elements

Initial finite element formulations for convective transport problems also used the Galerkin method, but with mixed results. In fluid flows or convective heat transfer, the matrix associated with the convective term is non symmetric, and as a result, the 'best approximation' property is lost. In practice, solutions are often corrupted by spurious node-to-node oscillations or 'wiggles'. Wiggles are most likely to appear in convection dominated cases (high Peclet or Reynolds number) when a downstream boundary condition forces a rapid change in the solution. An example of this phenomenon is shown in the Figure 2.3 for fluid past a

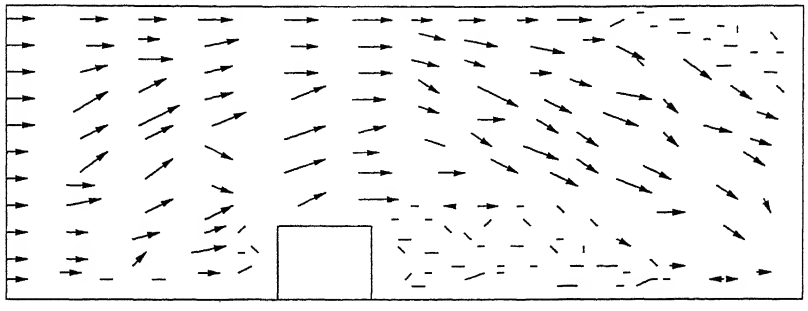

Figure 2.3: Oscillations generated upstream of a block for Reynolds number = 200

block in a narrow channel [68]. The only way to eliminate the oscillations is to severely refine the mesh such that convection no longer dominates on element levels. Obviously, mesh refinement is needed in regions where accurate representation of the solution is required. However, often only the global solution features are desired and in this case mesh refinement is required only to prevent oscillations. This provides motivation for development of an alternative to the Galerkin formulation which precludes spurious oscillations, regardless of mesh refinement. It is also well known that the Galerkin finite element method give rise to central-difference type approximations of differential operators. It is thus not surprising that 'wiggles' have also affected central-difference solutions. In fact, obtaining solutions at all has been problematic due to the reliance on iterative solvers in finite difference coupled-difference equations. It was discovered, however, that wiggle free solutions could be obtained by the use of 'upwind' differencing on the convective term. Upwind differencing amounts to approximating the convective derivative with solution values at the upstream and central nodes of a three node stencil. It is well known that the upwind convective term can be constructed simply by adding artificial diffusion to a central difference treatment. This artificial diffusion interpretation has been the basis for extensive criticism of upwind methods. In a finite element framework, upwind convective terms can be developed in several different ways. The initial upwind finite element formulation, for the one dimensional advection-diffusion equation, employed modified weighting functions to achieve the upwind effect. In essence, the element upstream of a node is weighted more heavily than the element downstream of a

node.

Many of the optimal upwind finite element formulations lead to the same system of matrix equations and give exact solutions for the one-dimensional model problem. Unfortunately, when generated to more complicated situations, some of these formulations are far from optimal. In multidimensional problems, solutions often exhibit excessive diffusion perpendicular to the flow direction. Overly, diffuse results also appear in transient problems, or when source terms are present. In addition, in many instances the Galerkin formulation gives oscillation-free solutions which are more accurate than upwind solutions. obviously, such results cause upwind techniques to be viewed with some suspicion (and even contempt). Some investigators believe that use of the Galerkin formulation, along with mesh refinement, is the only possible way to achieve solutions that are both accurate and wiggle free.

To illustrate upwind finite elements, consider the following example. Let Ω be a bounded region in $\Re^n$, $n \geq 2$, with piecewise smooth boundary. A general point in $\bar{\Omega}$ is denoted by x. The model equation under consideration is the steady advection-diffusion equation in an incompressible flow field:

$$u^T \nabla\phi = \nabla^T k \nabla\phi \tag{2.26}$$

where u is the flow velocity, k is the diffusivity and ∇ is the gradient operator. We assume k to be positive definite (both u and k are given functions of x). The boundary value problem for equation (2.26) consists of finding a function ϕ, satisfying equation (2.26), such that:

$$\left.\begin{array}{ll} \phi = f & \text{on } \Gamma_1 \\ n^T\, k\, \nabla\phi = g & \text{on } \Gamma_2 \end{array}\right\} \tag{2.27}$$

where f and g are given functions of x, n is the outward unit normal vector to Γ, and Γ_1 and Γ_2 are subregions of Γ satisfying $\overline{\Gamma_1 \cup \Gamma_2} = \Gamma$ and $\Gamma_1 \cap \Gamma_2 = \phi$. A weak form of the problem is given by

$$\int_\Omega \left(w\, u^T \nabla\phi + \nabla w^T k \nabla\phi \right) d\Omega = \int_{\Gamma_2} w\, g\, d\Omega \tag{2.28}$$

where ϕ is required to satisfy the first of equation (2.27) and w is required to be zero on Γ_1.

The second of equation (2.27) is a natural boundary condition implied by equation (2.28). The one dimensional version of equation (2.26) is

$$u \frac{d\phi}{dx} = \frac{d}{dx} k \frac{d\phi}{dx} \tag{2.29}$$

where u and k are given functions of x, k is positive, and $\Omega = (0, L)$. Various specializations of boundary conditions are possible. For example,

$$\left.\begin{array}{l} \phi(0) = f_0 \\ \phi(L) = f_L \end{array}\right\} \tag{2.30}$$

or

$$\left.\begin{array}{l} \phi(0) = f_0 \\ k(L)\ \frac{d\phi}{dx}(L) = g_L \end{array}\right\} \tag{2.31}$$

are allowable combinations, where f_0, f_L and g_L are given constants. Weak form of the one-dimensional problem, corresponding to equations (2.29) - (2.31), are given by

$$\int_0^L \left(w\, u \frac{d\phi}{dx} + \frac{dw}{dx}\, k\, \frac{d\phi}{dx} \right) dx = \left\{ \begin{array}{l} 0 \\ w(L)\ g_L \end{array}\right. \tag{2.32}$$

in the former case, ϕ is required to satisfy equation (2.30) and $w(0) = w(L) = 0$, whereas in the latter case, ϕ is required to satisfy only the first of equation (2.30) and $w(0) = 0$. Approximate solution of equations (2.28) and (2.32) may be constructed by the finite element method in which

$$\phi \leftarrow \sum_i N_i\, d_i \tag{2.33}$$

where N_i is the shape function associated with node 'i' and d_i is the approximate value of ϕ at node 'i'. In the standard Galerkin method (Bubnov-Galerkin method), w is taken to be, in turn,equal to each shape function which vanishes on Γ_1. In the one-dimensional case in which u and k are constant and element lengths are equal, employing piecewise linear shape functions, leads to a central difference approximation to the advection-diffusion term. Under

these circumstances it is well known that unless

$$h < \frac{2k}{|u|} \tag{2.34}$$

where h is the element length, the discrete solution will contain spurious oscillation called *wiggles* (move form side to side with rapid short moments). Analogous conditions to equation (2.34) holds in more general sense in which the Galerkin finite element method is employed and result in excessive mesh refinement in problems of interest.

To circumvent such difficulties upwind finite element formulation have been developed by a more general weighted residual method is which w is chosen from a wider class of functions than the shape functions. The procedure, although effective leads to grater evaluations than those used in the Galerkin formulation.

In general, there has been three basic techniques utilized to achieve the upwind effect in finite elements.

1. ARTIFICIAL DIFFUSION. Artificial diffusion, is added to the physical diffusion, and a conventional Galerkin finite element discretization is employed. This is actually a 'balance diffusion', in that it balances the negative diffusion of the Galerkin treatment.

2. QUADRATURE. The numerical quadrature rule for the convective term is modified to achieve the upwind effect.

3. PETROV-GALERKIN. The weighting functions for a typical node is modified to weight the element upwind of the node more heavily than the download element. An example is shown in Figure 2.4.

2.5 SUPG Strategy

The SUPGFEM has the robust qualities of a classical upwind method, but is not subject to any of the artificial diffusion criticisms. The basic idea of the Streamline Upwind method is

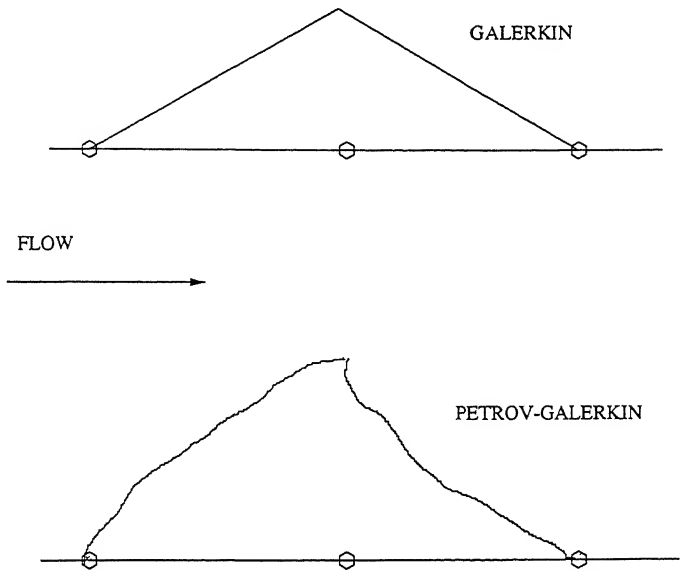

Figure 2.4: Galerkin weighting function and Upwind Petrov-Galerkin weighting function.

to add diffusion (or viscosity) which acts only in the flow direction. Extended to a Petrov-Galerkin formulation, the standard Galerkin weighting functions are modified by adding streamline upwind perturbation, which again acts only in the flow direction. The modified weighting function is applied to all terms in the equation, resulting in a consistent weighted residual formulation.

Let Ω be a bounded region in R^2 and assume Ω has a piecewise smooth boundary Γ. Let $x = \{x_i\}$, i = 1,2. denote a general point in $\bar{\Omega}$ and let $n = \{n_i\}$ be the outward normal vector to Γ. Let Γ_g and Γ_h be subsets of Γ which satisfy the following conditions:

$$\overline{\Gamma_g \cup \Gamma_h} = \Gamma$$

$$\Gamma_g \cap \Gamma_h = \phi$$

The superimposed bar in the above equation represents set closure and ϕ denotes the empty set. Consider a discretization of Ω into element subdomains Ω^e, $e = 1, 2..$ Let Γ^e denotes the boundary of Ω^e. Further, assume

$$\cup_e \bar{\Omega}^e = \Omega, \qquad \cap_e \Omega^e = \phi$$

Finally, define the 'interior boundary', Γ_{int} as follows:

$$\Gamma_{int} = \cup_e \Gamma^e - \Gamma$$

For the illustration of the strategy, consider the unsteady linear advection-diffusion equation for incompressible flow fields.

$$\phi_{,t} + \sigma_{i,i} = f \tag{2.35}$$

where

$$\sigma_i = \sigma_i^a + \sigma_i^d \quad \text{(total flux)}$$

$$\sigma_i^a = u_i \phi \quad \text{(advection flux)}$$

$$\sigma_i^d = - k_{ij} \phi_{,j} \quad \text{(diffusive flux)}$$

In the above, f is a source term, u_i is the flow velocity, and k_{ij} is the diffusivity. Each of f, u_i, and k_{ij} are assumed to be given functions of x and t. Further, the velocity field, u_i , is assumed to be divergence free. The initial-value problem defined by equation (2.35) consists of finding a function $\phi(x,t)$ which satisfies equation (2.35) on Ω and

$$\phi = g \quad \text{on } \Gamma_g$$

$$- \sigma_n^d = h \quad \text{on } \Gamma_h$$

$$\phi(x,0) = \phi_0$$

where g and h are given functions of x and t, and the initial condition ϕ_0 is a given function of x. In a usual Galerkin weighted residual method, the weighting functions are considered to be continuous across inter element boundaries. The Streamline Upwind/Petrov-Galerkin formulation, however needs discontinuous weighting functions of the form

$$\tilde{W} = w + P \tag{2.36}$$

where w is a continuous weighting function, and P is the discontinuous upwind contribution.

Both w and P are assumed to be smooth on the element interiors. Consider a point x in Γ_{int}. Designate (arbitrarily) one side of Γ_{int} to be the 'plus side' and the other to be the 'minus side'. Let n^+ and n^- be unit normal vectors to Γ_{int} at x which point in 'plus' and 'minus' directions, respectively. Clearly $n^- = n^+$. Let Γ_i^+ and Γ_i^- denote the values of Γ_i, obtained by approaching x from the positive and negative sides, respectively. The 'jump' in Γ_n at x is defined to be

$$[\,\sigma_n\,] = (\,\sigma_i^+ - \sigma_i^-\,)n_i^+ = \sigma_i^+ n_i^+ + \sigma_i^- n_i^-$$

it is also to be noted that 'jump' is invariant with respect to reversing the 'plus' and 'minus' designations. We shall also assume that the trial solutions, ϕ satisfy $\phi = g$ on Γ_g and weighting functions, w, satisfy $w = 0$ on Γ_g.

The Streamline Upwind /Petrov-Galerkin weighted residual formulation for the initial boundary value problem defined by equation (2.35) is

$$\int_\Omega w\,(\dot{\phi} + \sigma^a_{i,i})\,d\Omega - \int_\Omega w_{,\,i}\,\sigma_i^d\,d\Omega + \sum_e \int_{\Omega^e} P\,(\dot{\phi} + \sigma_{i,i} - f)\,d\Omega = \int_\Omega w\,f\,d\Omega + \int_{\Gamma^h} w\,h\,d\Gamma.$$

Integration by parts yields

$$\sum_e \int_{\Omega^e} \tilde{W}\,(\dot{\phi} + \sigma_{i,i} - f)\,d\Omega - \int_{\Gamma_h} w\,(\sigma_n^d + h)\,d\Gamma - \int_{\Gamma_{int}} w\,[\sigma_n^d]\,d\Gamma = 0.$$

As shown in the Figure 2.4, upwind finite elements may be constructed via the Galerkin method with added artificial diffusion. In the one-dimensional case, the artificial diffusion, when optimally selected, balanced the negative diffusion inherent in the Galerkin method, resulting in exact nodal solutions for the model problem. However, the multidimensional generalizations like flow of lubricant in parallel slider bearings of some finite element upwind schemes were unsuccessful due to the cross wind diffusion problem. It was apparent that the upwind effect, arrived at by whatever means, was needed only in the direction of flow. In

As shown in the equation (2.36) the perturbation is seen to be

$$P = \frac{\tilde{k}\ \hat{u}_j\ w_{,j}}{\|u\|}$$

Clearly, if w is continuous across element boundaries, then P, and thus $\tilde{W}$, will be discontinuous. Examples of w and $\tilde{W}$ for one-dimensional linear finite elements are shown in Figure 2.5.

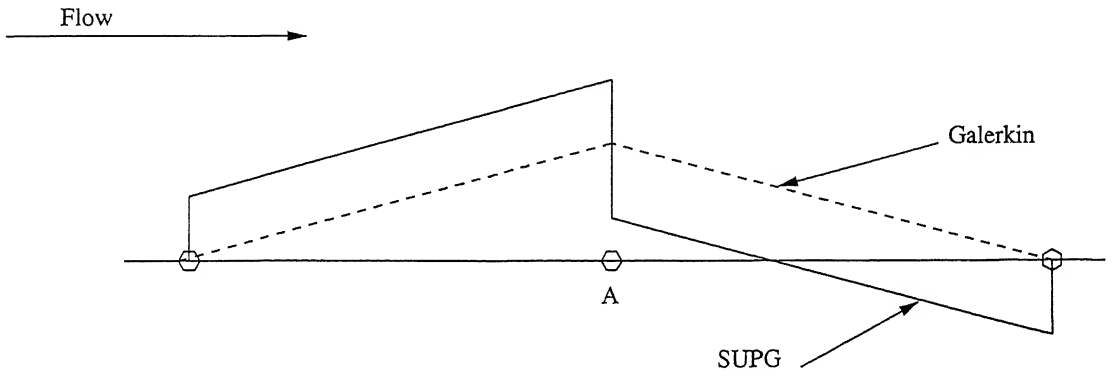

Figure 2.5: Comparison of Streamline Upwind/Petrov-Galerkin (SUPG) and Galerkin weighting functions for a node A

2.6 Implementation of the Finite Element Method

The final ingredient of the finite element method is the way in which the nodal equations are constructed. As seen in the example, the integration involved in the *weakformulation* leads to a sum of contributions on elements adjacent to the node which is treated. Instead of performing the integration on the set of elements adjacent to a node we could of course perform the integration on all elements separately and then afterwards construct the nodal equations by adding contributions from adjacent elements. This is called assembly. It has the advantage that the integration on all elements can be done in the same way and, as a consequence, with the same routine. For instance, for the equation (2.22), the integral in the left hand side, on an element Ω^e, is

$$\lambda \int_{\Omega^e} \frac{dw}{dx}\frac{d\hat{u}}{dx}\ dx = \lambda \int_{\Omega^e} [\frac{d\phi_1^e}{dx}\ w_1^e + \frac{d\phi_2^e}{dx}\ w_2^e]\ [\frac{d\phi_1^e}{dx}\ u_1^e + \frac{d\phi_2^e}{dx}\ u_2^e]\ dx$$

An element matrix K^e can be defined by

$$K_{ij}^e = \lambda \int_{\Omega^e} \frac{d\phi_i^e}{dx} \frac{d\phi_j^e}{dx} \, dx$$

The component of the system matrix in the global discrete system

$$K\,U = F \tag{2.37}$$

can now be found by adding components from the element matrices. The system matrix K is called *stiffness matrix*. In general problems, the computation of the element stiffness matrix and the element right hand side can not be performed analytically due to complexity of the integrand and due to the complexity of the element. In such cases it is generally advisable to go directly for an iterative technique.

Chapter 3

Lubrication in Tilted Pad Slider Bearings: Effect of Flux Boundary Conditions on the Pad[1]

3.1 Introduction

A tilted pad slider bearing consists of two surfaces (as shown in the Figure 3.1 separated by a lubricant film. One surface is stationary while the other moves with a uniform velocity. The direction of motion and the inclination of planes are such that a converging oil film is formed between the two surfaces and the physical wedge pressure generating mechanism is developed in the lubricant film. It is this pressure generating mechanism that enables the bearing to support a load. Several researchers have considered this basic geometry under various situations.

However, the parallel sliding has not been investigated so thoroughly. Parallel sliding of surfaces in the presence of a lubricant represents a common bearing configuration which can be found, in many engineering applications like Mechanical seals, Machine tool ways, Piston rings, Plain collar thrust bearings etc.

Several researchers like Fogg [36] , Osterle et al. [38], Lewicki [39], Cameron [43] ,

[1]Accepted for publication in the **"International Journal of Numerical Heat Transfer"**

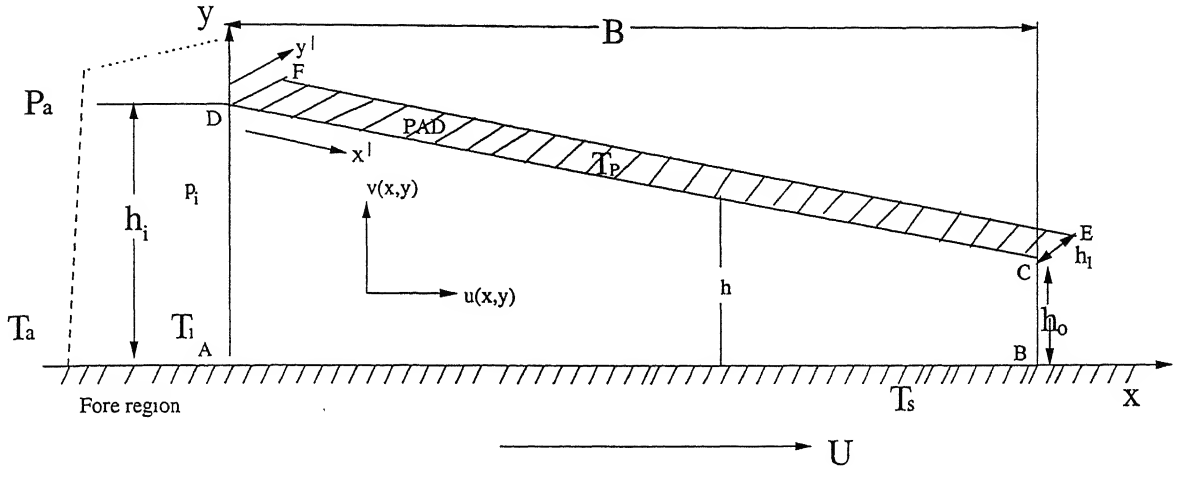

Figure 3.1: Geometry of the slider bearing

Young [69], Lebeck [47, 48] etc., have experimentally investigated the thermal influence on load carrying capacity of parallel slider bearings. Recently Rodkiewicz and Sinha [58] and Schumack [19] have numerically analyzed the problem of thermohydrodynamic lubrication with Dirichlet boundary prescription on the pad and slider. But the actual slider bearing configuration would require zero/nonzero flux boundary prescriptions. Gero and Ettles [18] has attempted the problem but his study was focussed on scheme development. Further he has dealt with either constant viscosity/density or linearized viscosity with constant density. The influence of thermal boosting, which amounts to considering slider, pad and inflow lubricant at different temperatures, on load carrying capacity, drag force etc of the lubricant in thermohydrodynamic slider bearing context has not been investigated.

So the aim of the study in this Chapter is to numerically investigate the influence of various temperature boundary prescriptions and thermal boosting on velocity distribution, temperature distribution, pressure distribution, load carrying capacity and frictional drag force in the lubricant film by analyzing the non-linear governing equations with temperature dependent viscosity and density at industrially significant (Rodkiewicz and Sinha [58], Gethin [17]) flow speeds and inlet pressures. For the numerical simulation of hydrodynamic lubrication problems Reddi [70] has proposed a variational principle based on Reynolds

Equation. Later Huebner [14] has shown the applicability of finite element method for thermohydrodynamic lubrication analysis based on variational principle for pressures, and Bubnov-Galerkin weighted residual approach for energy equation. He assumed the viscosity and density to be temperature dependent and obtained results considering high inlet pressures and high speeds. The scheme proposed by Huebner [14] suffer from well known node to node spurious oscillations. As we discussed in Chapter 2, Upwind strategies are known to preclude such oscillations in the solution. Brooks and Hughes [68] proposed SUPG Galerkin formulation for convection dominated flows with particular emphasis on the incompressible Navier-Stokes equations. SUPG Finite Element Method has been successfully used for thermal flow analysis by Grygiel and Tanguy [71] in advection diffusion problems. In the present Chapter the problem of thermohydrodynamic lubrication of slider bearing with temperature dependent density and viscosity which brings in extra pseudo compressibility terms into the energy equation has been successfully solved by using SUPGFEM. The results from the numerical simulations have been presented in computer generated plots and in Tables and the method has been validated for a hydrodynamic lubrication where analytical solution is available.

3.2 Governing Equations

The geometry and the coordinate system for a slider bearing analyzed in this Chapter is shown in Figure 3.1 Note that the dimensions are not shown to scale, the length of the bearing is typically of the 1000 times larger than the distance between the two surfaces. The basic assumptions for the lubrication flows are as follows.

- Pressure is invariant across the fluid film (in the y direction)
- Inertia forces are negligible
- Velocity gradients in all but the y direction are negligible
- The height of the fluid film y is very small compared to the span and length x. This

permits to ignore the curvature of the fluid film

- The flow is laminar., no vortex flow and no turbulence occur any where in the film.
- No external forces act on the film
- No slip at the bearing surfaces

In addition, the flow is assumed to be steady and laminar The Navier-Stokes equations thus reduce to

$$\frac{\partial p}{\partial x} = \frac{\partial}{\partial y}(\mu \frac{\partial u}{\partial y}) \tag{3.1}$$

and the continuity equation is

$$\frac{\partial}{\partial x}(\rho u) + \frac{\partial}{\partial y}(\rho v) = 0 \tag{3.2}$$

where, $\rho = \rho(T)$, $\mu = \mu(T)$. The boundary conditions are:

$$u = U \text{ and } v = 0 \text{ at } y = 0, \quad u = v = 0 \text{ at } y = h \tag{3.3}$$

Combining equations (3.1), (3.2) and applying the boundary conditions given in equation (3.3) leads to the steady Reynolds equation for the pressure distribution.

$$\frac{\partial}{\partial x}(\frac{h^3}{6\mu}\frac{\partial p}{\partial x}) = U\frac{\partial h}{\partial x} \tag{3.4}$$

The assumptions for the energy equation are as follows.

- Conduction terms other than those across the fluid film (in the y direction) are negligible.
- Thermal conductivity and specific heat are constant.

These assumptions combined with previous assumptions lead to the following form of the energy equation.

$$\rho\, c\ (u\frac{\partial T}{\partial x} + v\frac{\partial T}{\partial y}) = k\,\frac{\partial^2 T}{\partial y^2} + \mu\,(\frac{\partial u}{\partial y})^2 + u\,\frac{dp}{dx} \tag{3.5}$$

Viscosity and density are related to temperature via the following relationship.

$$\rho = \rho_a\,[1 - \lambda(T - T_a)], \qquad \mu = \mu_a\,\exp[-\beta(T - T_a)] \tag{3.6}$$

Now the following non dimensional variables (Schumack [19]) are introduced.

$$u^+ = \frac{u}{U}, \quad v^+ = \frac{vB}{Uh_o}, \quad x^+ = \frac{x}{B}, \quad y^+ = \frac{y}{h_o},$$

$$T^+ = \frac{T}{T_a} \quad \text{(subscript "a" indicates ambient condition)},$$

$$\mu^+ = \frac{\mu}{\mu_a}, \quad \rho^+ = \frac{\rho}{\rho_a}, \quad p^+ = \frac{ph_o^2}{\mu_a UB} \quad \text{(p is the gage pressure)},$$

$$p_i^+ = \frac{p_i h_o^2}{\mu_a UB}, \quad h_o^+ = \frac{h_o}{B}, \quad h^+ = \frac{h}{h_o}, \quad \beta^+ = \beta T_a,$$

$$\lambda^+ = \lambda T_a, \quad P_r E_c = \frac{\mu_a U^2}{kT_a}, \quad P_e = \frac{\rho_a U c h_o^2}{kB}.$$

With this non dimensionalization, the governing equations are rewritten as follows.

$$\frac{\partial}{\partial x^+}\left(\frac{h^{+3}}{6\mu^+}\frac{\partial p^+}{\partial x^+}\right) = \frac{\partial h^+}{\partial x^+} \tag{3.7}$$

with the boundary conditions

$$p^+ = p_i^+ \text{ at } x^+ = 0 \quad \text{and} \quad p^+ = 0 \text{ at } x^+ = 1 \tag{3.8}$$

and the corresponding energy equation in non dimensional form is as follows:

$$\rho^+ \left(u^+\frac{\partial T^+}{\partial x^+} + v^+\frac{\partial T^+}{\partial y^+}\right) = \frac{1}{P_e}\frac{\partial^2 T^+}{\partial y^{+2}} + \frac{P_r E_c}{P_e}\mu^+\left(\frac{\partial u^+}{\partial y^+}\right)^2 + \frac{P_r E_c}{P_e}u^+\frac{dp^+}{dx^+} \tag{3.9}$$

where ρ^+ and μ^+ are given by:

$$\rho^+ = 1 - \lambda^+(T^+ - 1), \quad \mu^+ = \exp[-\beta^+(T^+ - 1)] \tag{3.10}$$

In view of the various industrial applications, the energy equation has been solved under the following different temperature boundary conditions:

- Case1: Full Dirichlet model

  $T^+(x^+, 0) = T_s^+$, on slider,

  $T^+(x^+, h^+) = T_p^+$, on pad, where, $T_p^+ = T_s^+ = T_i^+$

- Case2: Zero half flux model

  $T^+(x^+, 0) = T_s^+$, on slider,

  $\frac{\partial T^+}{\partial \vec{n}}(x^+, h^+) = 0$, on pad (where $\vec{n}$ is the unit outward normal vector).

- Case3: Non zero half flux model

  $T^+(x^+, 0) = T_s^+$, on slider,

$\frac{\partial T^+}{\partial \vec{n}}(x^+, h^+) \neq 0$, on pad.

- Case4: Zero full flux model

  $\frac{\partial T^+}{\partial \vec{n}}(x^+, 0) = 0$, on slider,

  $\frac{\partial T^+}{\partial \vec{n}}(x^+, h^+) = 0$, on pad

- Case5: Thermal boosting model

  $T^+(x^+, 0) = T_s^+$, on slider,

  $T^+(x^+, h^+) = T_p^+$, on pad with,

  (a) $T_p^+ = T_s^+ > T_i^+$ (b) $T_p^+ > T_s^+ > T_i^+$ (c) $T_s^+ > T_p^+ > T_i^+$

  (d) $T_p^+ = T_s^+ < T_i^+$ (e) $T_p^+ > T_s^+ < T_i^+$ (f) $T_s^+ > T_p^+ < T_i^+$

Actually, the combination of T_p^+, T_s^+, T_i^+ which enhances the load carrying capacity of a slider bearing constitutes a thermal boosting model. At the inlet/outlet the following boundary conditions are used.

$T^+(0, y^+) = T_i^+$ at the inlet boundary and $\frac{\partial T^+}{\partial x^+}(1, y^+) = 0$ at the outlet boundary.

The load carrying capacity (W^+) and the frictional drag (F^+) have been determined from the following expressions.

$$W^+ = \int_0^1 p^+ \, dx^+ \tag{3.11}$$

$$F^+ = \int_0^1 (\mu^+ \frac{\partial u^+}{\partial y^+})_{\text{at } y^+=0} \, dx^+ \tag{3.12}$$

where, $W^+ = \frac{W}{\rho_a U^2 B}$ and $F^+ = \frac{F h_o}{\mu_a U B}$

3.3 Numerical Formulation of the Problem

3.3.1 Variational/Weak Formulation

Let Ω the domain of interest be bounded in R^2 with a piecewise smooth boundary Γ. Let (x^+, y^+) denote the vector of spatial coordinate of a generic point in $\bar{\Omega}$ and $\vec{n}$ is the outward unit normal vector drawn at any point (x^+, y^+) on Γ. Now the variational principle $\Pi(p)$ for the Reynolds equation (3.7) in Ω is derived as follows. Define the first variation in the integral

form:

$$\delta\Pi(p) = \int_\Omega \frac{\partial}{\partial x^+}[\frac{h^{+3}}{6\mu^+}\frac{\partial p^+}{\partial x^+} - h^+]\ \delta p^+ \tag{3.13}$$

And the stationary of $\Pi(p)$ with respect to variations in p among the set of functions satisfying the boundary conditions requires that

$$\int_\Omega \delta p^+ \frac{\partial}{\partial x^+}[\frac{h^{+3}}{6\mu^+}\frac{\partial p^+}{\partial x^+}]\ d\Omega - \int_\Omega \delta p^+ \frac{\partial h^+}{\partial x^+}\ d\Omega = 0 \tag{3.14}$$

Simplifying further

$$[\int_\Omega \frac{\partial}{\partial x^+}\{\delta p^+(\frac{h^{+3}}{6\mu^+}\frac{\partial p^+}{\partial x^+})\} - \int_\Omega \frac{h^{+3}}{6\mu^+}\frac{\partial p^+}{\partial x^+}\frac{\partial}{\partial x^+}(\delta p^+) - \int_\Omega \frac{\partial}{\partial x^+}(\delta p^+ h^+) + \int_\Omega h^+\frac{\partial}{\partial x^+}(\delta p^+)]\ d\Omega = 0$$

Now using the Green-Gauss identity and boundary conditions, the above equation leads to the following variational principle.

$$\Pi(p) = \int_\Omega [\frac{h^{+3}}{12\mu^+}(\frac{\partial p^+}{\partial x^+})^2 - h^+\frac{\partial p^+}{\partial x^+}]\ d\Omega \tag{3.15}$$

where, μ^+ and ρ^+ are defined in equation (3.10). The Bubnov-Galerkin weighted residual formulation of convection dominated flows are known to lead to spurious node to node oscillations in the solution. A similar situation has been encountered with the energy equation in the present study too. In this study to preclude such oscillations in the solution, the weighted residual formulation of the energy equation based on SUPG weight function is considered. The modified weighted residual formulation of the energy equation is given by:

$$\int_\Omega \tilde{W}_l[\rho^+(u^+\frac{\partial T^+}{\partial x^+} + v^+\frac{\partial T^+}{\partial y^+}) - \frac{1}{P_e}\frac{\partial^2 T^+}{\partial y^{+2}} - \frac{P_r E_c}{P_e}\mu^+(\frac{\partial u^+}{\partial y^+})^2 - \frac{P_r E_c}{P_e}u^+\frac{dp^+}{dx^+}]\ d\Omega = 0 \tag{3.16}$$

where, $\tilde{W}_l$ is the SUPG weight function. It is to be noted that ρ^+, μ^+ are dependent on T^+ and are given in equation (3.10)

3.3.2 Finite Element Formulation

The finite element discretization procedure reduces the lubrication problem to one of finite number of unknowns. This is accomplished by dividing the solution domain into bilinear rectangular elements and by expressing the field variables (pressure, velocities and tem-

perature) in terms of approximating trial functions (N_i) within each element. Now Ω is discretized into N_e bilinear rectangular elements such that:

$$\cup_{e=1}^{N_e} \bar{\Omega}^e = \bar{\Omega} \qquad \cap_{e=1}^{N_e} \bar{\Omega}^e = \phi \tag{3.17}$$

where, Ω^e denotes the interior domain of an element. Let Γ^e be the boundary of Ω^e. The discretized representation of the field variables are given by:

$$u_e^+ \approx \sum_{k=1}^{N_{el}} N_k u_k^{+^e}, \qquad v_e^+ \approx \sum_{k=1}^{N_{el}} N_k v_k^{+^e}, \qquad p_e^+ \approx \sum_{k=1}^{N_{el}} N_k p_k^{+^e}, \qquad T_e^+ \approx \sum_{k=1}^{N_{el}} N_k T_k^{+^e}. \tag{3.18}$$

where, $N_{el} = 2$ for pressure case and $N_{el} = 4$ for velocities and temperatures. On introducing these elemental discretization details into equation (3.15) and (3.16), we would obtain element level representations.

The element level representation of equation (3.15) is given by:

$$\int_{\Omega^e} \{\frac{h^{+3}}{12\mu^+}[\frac{\partial}{\partial x^+}(\sum_{j=1}^{N_{el}} p_j^{+^e} N_j^e)]^2 - h^+ \frac{\partial}{\partial x^+}(\sum_{j=1}^{N_{el}} p_j^{+^e} N_j^e)\}\ d\Omega^e = 0 \tag{3.19}$$

On minimizing the Reynolds equation (3.15) with respect to variables p_j^e, That is.

$$\frac{\partial \Pi(p)}{\partial p_i} = 0.$$

$$\frac{\partial \Pi(p)}{\partial p_i} = \frac{\partial}{\partial p_i} \{\int_\Omega \frac{h^{+3}}{\partial 12\mu^+} (\frac{\partial}{\partial x^+}(\sum_{j=1}^{n} p_j N_j))^2 - h^+ \frac{\partial}{\partial x^+}(\sum_{j=1}^{n} p_j N_j)\}\ d\Omega = 0$$

On further simplification, we arrive at the following equation:

$$\sum_{j=1}^{N_{el}} \int_{\Omega^e} [\frac{h^{+3}}{6\mu^+} \frac{\partial N_j^e}{\partial x^+} \frac{\partial N_i^e}{\partial x^+}]\ p_j^{+^e}\ d\Omega^e = \int_{\Omega^e} h^+ \frac{\partial N_i^e}{\partial x^+}\ d\Omega^e \tag{3.20}$$

$i = 1, 2, 3, \cdots, N_{el}$. On expanding the above equation and $N_{el} = 2$ for nodal pressures, we get the following elemental matrix equation.

$$\begin{bmatrix} \int_{\Omega^e} \frac{h^+}{6\mu^+} \frac{\partial N_1}{\partial x^+} \frac{\partial N_1}{\partial x^+}\ d\Omega^e & \int_{\Omega^e} \frac{h^+}{6\mu^+} \frac{\partial N_1}{\partial x^+} \frac{\partial N_2}{\partial x^+}\ d\Omega^e \\ \int_{\Omega^e} \frac{h^+}{6\mu^+} \frac{\partial N_2}{\partial x^+} \frac{\partial N_1}{\partial x^+}\ d\Omega^e & \int_{\Omega^e} \frac{h^+}{6\mu^+} \frac{\partial N_2}{\partial x^+} \frac{\partial N_2}{\partial x^+}\ d\Omega^e \end{bmatrix} \begin{bmatrix} p1 \\ p2 \end{bmatrix} = \begin{bmatrix} \int_{\Omega^e} h^+ \frac{\partial N_1}{\partial x^+}\ d\Omega^e \\ \int_{\Omega^e} h^+ \frac{\partial N_2}{\partial x^+}\ d\Omega^e \end{bmatrix} \tag{3.21}$$

To evaluate the integrals in the above matrix equation (3.21), we have used, Simpson's $\frac{1}{3}^{rd}$ rule. Thus, solving the system of matrix algebraic equations using the well known Gaussian elimination scheme we obtain the nodal pressures. In the iteration process for the

first iteration μ^+ is a constant. But in the subsequent iteration onwards it is a function of temperature defined by the relation given in the equation (3.10). Since the bearing solids are assumed to be rigid and the lubricant thermal effects are to be incorporated, it is essential that the bearing analyst must take into account viscous heating in the lubricant film and the resulting changes in lubricant viscosity. Such kind of analysis must include not only the generalized Reynolds equation, but also the conservation equation of thermal energy. The Reynolds and the energy equation must be solved simultaneously using SUPG finite element method.

Now with the SUPG analysis of Brooks and Hughes [68] and Grygiel and Tanguy [71] one obtains the following simplified discretized elemental energy equation:

$$\sum_j \int_{\Omega^e} \{ \tilde{W} \, (1 - \lambda^+ \, (\sum_k N_k^e T_k^{+^e} - 1)) \; [\, (\sum_k u_k^{+^e} N_k^e) \, \frac{\partial N_j^e}{\partial x^+} \; + \; (\sum_k v_k^{+^e} N_k^e) \, \frac{\partial N_j^e}{\partial y^+} \,]$$

$$+ \; \frac{1}{P_e} (\, \frac{\partial w_i}{\partial y^+} \, \frac{\partial N_j^e}{\partial y^+}) \} \; T_j^{+^e} \; d\Omega^e = \int_{\Omega^e} \tilde{W} [\, \frac{P_r E_c}{P_e} (\exp(-\beta^+ (\sum_k N_k^e T_k^{+^e} - 1))) \, (\frac{\partial}{\partial y^+} (\sum_k N_k^e u_k^{+^e}))^2$$

$$- \, (\sum_k N_k^e u_k^{+^e}) \, (\frac{d}{dx^+} (\sum_k N_k^e p_k^{+^e}))] \; d\Omega^e \qquad (3.2$$

With $\tilde{W} = w_i + P_i$ and $w_i = N_i \quad P_i = \frac{\tilde{k} \hat{u_j} w_{i,j}}{\|u\|}$. The upwind parameter $\hat{k}$ is calculated using elemental dimensions and elemental velocity (Grygiel and Tanguy [71], Brooks and Hughes [68]).

3.3.3 SUPG Algorithm for Energy Equation

Brooks and Hughes [68] SUPG algorithm has been incorporated for the present investigation.

- **step1**: Calculate (u^+, v^+) at the element center.
- **step2**: Calculate e_ξ, e_η (unit vectors)
- **step3**: Calculate u_ξ, v_η where $u_\xi = \bar{e}_\xi . \bar{u}$, $v_\eta = \bar{e}_\eta . \bar{v}$
- **step4**: Calculate h_ξ, h_η (elemental characteristic lengths)
- **step5**: Calculate α_ξ, α_η where $\alpha_\xi = \frac{u_\xi h_\xi}{2k}$, $\alpha_\eta = \frac{u_\eta h_\eta}{2k}$

- **step6:** Calculate $\tilde{\xi}$, $\tilde{\eta}$ where $\tilde{\xi} = (\text{Coth } \alpha_\xi) - \frac{1}{\alpha_\xi}$ and $\tilde{\eta} = (\text{Coth } \alpha_\xi) - \frac{1}{\alpha_\eta}$
- **step7:** Calculate $\tilde{k}$ where $\tilde{k} = \frac{(\tilde{\xi} u_\xi h_\xi + \tilde{\eta} u_\eta h_\eta)}{2}$
- **step8:** Calculate P_i where $P_i = \tilde{k}(\frac{\hat{u}_1}{\|u\|} w_{i,1} + \frac{\hat{u}_2}{\|u\|} w_{i,2})$ and $\|u\| = u^2 + v^2$ (sum).

Now based on equations (3.21), (3.22) the numerical simulations have been carried out on a 30×30 finite element mesh as shown in the Figure 3.2. The results have been obtained to an accuracy of $\epsilon = 5.0 \times 10^{-4}$ i.e.

$$\{\max \left(\frac{| \gamma_j^{New} - \gamma_j^{Old} |}{| \gamma_j^{New} |} \right)\} \leq \epsilon$$

for $j = 1, 2, \cdots, \text{n}, \cdots$

where γ_j represents any of the field variables p_j^+, u_j^+, v_j^+, T_j^+.

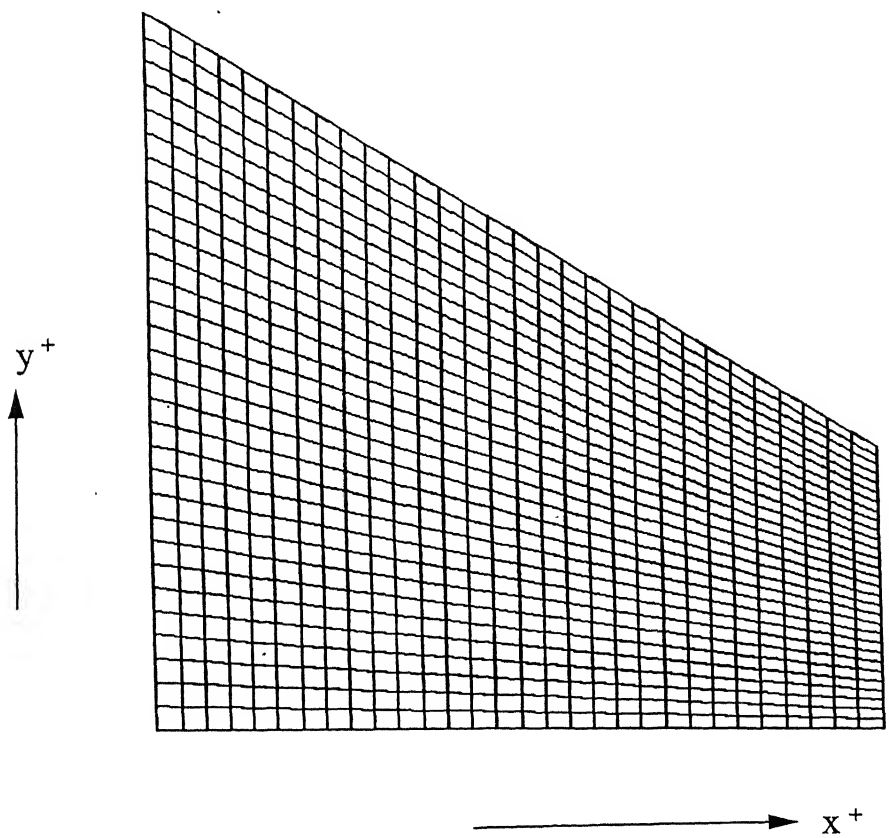

Figure 3.2: Domain discretization for 30×30 mesh system

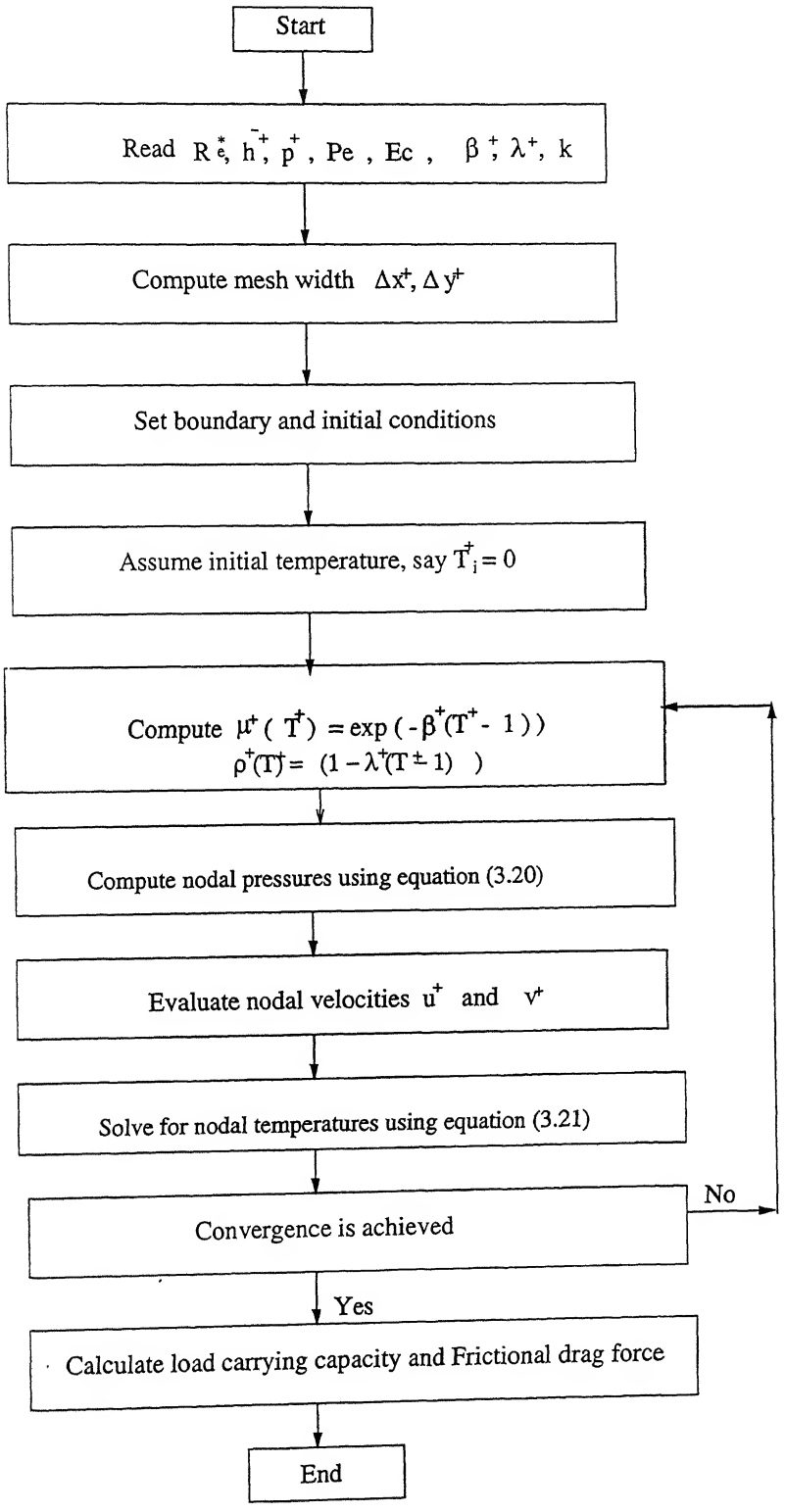

Figure 3.3: Flow chart for solution methodology

3.4 Results and Discussion

The bearing characteristics in the present study appear as functions of λ^+, β^+, k and dimensionless parameters P_r, P_e, E_c . For the present investigation, the value of these parameters are chosen in accordance with Lebeck [47, 48] and are as follows.

U = 20 m/s, h_i = 0.00005 m, B = 0.1 m, c = 1926 j/kg K, T_a = 310 K, ρ_a = 897.1 kg/m^3, μ_a = 0.0174 Pa.s, β = 0.035/K, λ = 0.0012/K. The simulations have been carried out for various values of k, p_i^+, β^+ and with the fixed values for the parameters P_r (Prandtl number),E_c (Eckert number) and P_e (Peclet number). The results have been analyzed for load carrying capacity, drag force and velocity, pressure, temperature fields and are presented in the form of computer generated plots and Tables. To ensure the grid independence of the results, the numerical simulations were carried out on different mesh systems consisting of $10 \times 10, 20 \times 20, 30 \times 30$ and 40×40 bilinear rectangular elements. The results for load carrying capacity for different mesh systems are shown in Figure 3.4.

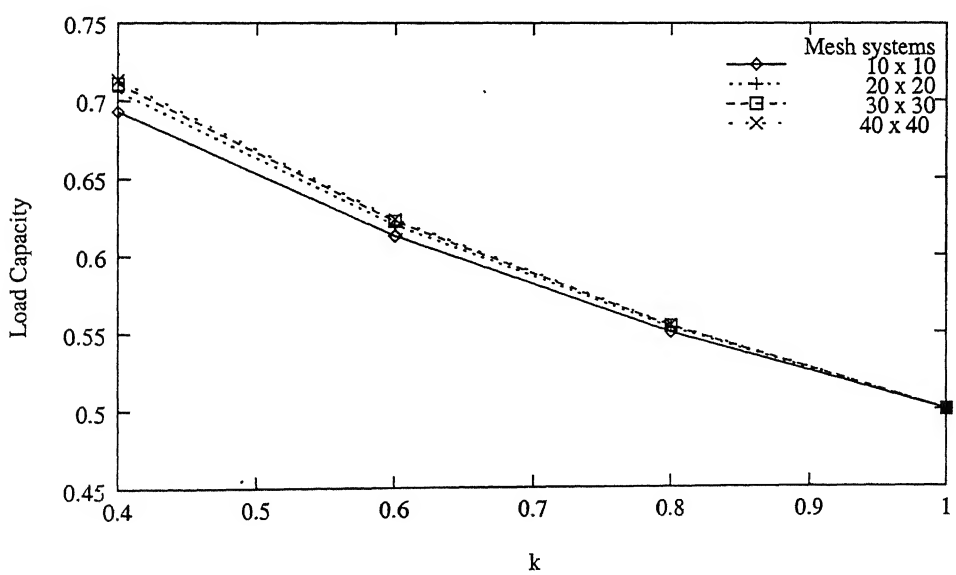

Figure 3.4: Load carrying capacity on different mesh systems

From the Figure 3.4, it can be easily concluded that the 30×30 mesh system yields a grid independent solution. Further the results have also been validated by comparing the

load carrying capacity with the analytical solution for the hydrodynamic lubrication. These comparisons are given in the Figure 3.5 for various inclinations of the slider bearing, i.e. with $k = 0.4, 0.6, 0.8, 1.0$ and at $p_i^+ = 1, 10, 50$. Here "analy" stands for analytical solution and "nume" stands for numerical solution.

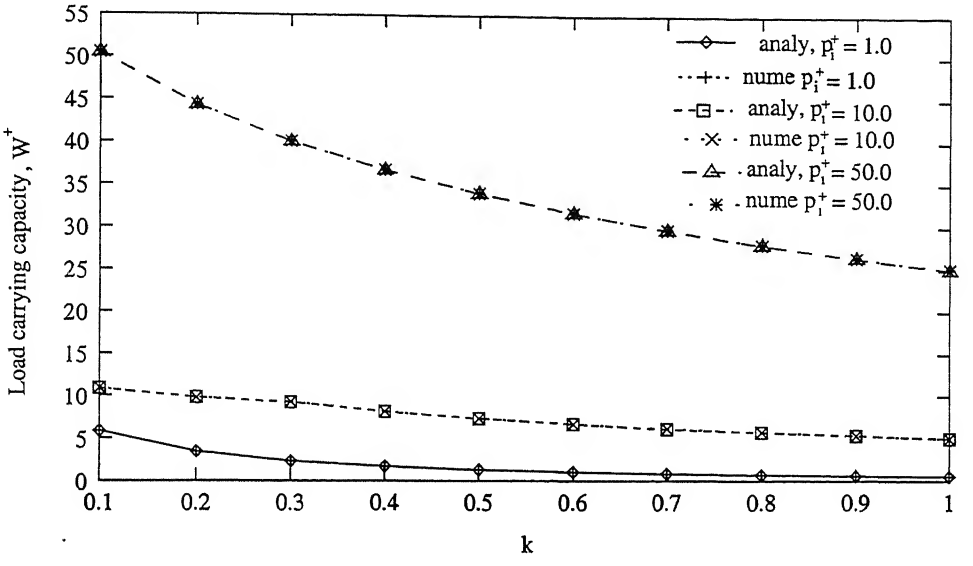

Figure 3.5: Comparison of analytical and numerical load carrying capacity

The dimensionless pressures at different locations in the sliding direction with $k = 0.4$ at different inlet pressures have been shown in Figure 3.6. Also for the cases $k = 0.8$, $k = 1$ the non dimensional pressures in the direction of the sliding for values of $p_i^+ = 1, 2, 5, 8$ have been plotted and are shown in Figures 3.7 and 3.8.

It is clearly seen from the Figures 3.6, 3.7 and 3.8 that for a fixed value of x^+, as the inlet pressure is raised the fluid pressure becomes higher. As a consequence the load carrying capacity is expected to be higher when the inlet pressure is higher for all values of k.

From Table 3.1, it can be seen that consideration of non-zero inlet pressure leads to increased load carrying capacity. Further with Reynolds equation for pressure and temperature dependent viscosity, different flux boundary conditions do not alter the load carrying capacity of slider bearings with fixed values of k (inclination of the pad) and p_i^+ (inlet pressure) significantly.

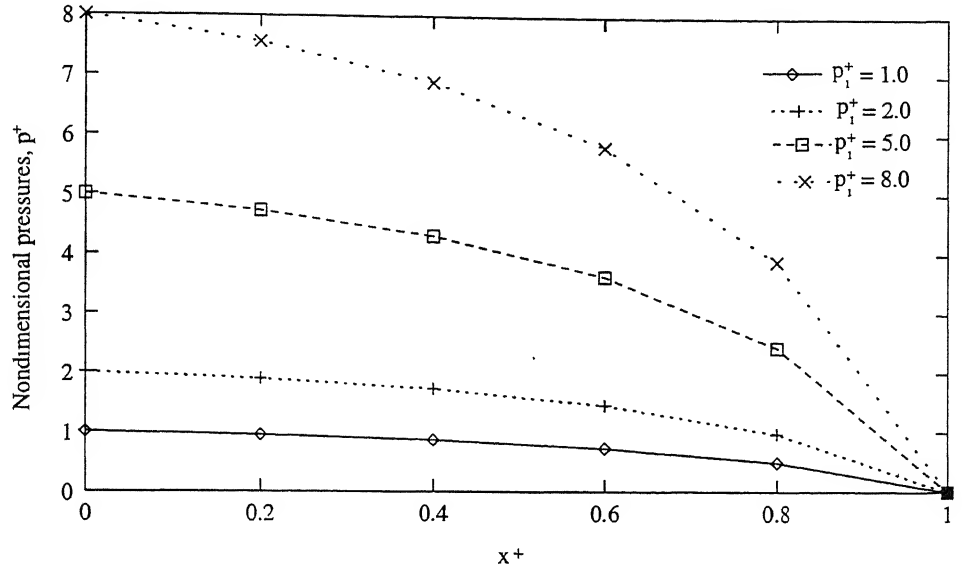

Figure 3.6: Pressure distribution for the case $k = 0.4$

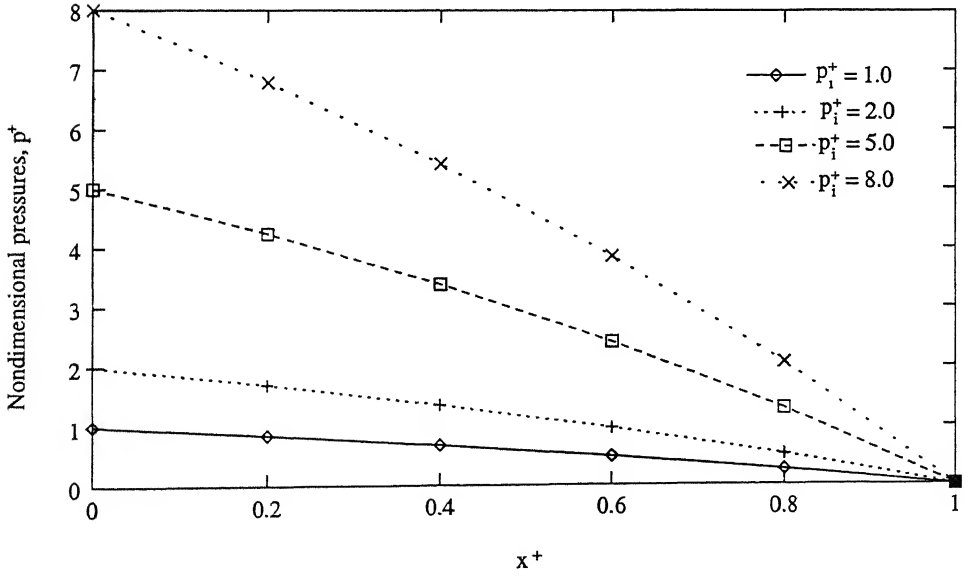

Figure 3.7: Pressure distribution for the case $k = 0.8$

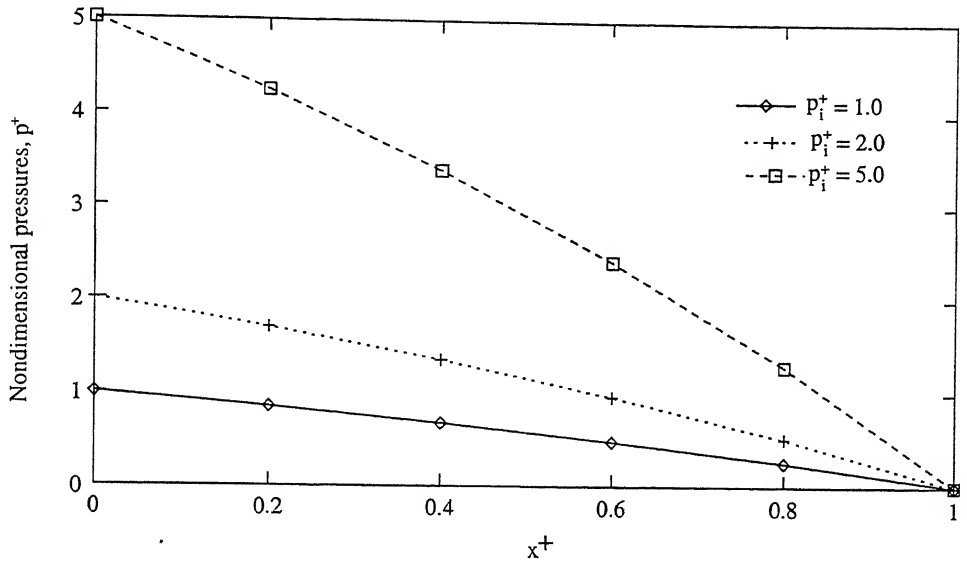

Figure 3.8: Pressure distribution for the case $k = 1$

Table 3.1: Comparison of load carrying capacity with k for different flux boundary conditions at: $T_i^+ = T_p^+ = T_s^+ = 1.5$

k	0.4	0.6	0.8	1.0
with $p_i^+ = 0$				
W^+(no flux)	0.0003886	0.00016031	0.00005461	0.000005785
W^+(half flux)	0.0003887	0.00016041	0.00005428	0.000005784
W^+(full flux)	0.0003881	0.00016031	0.00005405	0.000005651
with $p_i^+ = 1$				
W^+(no flux)	0.7108	0.6224	0.55424	0.5000002
W^+(half flux)	0.7104	0.6239	0.554245	0.5000002
W^+(full flux)	0.71047	0.623939	0.5542461	0.5000002
with $p_i^+ = 5$				
W^+(no flux)	3.5387	3.1056	2.76905	2.4999
W^+(half flux)	3.5385	3.1055	2.7689	2.4999
W^+(full flux)	3.53857	3.10554	2.76898	2.4999

In Figure 3.9 pressure generated along the pad for $k = 0.6,\ 0.4$ at inlet pressure $p_i^+ = 0$ have been plotted.

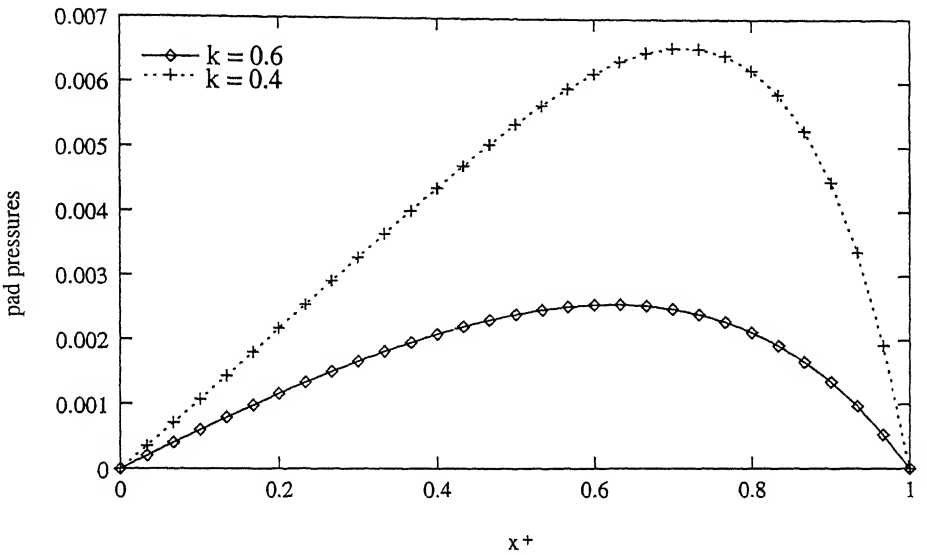

Figure 3.9: Pad pressures at $p_i^+ = 0$

In both the cases the peak pad pressures are noticed closer to the outlet. The quantitative behavior is in conformity with the existing results for a slider bearing. It is also further observed from these Figures 3.6 - 3.8 that the pressure profiles are nonlinear for $k = 0.4$ and $k = 0.8$, whereas for $k = 1$, they are almost linear, indicating that no appreciable fluid pressure is generated for parallel slider bearing. From Table 3.2, It is observed that, lubri-

Table 3.2: Effect of β^+ on load carrying capacity at different inlet pressures

β^+	10.0	8.0	6.0	4.0	2.0	0.0
$p_i^+ = 0$						
W^+	0.0003886	0.0011669	0.0035013	0.1049528	0.31444689	0.95129
$p_i^+ = 1$						
W^+	0.71086720	0.718673	0.7420864	0.8123493	1.022427	1.658269
$p_i^+ = 5$						
W^+	3.5387	3.546638	3.570199	3.641908	3.85248	4.486161

cants with low values of viscosity coefficient (β^+) enhance the load carrying capacity of a slider bearing irrespective of the inlet pressure. According to equation (3.10), decreasing β^+ (with fixed T^+) increases the viscosity of lubricant. Lubricants with high viscosity has higher thresholds for thermal deformation and hence are associated with larger load carrying capacity.

In Figure 3.10 drag force in the sliding direction for different values of k at different inlet pressures ranging from $p_i^+ = 0$ to 8 along the slider have been drawn. From this Figure, one can conclude that as k increases the drag force continuously increases for a fixed inlet pressure (Pinkus [31]).

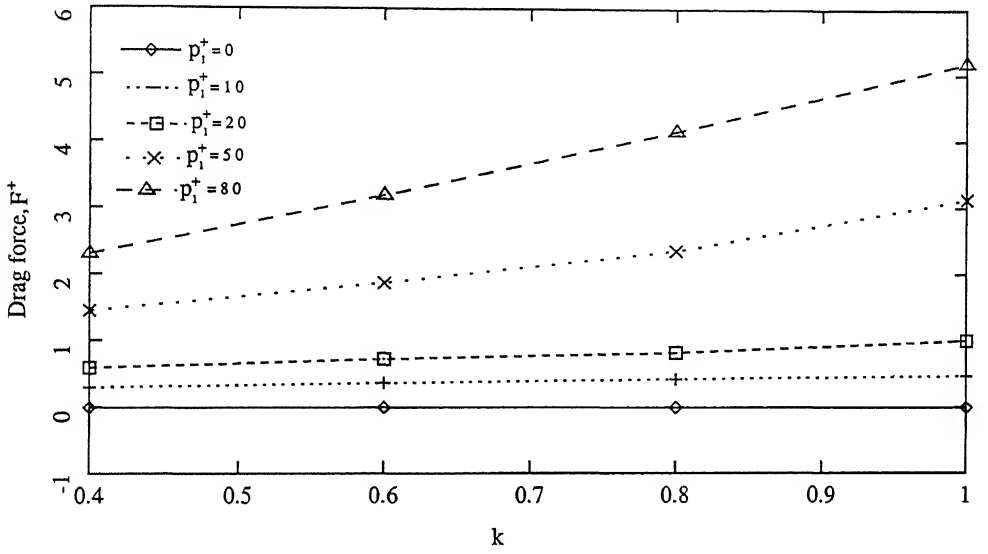

Figure 3.10: Variation of drag force with k at different inlet pressures

Temperatures along the pad with different boundary conditions have been plotted and are shown in Figure 3.11 One can observe that the full flux pad temperatures are higher than the corresponding half flux pad temperatures everywhere slightly away from the outlet. More prominently, one can notice the existence of thermal boundary layer near the inlet in both the cases. In Table 3.3, load carrying capacity for the cases corresponding to no flux and half flux models have been presented. Here the no flux model has been analyzed by fixing $T_s^+ = T_p^+ = 1.5$, $T_i^+ = 1$, and $p_i^+ = 1$ for varying values of k. And the half flux

model has been analyzed by fixing $\frac{\partial T_p^+}{\partial \bar{n}} = 0.2$, $T_s^+ = 1.5$, $T_i^+ = 1$ and $p_i^+ = 1$ for different values of k.

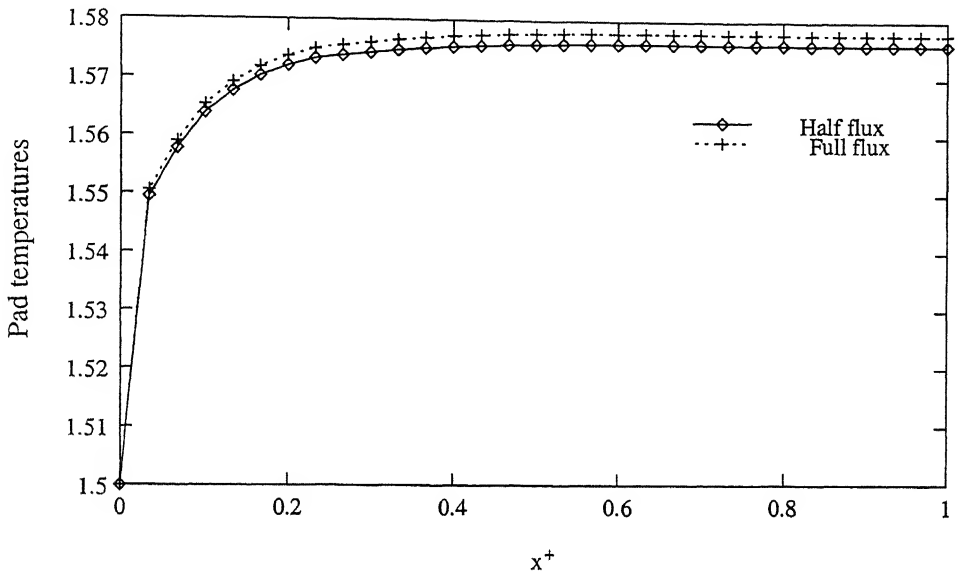

Figure 3.11: Pad temperatures at different flux boundary conditions for the case $k = 0.4, p_i^+ = 1$

In Table 3.3, load carrying capacity corresponding to above two cases with $T_i^+ = 1.5$ and $\frac{\partial T_p^+}{\partial \bar{n}} = 0.0$ have been presented. From these one can notice that both the models corresponding to Table 3.3 thermally boost the load carrying capacity of the slider bearing with the non zero half flux model having an upper hand.

Table 3.3: Effect of non zero flux boundary conditions on load carrying capacity at: $T_i^+ = 1.0$, $T_p^+ = T_s^+ = 1.5$, $p_i^+ = 1.0$

k	0.4	0.6	0.8	1.0
$W^+(no\ \ flux)$	0.7152418	0.6274425	0.5569304	0.500002
$W^+(\text{flux} = 0.2)$	0.7301611	0.6446275	0.5657586	0.500002

The increase in load carrying capacity brought in models corresponding to Table 3.3 is due to increase in the viscosity of the lubricant. From equation (3.10), one can see that an increase in $\mu^+(T^+)$ may be possible by either decreasing β^+ or T_i^+. Here as β^+ is fixed, the increase in $\mu^+(T^+)$ should be due to decrease in T^+. And this is precisely the case as the

averaged T^+ of the lubricant from the calculations turn out to be around 1.2. But in the simulations corresponding to Table 3.1, the average T^+ turns out to be 1.5.

The study of the effect of considering slider and pad at different temperatures ($T_s^+ > T_p^+$ or $T_p^+ > T_s^+$) on load carrying capacity and frictional drag force of a slider bearing is of high practical relevance (ref. Pinkus [31], page 101). Zienkiewicz [42] in his investigation considered slider and pad at different temperatures and analytically investigated the issue of load carrying capacity with a linear model. As his focus was on parallel slider bearing, he has fixed $k = 1$ and $p_i^+ = 0$. His studies reveal that if pad temperature (T_p^+) is greater than the slider temperature (T_s^+), then a suctional effect, which may lead to a drastic fall in load carrying capacity and hence a collapse in bearing is possible. In reality, the stationary surface (pad) is usually hotter than the moving surface (slider) (ref: Pinkus [31]), so in this investigation the following two models have been analyzed: (a) $T_s^+ = T_i^+ = 1.5$ and $T_p^+ = 1.7$ (b) $T_p^+ = T_i^+ = 1.5$ and $T_s^+ = 1.7$ with $p_i^+ = 1.0$ and $0.4 \leq k \leq 1.0$. The load carrying capacity corresponding to these two models are presented in Tables 3.4 and 3.5.

Table 3.4: Comparison of load carrying capacity and drag force for slider and pad setting at: $T_i^+ = 1.5$, $T_p^+ = 1.7$, $T_s^+ = 1.5, p_i^+ = 1$

k	0.4	0.6	0.8	1.0
W^+	0.7097811	0.6216089	0.5546017	0.500002
F^+	0.2908928	0.3604844	0.4168325	0.4692305

Table 3.5: Comparison of load carrying capacity and drag force for slider and pad setting at: $T_i^+ = 1.5$, $T_p^+ = 1.5$, $T_s^+ = 1.7, p_i^+ = 1$

k	0.4	0.6	0.8	1.0
W^+	0.7097811	0.6219599	0.5541165	0.500002
F^+	0.22216296	0.2711326	0.2776720	0.3321671

Interestingly, when $p_i^+ = 1.0$, both the models are associated with almost same load carrying capacity for $0.4 \leq k \leq 1.0$. However the frictional drag associated with the model(a), are higher than those associated with model(b).

Another important slider bearing case is, considering inlet lubricant temperature to be higher than that of both the pad and slider temperatures. Only two test cases are considered. (a) $T_i^+ = 1.5,\ T_p^+ = 1.2,\ T_s^+ = 1.4$ and (b) $T_i^+ = 1.5,\ T_p^+ = 1.4,\ T_s^+ = 1.2$. These results are presented in Tables 3.6 and 3.7.

Table 3.6: Variation of load carrying capacity for the setting at: $T_i^+ = 1.5,\ p_i^+ = 1.0$

k	0.4	0.6	0.8	1.0
$T_p^+ = 1.2,\ T_s^+ = 1.4$ W^+	0.7217854	0.6260851	0.5550337	0.5000006
$T_p^+ = 1.4,\ T_s^+ = 1.4$ W^+	0.7198654	0.6243347	0.5546634	0.5000005

Table 3.7: Influence of non zero flux boundary condition on load carrying capacity for the setting at: $T_i^+ = 1.5,\quad p_i^+ = 1.0$ with flux $= 0.2$

k	0.4	0.6	0.8	1.0
$T_s^+ = 1.4$ W^+	0.7219934	0.6263183	0.5552484	0.5000004
$T_s^+ = 1.2$ W^+	0.7165319	0.6245772	0.5548232	0.4999996

It is observed from Tables 3.6 and 3.7 (with non zero flux) when the slider is at a higher temperature as compared to the pad temperature, the load carrying capacity is higher for all values of k. Similar result were observed in Tables 3.4 and 3.5. However the cooling of the pad and slider (i.e. $T_s^+ < T_i^+$ and $T_p^+ < T_i^+$) yields a higher load as compared to the case when $T_s^+ > T_i^+$ and $T_p^+ > T_i^+$.

Other important case is when the inlet lubricant temperature is lower than that of both the slider as well as the pad temperature. In this investigation, the following test cases have been analyzed (a) $T_i^+ = 1.0,\ T_p^+ = 1.2,\ T_s^+ = 1.5$ (b) $T_i^+ = 1.0,\ T_s^+ = 1.2,\ T_p^+ = 1.5$ and (c) $T_i^+ = 1.5,\ T_s^+ = T_p^+ = 1.5$. The load carrying capacity associated with these models for $0.4 \leq k \leq 1.0$ and $p_i^+ = 1.0$ have been computed and compared in Figure 3.12.

The calculated average temperatures of the lubricant with above three models is in the

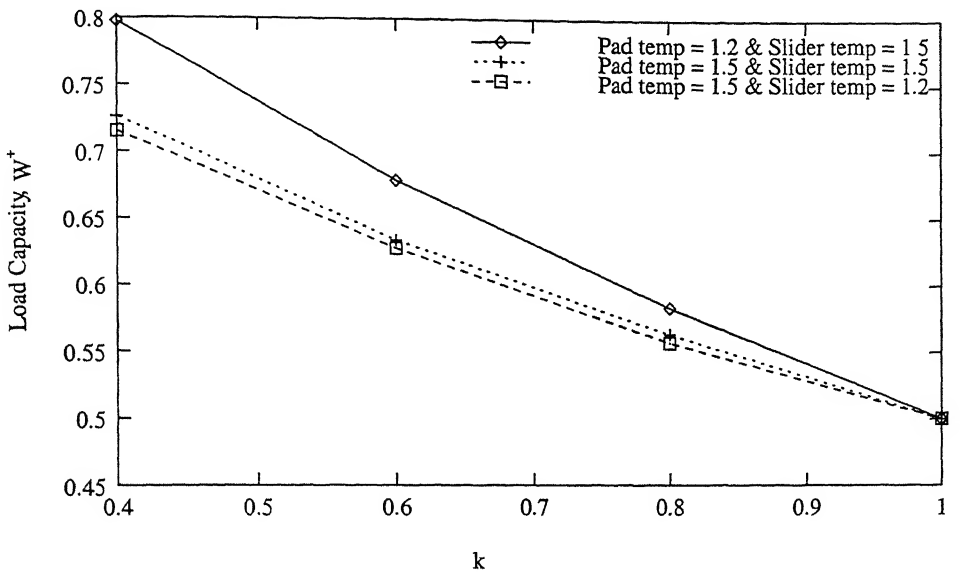

Figure 3.12: Effect of load carrying capacity with k for different slider/pad temperatures at $p_i^+ = 1$

order: $1.0 < T_a^{ave} < T_c^{ave} < T_b^{ave} < 1.5$ which leads to a reverse order in viscosities $\mu^+(T^+)$. This justifies the order of the load carrying capacity as seen in Figure 3.12.

To further understand the effect of zero/nonzero flux boundary conditions on load carrying capacity, simulations have been carried out with $p_i^+ = 1$, $T_s^+ = 1.5$, $T_i^+ = 1$, $\frac{\partial T_p^+}{\partial \vec{n}} = 0, -2.0, 0.2$ and the corresponding results are presented in Table 3.8 and Figure 3.13.

Table 3.8: Effect of non zero flux boundary conditions on load carrying capacity at: $T_i^+ = 1.0$, $T_s^+ = 1.5, p_i^+ = 1$

k	0.4	0.6	0.8
non zero flux = 0.2 W^+	0.7301611	0.6446275	0.567586
non zero flux = -0.2 W^+	0.7467269	0.6854924	0.6181974

From the plots in Figure 3.13 one may notice that the pad temperatures, at any flux namely, positive (influx), zero (adiabatic), and negative (out flux) boundary prescriptions are in the decreasing order of magnitude. Also a boundary layer is noticed near the inlet boundary. The load carrying capacity in Table 3.8 indicate that the out flux boundary

prescription , of the order of - 0.2, with $T_i^+ < T_s^+$ will enhance the load carrying capacity in the lubricant and hence constitutes a thermal boosting model. This happens because the pad temperatures, as shown in Figure 3.13 are linear and hence the viscosity will be higher.

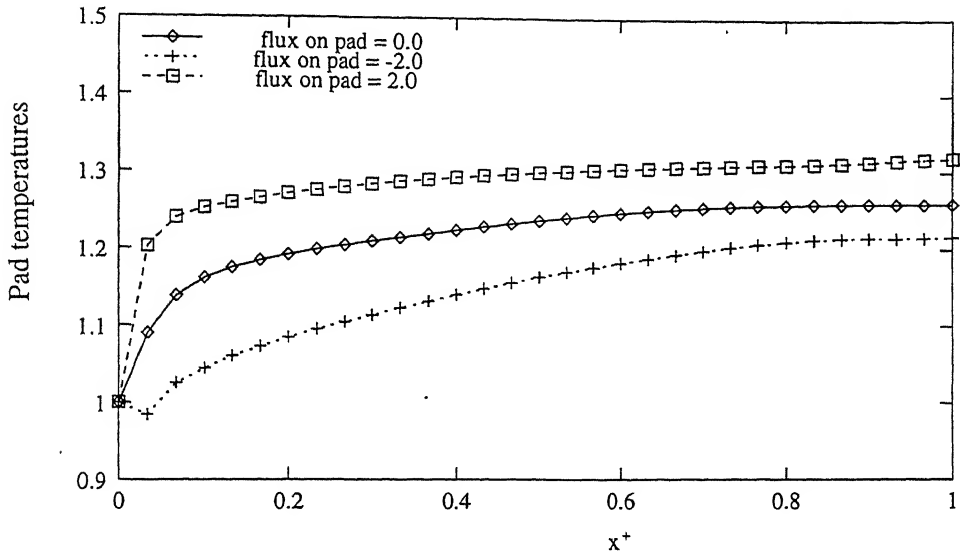

Figure 3.13: Effect of flux boundary conditions on pad temperatures at k = 0.4 and $p_i^+ = 1$

For $k = 0.4$, the streamline pattern corresponding to the inlet pressures $p_i^+ =$ 0, 1, and 5 are presented in Figure 3.14. From these patterns one can see that the laminarity of the lubricant flow is fully lost as the inlet pressure is raised from 0 to 5. The circular streamline pattern is observed at $p_i^+ = 1$ can be directly attributed to the bolus like effect caused by the higher gage pressure of the order $10^8 N/m^2$. As the inlet pressure is further raised to 5, a bolus like effect with turbulent looking pattern manifests in the lubricant flow domain.

Streamlines corresponding to the cases (a) $T_i^+ = 1.2$, $T_p^+ = 1.4$, $T_s^+ = 1.0$, $k = 0.4$ and $p_i^+ = 1$ (b) $T_i^+ = 1.2$, $T_p^+ = 1.0$, $T_s^+ = 1.4$, $k = 0.4$ and $p_i^+ = 1$ are shown in Figure 3.15. The flow is clearly nonlinear with a bolus like pattern close to either pad or slider, on the converging part of the domain, depending on whether $T_p^+ \geq T_i^+$ or $T_s^+ \leq T_i^+$. These features in (Figure 3.15) the flow pattern can be attributed to the combined effect of

thermal boosting and high gage pressure.

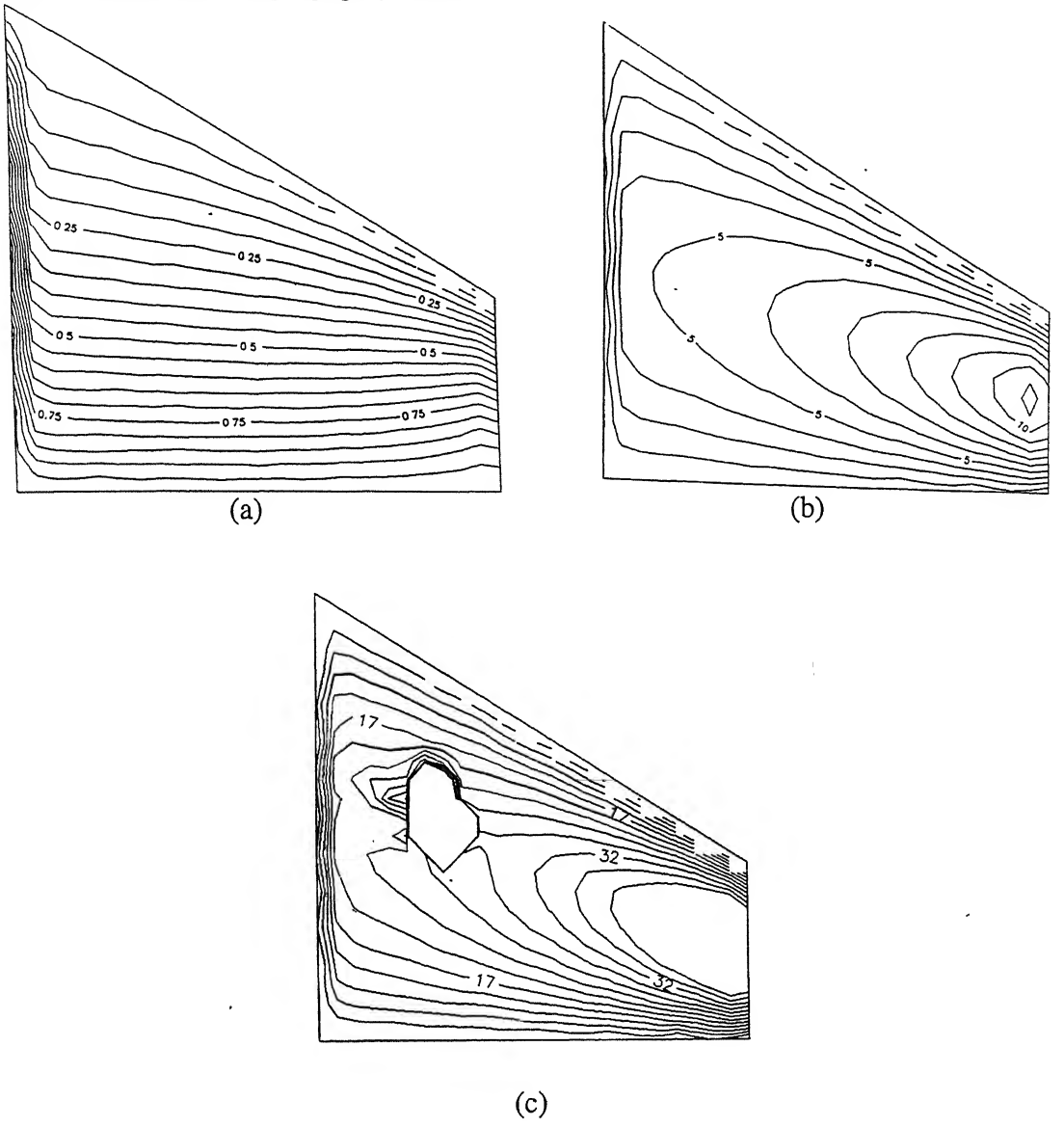

Figure 3.14: Constant u-velocities at k = 0.4 for (a) $p_i^+ = 0$ (b) $p_i^+ = 1$ (c) $p_i^+ = 5$

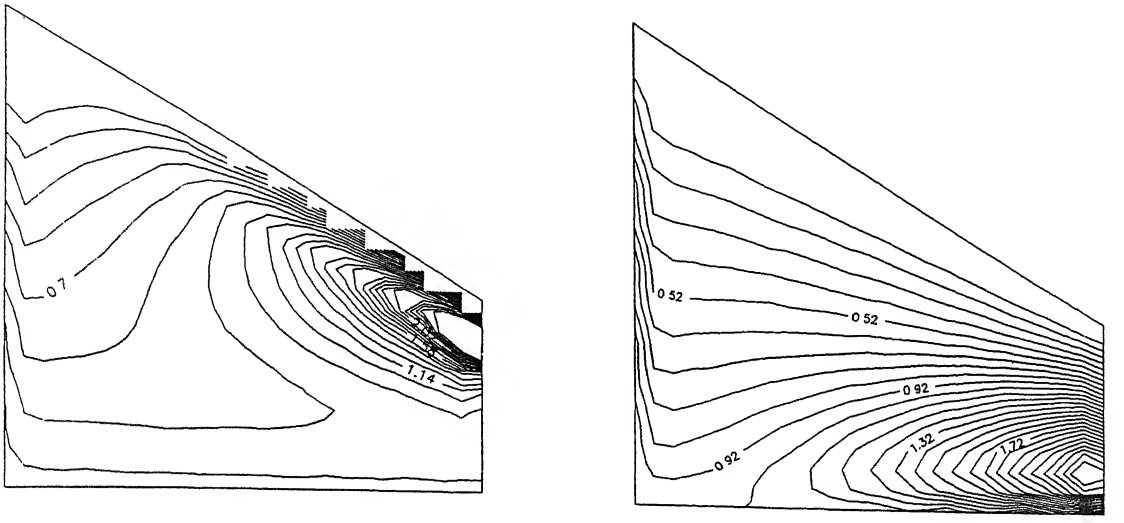

(a) (b)

Figure 3.15: Constant u-velocities for $k = 0.4$, $p_i^+ = 1$, $T_i^+ = 1.2$ (a) $T_p^+ = 1.4$, $T_s^+ = 1$ (b) $T_p^+ = 1.0$, $T_s^+ = 1.4$

To get a better understanding of the thermal characteristics of the lubricant, the isotherms corresponding to the above two cases are presented in Figure 3.16. Presence of the thermal boundary layers on the inlet starting from pad and slider, support the observation corresponding to the temperature distribution on the pad. These boundary layers are attributed to the difference in the inflow temperature (T_i^+) from that of the pad/slider temperatures.

In Figure 3.17 streamlines and in Figure 3.18 isotherms corresponding to models with unequal slider, pad temperatures for $k = 1$ (parallel slider bearing) are presented. Again as in the tilted pad case one may observe nonlinear and bolus like flow pattern in streamlines and boundary layer features in isotherms. One may also observe that the change in slider geometry also has its share of influence on the streamline and isotherm pattern.

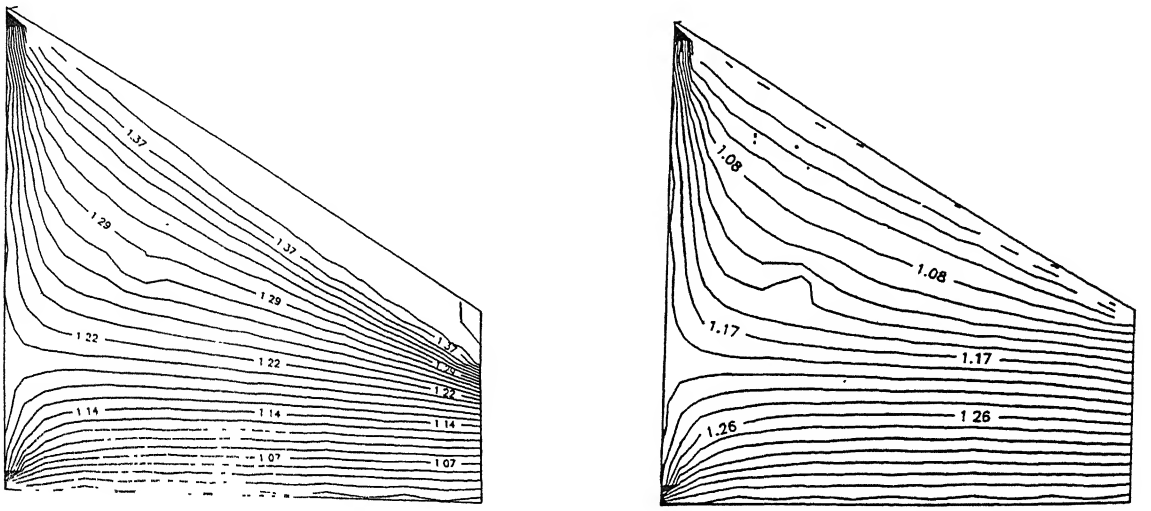

(a) (b)

Figure 3.16: Temperature contours for $k = 0.4$, $p_i^+ = 1$, $T_i^+ = 1.2$ (a) $T_p^+ = 1.4$, $T_s^+ = 1.0$ (b) $T_p^+ = 1.0$, $T_s^+ = 1.4$

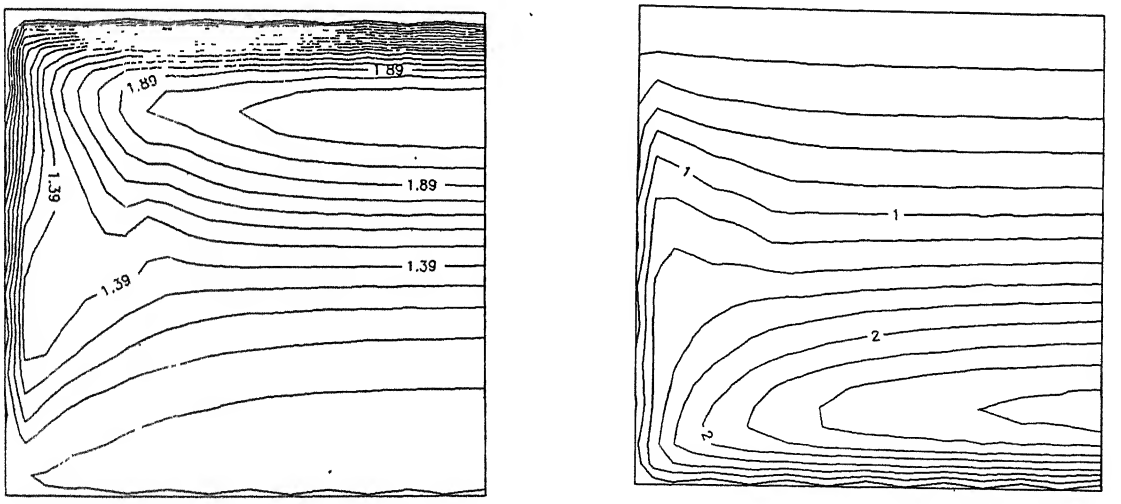

(a) (b)

Figure 3.17: Constant u-velocity contours at $k = 1, p_i^+ = 1$, $T_i^+ = 1.2$ (a) $T_p^+ = 1.4$, $T_s^+ = 1.0$ (b) $T_p^+ = 1.0$, $T_s^+ = 1.4$

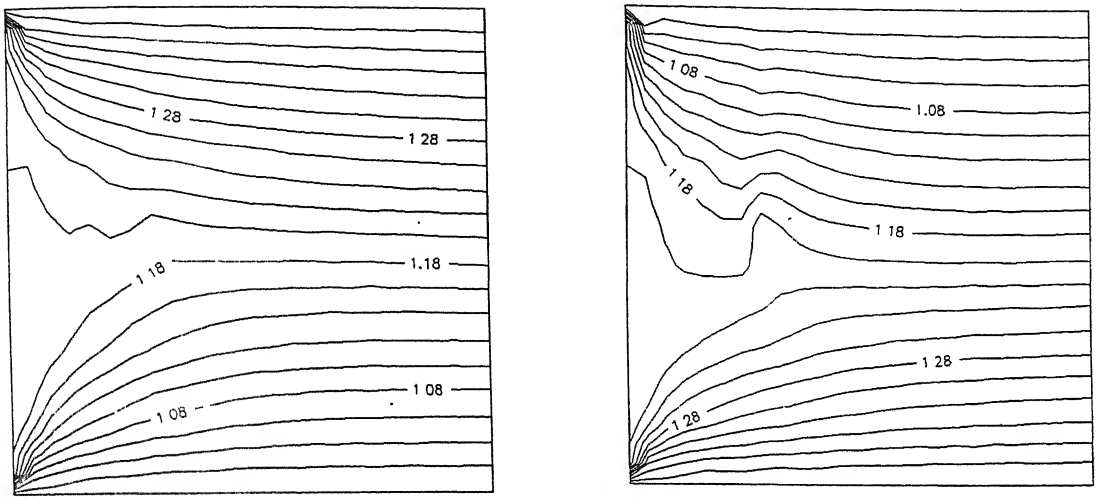

(a) (b)

Figure 3.18: Temperature contours at $k = 1$, $p_i^+ = 1$, $T_i^+ = 1.2$ (a) $T_p^+ = 1.4$, $T_s^+ = 1.0$. (b) $T_p^+ = 1.0$, $T_s^+ = 1.4$

In this Chapter, we have chosen some ad-hoc values for the non-zero flux boundary condition on the pad in order to simulate the results (i.e. we have taken 0.2 and also - 0.2). In the next Chapter, we have incorporated the heat conduction in the pad. In that simulations, the pad flux values turns out to be approximately 0.003. So comparisons are made for load carrying capacity with these three values for the setting $k = 0.4$, $p_i^+ = 1, T_i^+ = 1, T_s^+ = 1.5$ for Case1 and are shown in Figure 3.19.

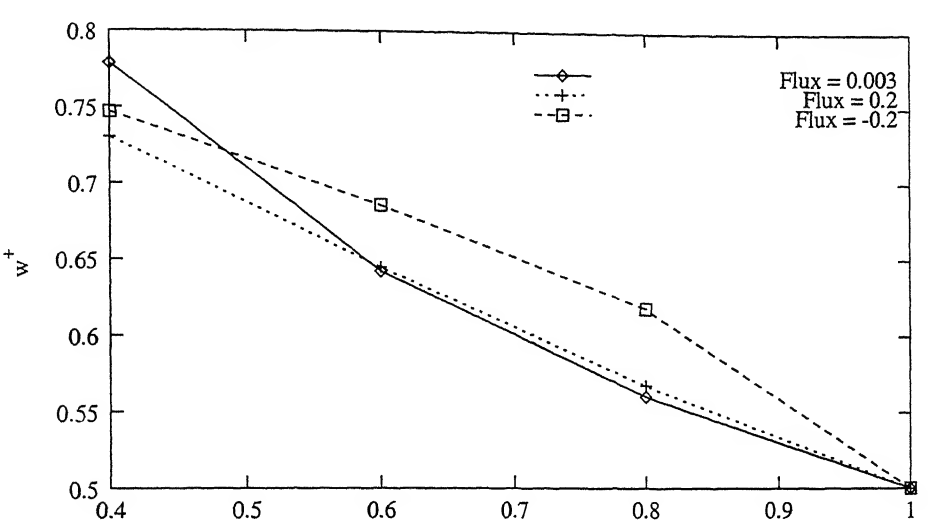

Figure 3.19: Comparison of load carrying capacity with k for various flux prescriptions on the pad

3.5 Conclusions

Thermal effects on load carrying capacity in slider bearings has been numerically analyzed by SUPGFEM. A thorough investigation of several models has been done. An orderly analysis identifying the influence of various factors viz. slider bearing geometry, thermal boosting, inlet pressure, inlet temperature and temperature dependent viscosity coefficient of the lubricant, on the pressure generating mechanism in slider bearings has been provided. Clearly, the study reveals that the consideration of (a) Lubricant with low values of temperature viscosity coefficient (b) Non zero inlet pressure and (c) $T_i^+ < T_s^+ < T_p^+$ (or) $T_i^+ < T_s^+$ with non-zero flux on pad constitutes a desirable setup for enhancing the Load Carrying Capacity of a Slider Bearing. The numerical formulation presented here is suitable for thermal analysis of both, high and low speed lubrication flow problems of industrial significance, where higher accuracy is required.

Chapter 4

Performance of a Tilted Pad Slider Bearing Considering Heat Conduction in the Pad

4.1 Introduction

Lubrication under high load and high speed is common in engineering practice today. In the thin film that separates the two rubbing surfaces a large amount of heat may be generated. Yet, beyond the classical theory for isothermal and rigid hydrodynamic lubrication, little is known about the combined effect of temperature and heat conduction in the solid pad. Undoubtly there is a need for a fundamental study of the conditions which surround the fluid film (Khonsari and Wang [72]). Several researchers, as discussed in Chapter 3 (page: 53, 54) have numerically analyzed the thermohydrodynamic performance of slider bearings. Studies of Schumack [19] were focussed on the applicability of spectral element scheme for thermohydrodynamic lubrication (THDL) analysis. Whereas Rodkiewicz and Sinha [58], Kumar et al. [73] analyzed the load carrying mechanism of a slider bearings under thermal influence by solving nonlinear coupled partial differential equations governing the fluid film with either isothermal or adiabatic boundaries or with boundaries having non-zero thermal flux prescriptions.

Actual bearing configurations have solid pad/slider. To analyze this configuration one has to couple the p.d.e's governing the fluid film in the slider bearing with the heat conduction equation for the solid pad/slider. Ezzat and Rohde [15] and later Gero and Ettles [18] have considered such models for THD lubrication studies. Ezzat and Rohde considered viscosity related to two specified temperatures and treated density to be constant. Both viscosity and density were treated to be constants by Gero and Ettles [18]. The influence of thermal boosting and various geometric configurations on load carrying capacity, drag force etc., of the lubricant has been investigated by them.

In the present Chapter, we investigate the hydrodynamic lubrication of a finite width slider bearings, taking into account not only the temperature variation in the fluid film but also the effect of heat conduction to the pad. Influence of thermal boosting, various geometric configurations and several practical thermal boundary prescriptions on load carrying capacity and frictional drag has been analyzed. Following Brooks and Hughes [68] and Grygiel and Tanguy [71] finite element numerical scheme with Streamline Upwind Petrov-Galerkin weight functions have been used to preclude the numerical oscillations arising in the flow field.

4.2 Governing Equations

The geometry and the coordinate system for a slider bearing has been shown in Figure 3.1. Introducing the following non dimensional variables Schumack [19]:

$$u^+ = \frac{u}{U}, \quad v^+ = \frac{vB}{Uh_o}, \quad x^+ = \frac{x}{B}, \quad y^+ = \frac{y}{h_o}$$

$T^+ = \frac{T}{T_a}$ (subscript "a" indicates ambient condition),

$$\mu^+ = \frac{\mu}{\mu_a}, \quad \rho^+ = \frac{\rho}{\rho_a}, \quad p^+ = \frac{ph_o^2}{\mu_a UB} \text{ (p is the gage pressure)},$$

$$p_i^+ = \frac{p_i h_o^2}{\mu_a UB}, \quad h_o^+ = \frac{h_o}{B}, \quad h^+ = \frac{h}{h_o}, \quad \beta^+ = \beta T_a,$$

$$\lambda^+ = \lambda T_a, \quad P_r E_c = \frac{\mu_a U^2}{kT_a}, \quad P_e = \frac{\rho_a U c h_o^2}{kB}.$$

$$T_p{}^+ = \frac{T_p}{T_a}, \quad x'^+ = \frac{x'}{B}, \quad y'^+ = \frac{y'}{h_1}$$

$h_1^+ = \frac{h_1}{B}$. (where h_1 is the thickness of the pad).

Under the lubrication assumptions mentioned in Section 3.2 and using the above non-dimensionalization scheme, the standard Navier-Stokes equations together with the continuity equation reduce to the following form:

$$\frac{\partial p^+}{\partial x^+} = \frac{\partial}{\partial y^+} \left(\mu^+ \frac{\partial u^+}{\partial y^+} \right) \tag{4.1}$$

$$\frac{\partial}{\partial x^+} \left(\rho^+ u^+ \right) + \frac{\partial}{\partial y^+} \left(\rho^+ v^+ \right) = 0 \tag{4.2}$$

Combining equations (4.1) and (4.2) with the following boundary conditions $u^+ = 1, \quad v^+ = 0 \quad$ at $y^+ = 0$ and $u^+ = 0, \quad v^+ = 0 \quad$ at $y^+ = h^+$ will lead to the following steady state Generalized Reynolds equation for the pressure distribution.

$$\frac{\partial}{\partial x^+} \left(\frac{h^{+3}}{6\,\mu^+} \frac{\partial p^+}{\partial x^+} \right) = \frac{\partial h^+}{\partial x^+} \tag{4.3}$$

with the boundary conditions

$$p^+ = p_i^+ \text{ at } x^+ = 0 \text{ and } p^+ = 0 \text{ at } x^+ = 1 \tag{4.4}$$

The energy equation is as follows

$$\rho^+ \left(u^+ \frac{\partial T^+}{\partial x^+} + v^+ \frac{\partial T^+}{\partial y^+} \right) = \frac{1}{P_e} \frac{\partial^2 T^+}{\partial y^{+2}} + \frac{P_r\, E_c}{P_e} \mu^+ \left(\frac{\partial u^+}{\partial y^+} \right)^2 + \frac{P_r\, E_c}{P_e} u^+ \frac{dp^+}{dx^+} \tag{4.5}$$

where

$$\rho^+ = 1 - \lambda^+ \left(T^+ - 1 \right), \quad \mu^+ = \exp \left[-\beta^+ \left(T^+ - 1 \right) \right] \tag{4.6}$$

Equation governing the heat conduction in the pad is

$$(h_1{}^+)^2 \frac{\partial^2 T_p{}^+}{\partial x'^{+2}} + \frac{\partial^2 T_p{}^+}{\partial y'^{+2}} = 0 \tag{4.7}$$

In view of the various industrial applications, the energy equation has been solved under the following different temperature boundary conditions (see Figure 3.1 for AB, BC, AD, CD, DF, CE, EF positions):

- Case1:

  Lubricant boundary conditions:

  $T^+ = T_s^+ = 1.3$ (or 1.2 or 1.1 or 1.0), on AB

  $\frac{\partial T^+}{\partial x^+} = 0$, on BC

  $T^+ = T_i^+ = 1.3$, on AD

  Pad boundary conditions:

  $T_p^+ = 1.3$,, on DF

  $T_p^+ = 1.3$,, on CE

  $T_p^+ = 1.3$,, on EF

  Interface boundary conditions:

  $T^+ = T_p{}^+$ and $k_s \frac{\partial T_p{}^+}{\partial y'^+} = k_f \frac{\partial T^+}{\partial y^+}$, on CD

- Case2:

  Lubricant boundary conditions:

  $T^+ = T_s^+ = 1.3$ (or 1.2 or 1.1 or 1.0), on AB

  $\frac{\partial T^+}{\partial x^+} = 0$, on BC

  $T^+ = T_i^+ = 1.3$, on AD

  Pad boundary conditions:

  $\frac{\partial T_p{}^+}{\partial x'^+} = 0$, on DF

  $\frac{\partial T_p{}^+}{\partial x'^+} = 0$, CE

  $T_p{}^+ = 1.3$, on EF

  Interface boundary conditions:

  $T^+ = T_p{}^+$ and $k_s \frac{\partial T_p{}^+}{\partial y'^+} = k_f \frac{\partial T^+}{\partial y^+}$, on CD

- Case3:

  Lubricant boundary conditions:

  $T^+ = T_s^+ = 1.3$ (or 1.2 or 1.1 or 1.0), on AB

  $\frac{\partial T^+}{\partial x^+} = 0$, on BC

  $T^+ = T_i^+ = 1.3$, on AD

Pad boundary conditions:

$\frac{\partial T_p{}^+}{\partial x'^+} = 0$, on DF

$\frac{\partial T_p{}^+}{\partial x'^+} = 0$, on CE

$\frac{\partial T_p{}^+}{\partial \vec{n}} = 0$, on EF

Interface boundary conditions:

$T^+ = T_p{}^+$ and $k_s \frac{\partial T_p{}^+}{\partial y'^+} = k_f \frac{\partial T^+}{\partial y^+}$, on CD

- Case4:

Lubricant boundary conditions:

$T^+ = T_s^+ = 1.3$ (or 1.2 or 1.1 or 1.0), on AB

$\frac{\partial T^+}{\partial x^+} = 0$, on BC

$T^+ = T_i^+ = 1.3$, on AD

Pad boundary conditions:

$\frac{\partial T_p{}^+}{\partial x'^+} = 0$, on DF

$\frac{\partial T_p{}^+}{\partial x'^+} = 0$, on CE

$-k_s \frac{\partial T_p{}^+}{\partial \vec{n}} = -H\ (T_p{}^+ - 1)$, on EF

Interface boundary conditions:

$T^+ = T_p{}^+$ and $k_s \frac{\partial T_p{}^+}{\partial y'^+} = k_f \frac{\partial T^+}{\partial y^+}$, on CD

The load carrying capacity (W^+) and the frictional drag (F^+) have been determined using the equations (3.11) and (3.12).

4.3 Finite Element Formulation and Solution Procedure

Let Ω the domain of interest be bounded in R^2 with a piecewise smooth boundary Γ. Let (x^+, y^+) denote the vector of spatial coordinate of a generic point in $\bar{\Omega}$ and $\vec{n}$ is the outward unit normal vector drawn at any point (x^+, y^+) on Γ. Now the variational principle $\Pi(p)$ for

the Reynolds equation (4.3) in Ω is given by:

$$\Pi(p) = \int_{\Omega} [\ \frac{h^{+3}}{12\ \mu^{+}} (\ \frac{\partial p^{+}}{\partial x^{+}}\ )^2 - h^{+}\ \frac{\partial p^{+}}{\partial x^{+}}\ ]\ d\Omega \tag{4.8}$$

The weighted residual formulation of the energy equation is given by:

$$\int_{\Omega} \tilde{W}_l\ [\ \rho^{+}(u^{+}\ \frac{\partial T^{+}}{\partial x^{+}} + v^{+}\ \frac{\partial T^{+}}{\partial y^{+}}) - \frac{1}{P_e}\ \frac{\partial^2 T^{+}}{\partial y^{+2}} - \frac{P_r\ E_c}{P_e}\ \mu^{+}\ (\ \frac{\partial u^{+}}{\partial y^{+}}\ )^2 - \frac{P_r\ E_c}{P_e}\ u^{+}\ \frac{dp^{+}}{dx^{+}}\ ]\ d\Omega = 0 \tag{4.9}$$

where, $\tilde{W}_l$ is the modified SUPG weight function. It is to be noted that ρ^{+}, μ^{+} are dependent on T^{+} and are defined in equation (4.6).

And the Galerkin formulation for the heat conduction in the pad is given by:

$$\int_{\Omega'} [\ (h_1^{+})^2\ \frac{\partial^2 T_p{}^{+}}{\partial x'^{+2}} + \frac{\partial^2 T_p{}^{+}}{\partial y'^{+2}}\ ]\ w_l\ \ d\Omega' = 0 \tag{4.10}$$

Now to reduce the lubrication problem to one of finite number of unknowns, the solution domain is divided into bilinear rectangular elements and the field variables (pressures, velocities and temperatures) are expressed in terms of approximating trial functions N_i within each element. Now Ω is discretized into N_e bilinear rectangular elements such that:

$$\cup_{e=1}^{N_e}\ \bar{\Omega}^e = \bar{\Omega} \qquad \cap_{e=1}^{N_e}\ \bar{\Omega}^e = \phi \tag{4.11}$$

where, Ω^e denotes the interior domain of an element. Let Γ^e be the boundary of Ω^e. The discretized representation of the field variables are given by:

$$u_e^{+} \approx \sum_{k=1}^{N_{el}} N_k\ u_k^{+^e}, \qquad v_e^{+} \approx \sum_{k=1}^{N_{el}} N_k\ v_k^{+^e}, \qquad p_e^{+} \approx \sum_{k=1}^{N_{el}} N_k\ p_k^{+^e},$$

$$T_e^{+} \approx \sum_{k=1}^{N_{el}} N_k\ T_k^{+^e}. \qquad T_e^{p^{+}} \approx \sum_{k=1}^{N_{el}} N_k\ T_k^{p^{+^e}}$$

where, $N_{el} = 2$ for pressure case and $N_{el} = 4$ for velocities and temperatures. Introducing these elemental discretization details into equations (4.8)-(4.10) we obtain element level representations. The element level representation of equation (4.8) is given by:

$$\int_{\Omega^e} \{\ \frac{h^{+3}}{12\ \mu^{+}} [\ \frac{\partial}{\partial x^{+}} (\ \sum_{j=1}^{N_{el}} p_j^{+^e}\ N_j^e\ )\ ]^2 - h^{+}\ \frac{\partial}{\partial x^{+}} (\ \sum_{j=1}^{N_{el}} p_j^{+^e}\ N_j^e\ )\ \}\ d\Omega^e = 0 \tag{4.12}$$

on minimizing the equation with respect to variables p_j^e and on further simplification one would arrive at the following equation.

$$\sum_{j=1}^{N_{el}} \int_{\Omega^e} [\ \frac{h^{+3}}{6\ \mu^+} \frac{\partial N_j^e}{\partial x^+} \frac{\partial N_i^e}{\partial x^+}\ ]\ p_j^{+^e}\ d\Omega^e = \int_{\Omega^e} h^+ \frac{\partial N_i^e}{\partial x^+}\ d\Omega^e \tag{4.13}$$

Now with the SUPG analysis of Brooks and Hughes [68] and Grygiel and Tanguy [71] one would obtain the following discretized elemental energy equation.

$$\sum_j \int_{\Omega^e} \{\ \tilde{W}\ (1 - \lambda^+\ (\sum_k N_k^e T_k^{+^e} - 1))\ \ [\ (\sum_k u_k^{+^e} N_k^e)\ \frac{\partial N_j^e}{\partial x^+}\ +\ (\sum_k v_k^{+^e} N_k^e)\ \frac{\partial N_j^e}{\partial y^+}\ ]$$

$$+\ \frac{1}{P_e}(\ \frac{\partial w_i}{\partial y^+}\ \frac{\partial N_j^e}{\partial y^+})\}\ T_j^{+^e} d\Omega^e = \int_{\Omega^e} [\tilde{W} \frac{P_r E_c}{P_e} (\exp(-\beta^+ (\sum_k N_k^e T_k^{+^e} - 1))) (\frac{\partial}{\partial y^+} (\sum_k N_k^e u_k^{+^e}))^2$$

$$-\ (\sum_k N_k^e u_k^{+^e})\ (\frac{d}{dx^+} (\sum_k N_k^e p_k^{+^e}))]\ d\Omega^e = 0 \tag{4.14}$$

where,

$$\tilde{W} = w_i + P_i \quad w_i = N_i \quad \text{and} \quad P_i = \frac{\tilde{k}\ \hat{u_j}\ W_{i,j}}{\|u\|}$$

And the upwind parameter $\hat{k}$ is calculated using elemental dimensions and elemental velocity (Grygiel and Tanguy [71] and Brooks and Hughes [68].

And the discretized elemental level heat conduction equation is given by:

$$\int_{\Omega'^e} [\ w_i\ (h_1^+)^2\ \frac{\partial w_i}{\partial x'^+}\ \frac{\partial N_j{}^e}{\partial x'^+} + \frac{\partial w_i}{\partial y'^+}\ \frac{\partial N_j{}^e}{\partial y'^+}] \ T_{p_j}^{+^e}\ \ d\Omega'^e = 0 \tag{4.15}$$

Now based on equations (4.13) - (4.15) numerical simulations have been carried out on a 30×30 finite element mesh system. The results have been obtained to an accuracy of $\epsilon = 5.0 \times 10^{-4}$ i.e

$$(\ \max\ (\ \frac{|\ \gamma_j^{New} - \gamma_j^{Old}\ |}{|\ \gamma_j^{New}\ |}\ )\ ) \ \leq\ \epsilon$$

for $j = 1, 2, \cdots, \mathrm{n}, \cdots$. where γ_j represents any of the field variables $p_j^+, u_j^+, v_j^+,\ T_j^+$.

4.4 Results and Discussion

The simulations have been carried out on 30 × 30 mesh system. Computer generated plots are obtained for various values of k, p_i^+ and with the fixed values for the parameters P_r (Prandtl number) and E_c (Eckert number). The results have been analyzed for load carrying capacity, drag force and velocity, pressure, temperature fields and are presented in the form of plots and Tables.

The non dimensional pressures for Casel at different locations in the sliding direction with $k = 0.4$, $p_i{}^+ = 0$ for different slider temperatures $(T_s{}^+)$ are shown in Figure 4.1.

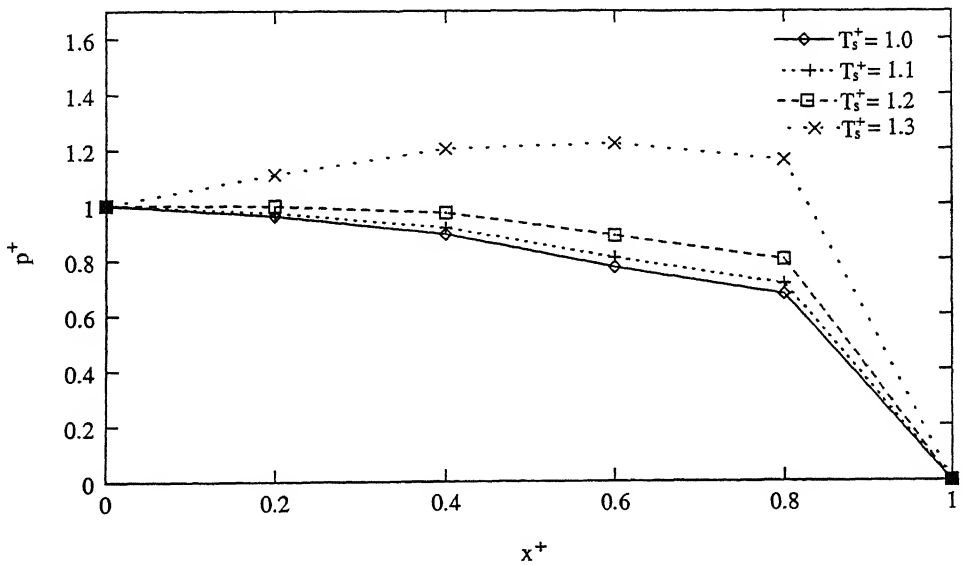

Figure 4.1: Pressure distribution along the sliding direction of the bearing at $p_i^+ = 1$, $k = 0.4$

From this Figure one can notice that for fixed values of x^+, lowering the slider temperature $(T_s{}^+)$ below the inlet lubricant temperature (T_i^+) enhances the pressure. So maintaining the slider at temperature lower than that of inlet lubricant temperature leads to thermal boosting of the slider bearing performance. In Figure 4.1 one can notice that when the non dimensional slider temperature is kept at $T_s{}^+ = 1.0$ and the inlet lubricant temperature at $T_i{}^+ = 1.3$, peak pressures are observed at $x^+ = 0.8$. Both of these observations can be attributed to the fall in the average temperature of the lubricant in the domain under con-

sideration, on lowering the slider temperature. From the expression for viscosity ($\mu^+(T^+)$) it is clear that for fixed β^+ lowering T^+ leads to higher values for viscosity. Higher the viscosity higher will be the threshold for thermal deformation of the lubricant and this leads to improved performance. Such a fall in the lubricant temperature can be ascertained by tracing the temperature distribution in the form of isotherms of the lubricant for different slider temperature set ups. So in Figure 4.2 isotherms for the set ups $T_s^+ = 1,\ 1.1,\ 1.2,\ 1.3$ with $T_p^+ = 1.3$ for all these cases are presented.

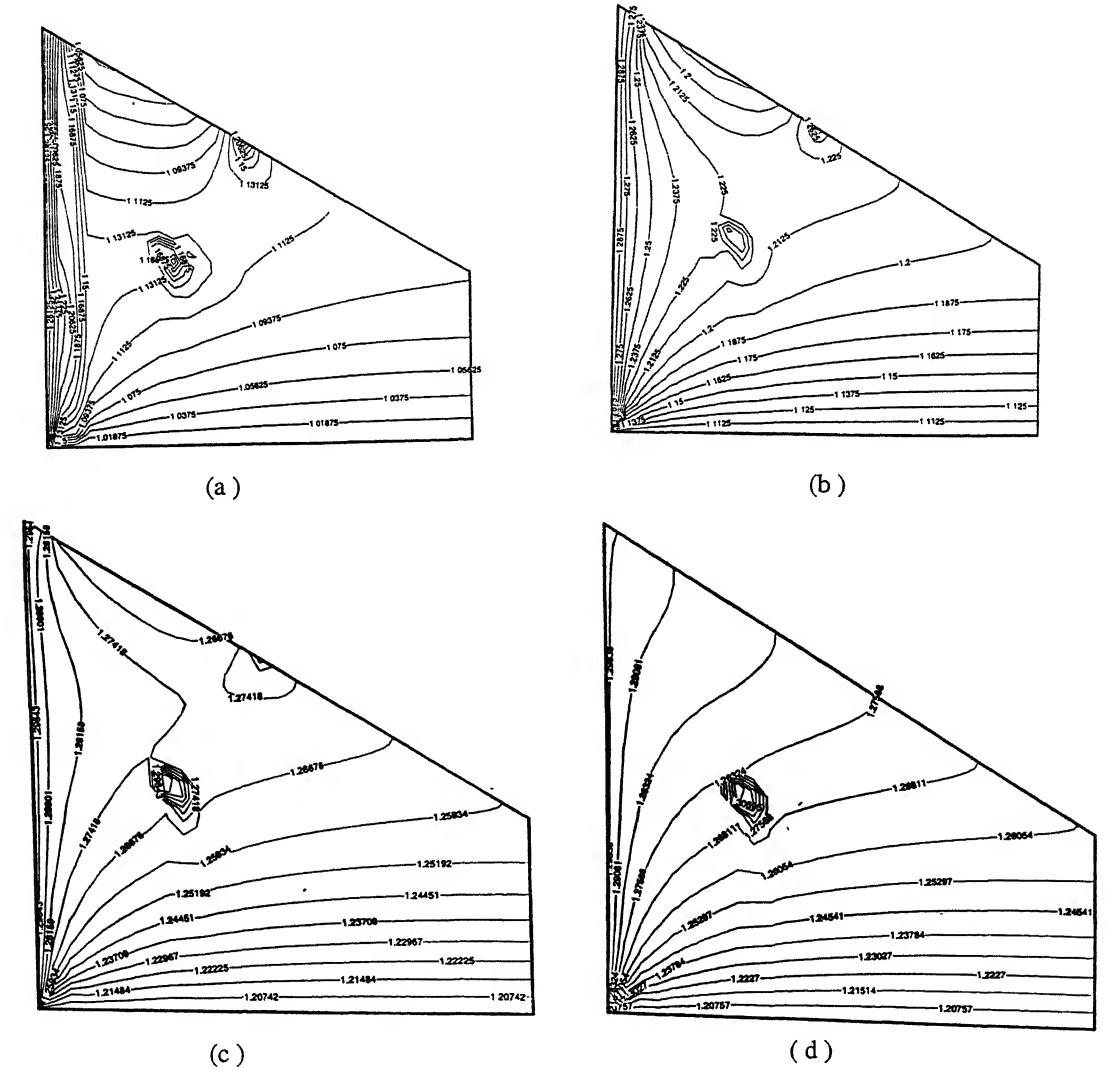

Figure 4.2: Isotherms at (a) $T_s^+ = 1.0$, (b) $T_s^+ = 1.1$, (c) $T_s^+ = 1.2$, (d) $T_s^+ = 1.3$

These plots fully support the observations regarding the lubricant temperature fall. One can notice that around $x^+ = 0.8,\ 0 \leq y^+ \leq h^+$ for all slider temperature set ups, average temperature distribution reaches a minimum and this lower bound can be lowered by decreasing ${T_s}^+$ which in turn can aid the pressure build up. Also on lowering ${T_s}^+$ a thermal boundary layer is seen to develop adjacent to the inlet. In the region R between $0.2 \leq x \leq 0.5,\ 0.35 \leq y \leq 0.5$ in the Figure 4.2 circular isotherms with increasing inner temperatures are noticed. In one case Figure 4.2 (d) the temperature goes beyond inlet temperature 1.3. These are hot spots in the domain and they indicate the presence of small recirculating fluid zones. To verify this, u-velocity contours (iso u-velocities or streamlines as $v << 1$) are presented in Figures 4.3 and 4.4 for $T_i^+ = 1.3,\ T_s^+ = 1.0,\ 1.1,\ 1.2,\ 1.3,\ p_i^+ = 1,\ k = 0.4,\ p_0^+ = 0.$

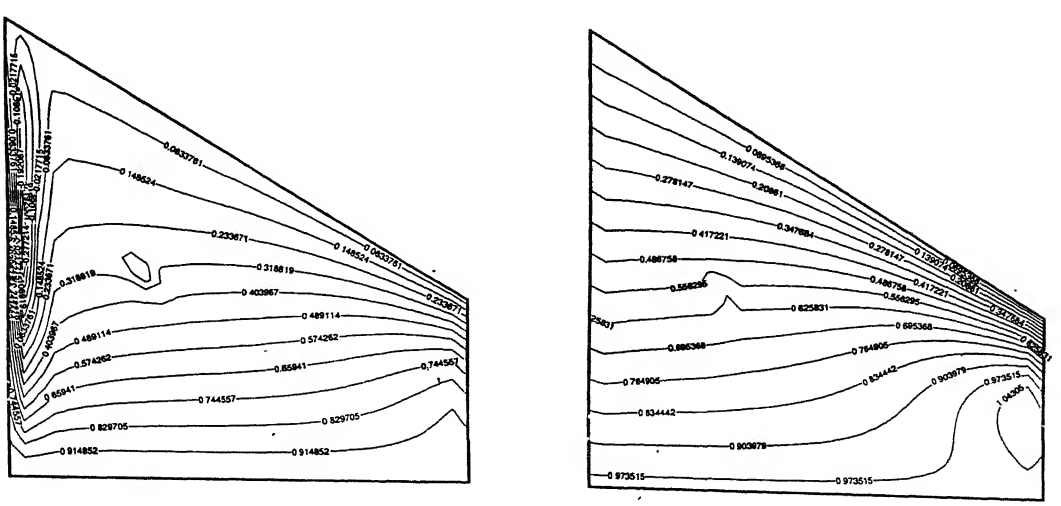

(a) (b)

Figure 4.3: u-velocity contours at (a) $T_s^+ = 1.0$, (b) $T_s^+ = 1.1$

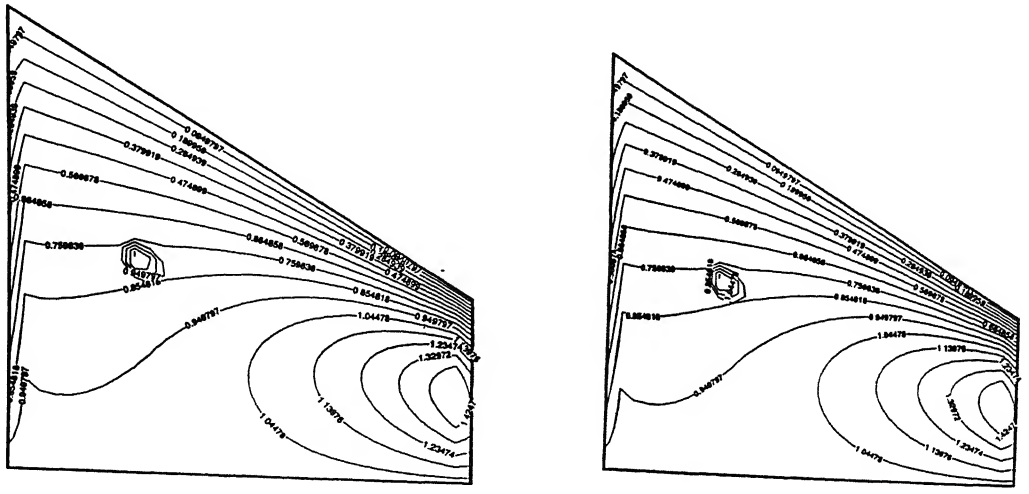

(c) (d)

Figure 4.4: u-velocity contours at (c) $T_s^+ = 1.2$, (d) $T_s^+ = 1.3$

In these Figures one can notice the manifestation or positive indication of recirculation zones in the region R. These circulation zones get prominent as T_s^+ is set closer to T_i^+. The isotherms in Figure 4.2 indicate that as the recirculation zones in region R in Figures 4.3 and 4.4 get prominent, the hot spots or circular isotherms too get stronger. From the Figure 4.2 (a) and (b) corresponding to $T_s^+ = 1.0$ and 1.1 one can notice that in the inlet region where a thermal boundary layer with plume like isotherm manifests, flow field gets concentrated with fluid boundary layer immediately followed by a long and slender recirculation zone. This can be attributed primarily to the thermal boundary conditions and partly to the geometric configuration of the slider bearing. In Figures 4.3 and 4.4 one can also see that as T_s^+ is raised boundary layer adjacent to the inlet vanishes and flow in the domain gets accelerated. The flow pattern for various values of T_s^+ suggest that on lowering T_s^+ flow gets more laminar excepting close to the inlet.

In Figure 4.5 the frictional drag force (F^+) corresponding to the above simulations along the sliding direction have been plotted. It is clear that $T_s^+ = 1.0$, $T_i^+ = 1.3$ not only leads to higher pressure generation but also to reduced frictional drag. From the formula for frictional drag force given in equation (3.12) as μ^+ is already seen to increase on lowering

slider temperature any reduction in F^+ should be due to fall in the velocity gradient $\frac{\partial u^+}{\partial y^+}$. The u-velocity contours in Figures 4.3 and 4.4 show that such a fall in velocity gradient does indeed take place.

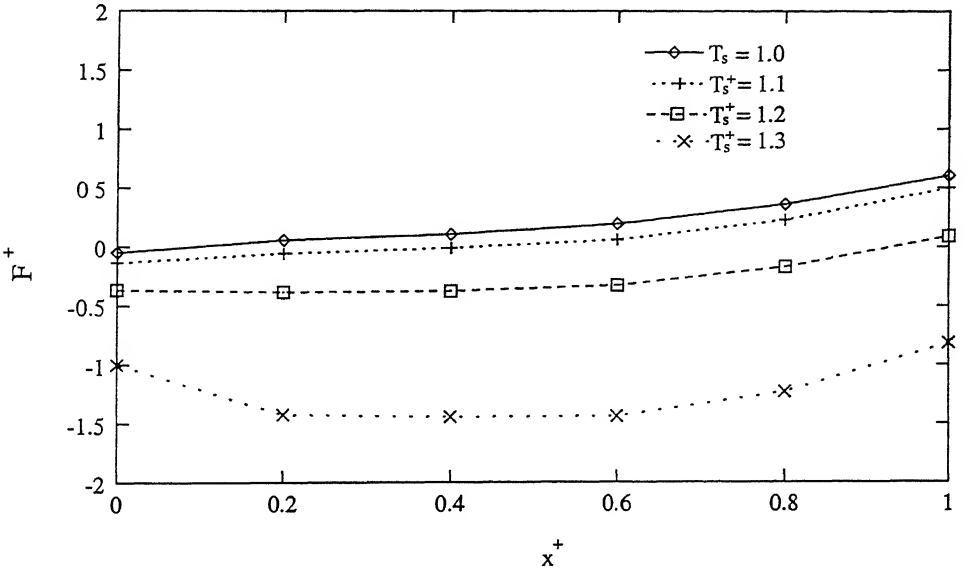

Figure 4.5: Frictional drag force along the sliding direction of the bearing at $p_i^+ = 1, T_i^+ = 1.3, k = 0.4$, Case1

The combined effect of thermal boosting and geometric configuration of slider bearing on load carrying capacity and the frictional drag are presented in Figures 4.6 and 4.7 respectively for Case4 at $p_i^+ = 1$. These plots show that decreasing either k or T_s^+ or both k and T_s^+ simultaneously enhances the load carrying capacity but lowers the frictional drag values. Further the combined influence of k and T_s^+ on frictional drag and load carrying capacity is stronger than their segregated effects. While the combined influence of k and T_s^+ on frictional drag is clearly seen at all k, it is predominantly seen for $0.4 \leq k \leq 0.6$ on load carrying capacity.

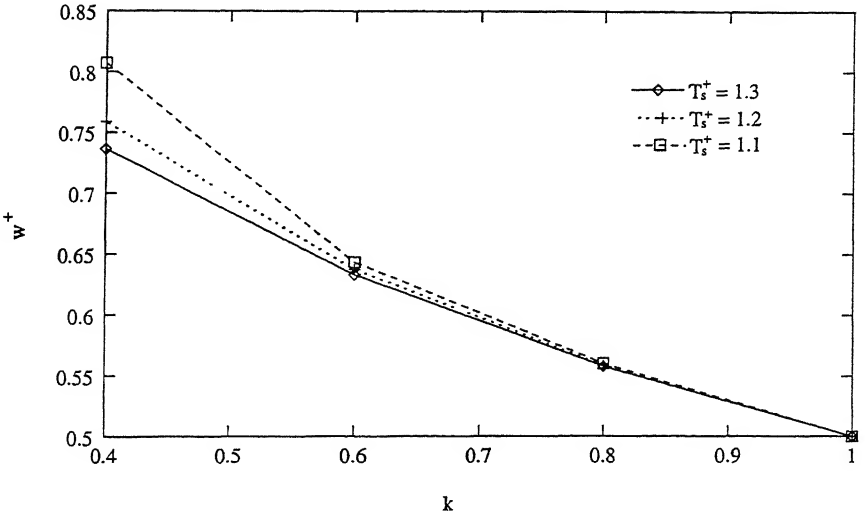

Figure 4.6: Variation of load carrying capacity with k at $p_i^+ = 1$, $T_i^+ = 1.3$, Case4

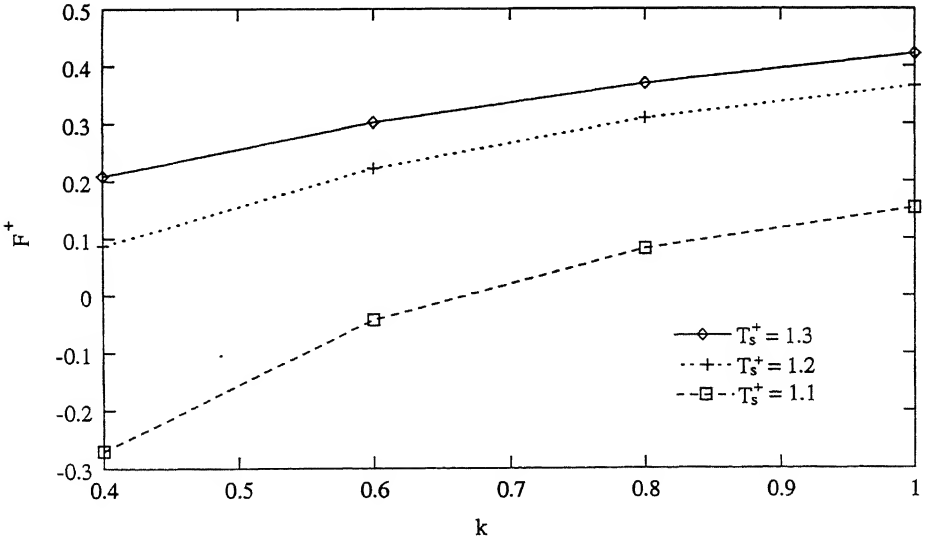

Figure 4.7: Variation of frictional drag force with k at $p_i^+ = 1$, $T_i^+ = 1.3$, Case4

In Figure 4.8 the combined influence of thermal boosting and the geometry of the slider bearing on load carrying capacity for $p_i^+ = 0$ is presented. One may notice that these results are similar to those obtained at $p_i^+ = 1$ (see Figure 4.6). Further these are in conformity with the remarks made by Pinkus and Sternlicht [74].

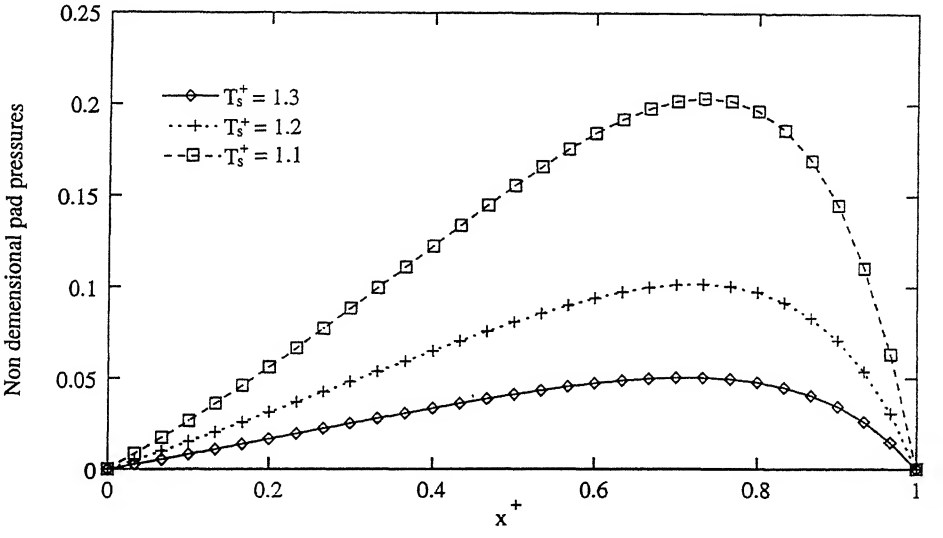

Figure 4.8: Pressures along the pad at $p_i^+ = 0, k = 0.4$

Also from Figures 4.6 and 4.8 it is seen that the thermal boosting has greater influence on load carrying capacity for smaller inlet pressures. In the case $k = 0.4$, thermal boosting i.e $T_s^+ = 1.1$, has brought in nearly four fold increase in the load carrying capacity. It may also be interesting to trace the pressures along the sliding direction on the pad for $k = 0.4$ at $p_i^+ = 0$.

From Figure 4.8 one may notice that for all T_s^+ prescriptions maximum pressure on the pad manifest around $x^+ = 0.75$ to 0.8 which is close to the outlet. This result is very much in conformity with the standard results reported on load carrying capacity for slider bearings (Rodkiewicz and Sinha [58]). A more interesting feature which one would notice in Figure 4.8 is that the thermal boosting effect on the pressure along the pad is also maximum around $x^+ = 0.75$ to 0.8.

Load carrying capacity of parallel slider bearing (k = 1) with zero inlet pressure (p_i^+) has

lot of significance in several applications. So the influence of thermal boosting on pressure generation in the fluid film for $k = 1$ with $p_i^+ = 1$ and Case4 boundary conditions has been analyzed and presented in Figure 4.9 for various values of T_s^+.

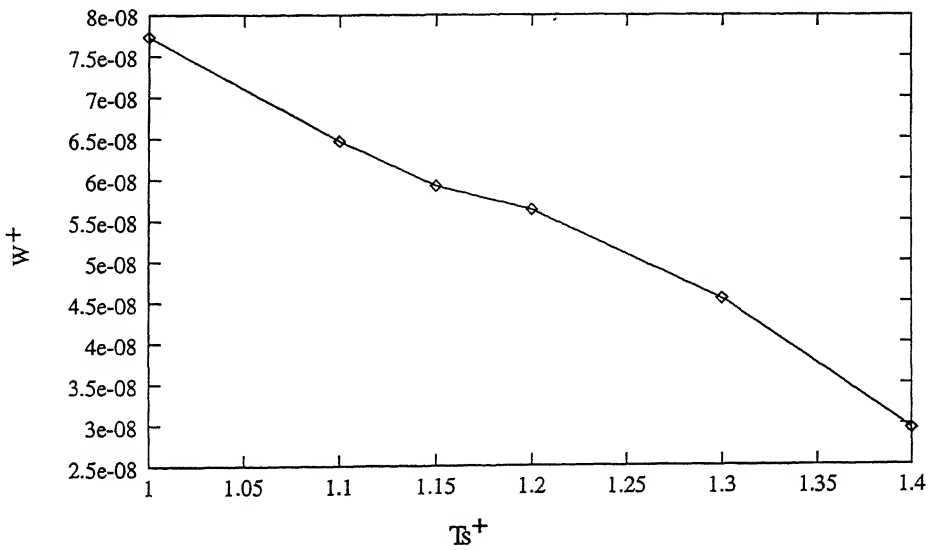

Figure 4.9: Load carrying capacity at different slider temperatures with $p_i^+ = 0, k = 1$, Case4

It is clear that on reducing T_s^+ from 1.4 to 1.0, the load carrying capacity is boosted more than two and half times. i.e from $3 \times e^{-08}$ to $7.75 \times e^{-08}$. This result supports the view that pressure generation is very much possible in parallel slider bearings. Here it is to be noticed that in this study, ρ^+, μ^+ are functions of temperature.

Next the influence of solid pads with various thermal boundary conditions as described by Case1 (pad with isothermal side and isothermal top face), Case2 (pad with adiabatic sides and top) and Case4 (pad with adiabatic sides and exposed top) on the load carrying capacity and frictional drag force in the fluid film has been analyzed for $T_s^+ = 1.3,\ 1.2,\ T_i^+ = 1.3,\ p_i^+ = 1,\ k = 0.4, 1$. These results are presented in Tables 4.1 - 4.4.

Table 4.1: Comparison of load carrying capacity and frictional drag force at different boundary conditions for $T_i^+ = 1.3, T_s^+ = 1.3, p_i^+ = 1, k = 0.4$

Boundary conditions	Case1	Case2	Case3	Case4
W^+	0.7364519	0.7364491	0.7364560	0.7364571
F^+	0.2086179	0.2086195	0.2086191	0.2086179

Table 4.2: Comparison of load carrying capacity and frictional drag force at different boundary conditions for $T_i^+ = 1.3, T_s^+ = 1.3, p_i^+ = 1, k = 1$

Boundary conditions	Case1	Case2	Case3	Case4
W^+	0.05000002	0.5000002	0.4999992	0.5000002
F^+	0.4217472	0.4217471	0.4217361	0.4217463

Table 4.3: Comparison of load carrying capacity and frictional drag force at different boundary conditions for $T_i^+ = 1.3, T_s^+ = 1.2, p_i^+ = 1, k = 0.4$

Boundary conditions	Case1	Case2	Case3	Case4
W^+	0.7599708	0.7599646	0.7588058	0.7587989
F^+	0.866119	0.0865929	0.08708	0.08708

Table 4.4: Comparison of load carrying capacity and frictional drag force at different boundary conditions for $T_i^+ = 1.3, T_s^+ = 1.2, p_i^+ = 1, k = 1$

Boundary conditions	Case1	Case2	Case3	Case4
W^+	0.4999992	0.5000011	0.5000002	0.5000002
F^+	0.3655055	0.3654333	0.3654611	0.3654560

From Tables 4.1 - 4.4, both at $T_s^+ = 1.3$ and $T_s^+ = 1.2$ only a marginal variation in load carrying capacity and frictional drag force is noticed. To further investigate this average temperature flux across the solid pad and lubricant interface are evaluated for Case1 , Case2 , Case3 and Case4 setups and these are found to be in the range of 0.002 to 0.005. To assess the influence of flux boundary values naturally getting set on the interface, a special slider bearing configuration without solid pad has been considered and a temperature flux boundary condition is prescribed on the pad side.

Experiments are carried out for different temperature flux prescriptions setting the remaining parameters at: $p_i^+ = 1$, $T_i^+ = 1.3$, $T_s^+ = 1.2$ and $0.4 \leq k \leq 1$. Results in the form of load carrying capacity obtained for flux prescriptions of 0.002 to 0.004 are presented in Table 4.5. One can see that small variation in flux values from 0.002 to 0.004 does not bring in a visible change in the load carrying capacity. These results agree with Rohde and Kong [49].

Table 4.5: Comparison of load carrying capacity at different flux values and at different values of k with $p_i^+ = 1$.

Flux	$k = 0.4, W^+$	$k = 0.6, W^+$	$k = 0.8, W^+$	$k = 1, W^+$
0.002	0.778611	0.6421080	0.5604001	0.500002
0.003	0.778603	0.6421075	0.5603997	0.500002
0.004	0.778595	0.6421067	0.560389	0.49999

Isotherms corresponding to the slider bearing with solid pad for the Case1 and Case4 are presented in Figure 4.10 (a) and (b). The isotherm patterns close to the interface clearly show the temperatures in the vicinity of interface, both on pad and lubricant side have only marginal changes and hence give raise to small flux values. Further it must be noticed that on the pad side little above the interface multiple circular isotherm pattern with almost fixed isotherm values are present. These go to say that fluxes on the interface, excepting close to the inlet and outlet will be very small. However, the influence of the Case4 on the temperature distribution in pad may be noticed from the isotherms density close to the

adiabatic sides and also from their magnitudes in the interior of the pad.

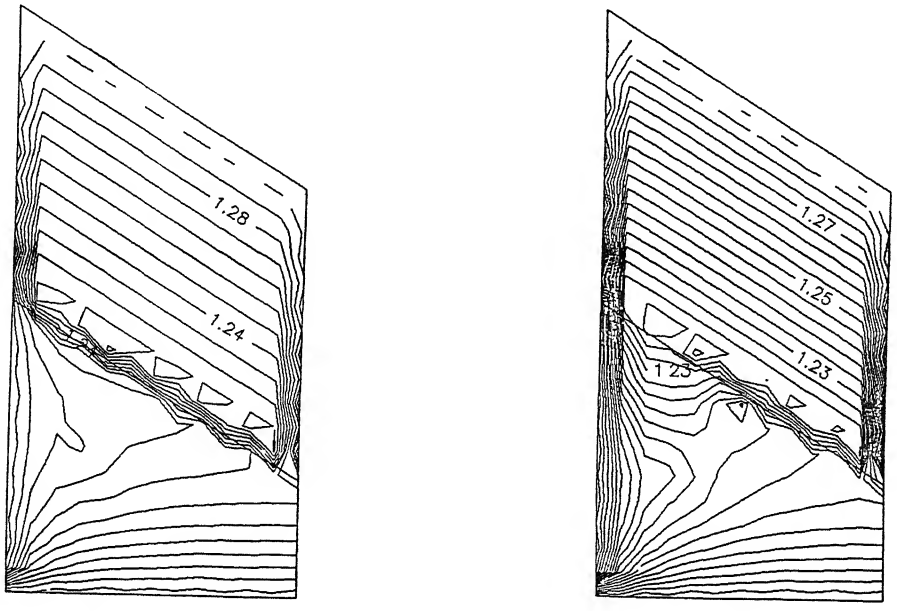

(a) (b)

Figure 4.10: Isotherms at $T_i^+ = 1.3, k = 0.4, p_i^+ = 1$ for (a) Case1, $T_s^+ = 1.3$ and (b) Case4, $T_s^+ = 1.2$.

In Table 4.6, the effective load carrying capacity for the case with conduction and no conduction in the pad are shown by fixing $T_i^+ = 1, T_s^+ + = 1.5, p_i^+ = 1$, Case4, flux = 0.003. From this Table 4.6, we notice that the load carrying capacity for the case of no conduction in the pad are higher for values of $k = 0.4, 0.6, 0.8$. Whereas for parallel case ($k = 1$) no change in the load carrying capacity is observed.

Table 4.6: Comparison of load carrying capacity for the case with conduction and no conduction in the pad for $p_i^+ = 1, T_i^+ = 1, T_s^+ = 1.5$, flux = 0.003, Case4

	k = 0.4	k = 0.6	k = 0.8	k = 1
W^+ (with conduction)	0.7365377	0.6255385	0.5560876	0.500002
W^+ (no conduction)	0.7786063	0.6421075	0.5603997	0.500002

4.5 Conclusions

Load carrying capacity and frictional drag of a high speed slider bearing with a solid pad for various thermal boundary conditions in conjunction with thermal boosting for various geometric configurations have been numerically analyzed using FEM. Density and the Viscosity in the mathematical model describing the slider bearing configuration are treated as functions of temperature. SUPG weight functions are found to be effective in precluding the numerical oscillations and in obtaining a convergent solution. Load carrying capacity of slider bearing can be thermally boosted by setting slider at temperatures lower than that of incoming lubricant. Thermal boundary layer in the inlet region, hot spots and recirculation zones in region R ($0.2 \leq x^+ \leq 0.5,\ 0.35 \leq y^+ \leq 0.5$) sensitive to T_s^+ are noticed in the temperature and flow fields respectively. Lowering of slider temperature takes the flow closer to the laminar regime and can make slider bearings more durable. Though solid pads with different boundary settings as chosen in this study from application point of view alters the the temperature field in the pad the thermal flux across the fluid-solid interface changes marginally and thus the load carrying capacity of the slider bearing remains unaffected. It is to be noted that the isothermal pads employed in the present study have been set at temperature similar to that of inlet flow.

Chapter 5

Thermohydrodynamic Analysis of a Tilted Pad Slider Bearing Considering Heat Conduction in the Pad and Slider[1]

5.1 Introduction

Tilted pads are widely used in many types of machinery because of their excellent stability, superior durability and high load carrying capacity. Numerous work has been done to investigate the behavior of tilted pads from various points of view. It is believed that performance of a tilted pad is affected by many factors, such as pad conduction, heat conduction in the moving slider, flux boundary conditions, effect of the inlet pressure buildup, etc.

The importance of thermohydrodynamic lubrication of slider bearings has been highlighted in the previous Chapter. In most of the works cited earlier the heat conduction in the slider and pad has not been considered. Dowson and Hudson [44] re-examined the mechanism of slider bearings allowing for the heat transfer to the bearing solids to determine the fluid film thermal boundaries. More recently Ezzat and Rohde [15] analyzed the thermohydrodynamic behavior of a steadily loaded inclined plane slider, taking into account

[1]Accepted for presentation and publication in the **STLE Annual Meeting Proceedings, May 2000**

the finite width of the bearing and heat transfer to the solids. Kumar et al. [73] have numerically analyzed the thermohydrodynamic performance of a slider bearing under thermal influence by solving nonlinear coupled partial differential equations governing the fluid film with either isothermal or adiabatic boundaries or with boundaries having non zero thermal flux prescriptions. Later Kumar et al [73] also analyzed the affect of heat conduction in the pad on bearing characteristics. But actual bearing configurations have slider and pad which are solids of finite thickness.To analyze this configuration one has to couple the p.d.e's governing the fluid film in the slider bearing with the heat conduction in the pad and as well as in the moving slider.

Rohde and Kong [49] and later Gero and Ettles [18] have considered only heat conduction in the pad but not both to the pad and slider. Rohde and Kong [49] have assumed viscosity related to two specified temperatures and density to be a constant, whereas Gero and Ettles [18] considered viscosity and density to be constants. The influence of thermal boosting and various inclinations of pad configuration on load carrying capacity, drag force etc., of the lubricant has not been investigated by them.

In the present Chapter, temperature sensitive density and viscosity, which brings in extra pseudo compressibility terms into the energy equation have been analyzed. Influence of thermal boosting, various geometric configurations and several realistic thermal boundary prescriptions on load carrying capacity and frictional drag has been analyzed. Following Brooks and Hughes [68] and Grygiel and Tanguy [71] finite element numerical scheme with Streamline Upwind Petrov-Galerkin weight functions has been used to preclude the numerical oscillations and results are depicted through computer generated plots and tables.

5.2 Problem Formulation

The geometry and the coordinate system for a slider bearing analyzed in this Chapter is shown in the Figure 5.1.

Introducing the following non dimensional variables Schumack [19]:

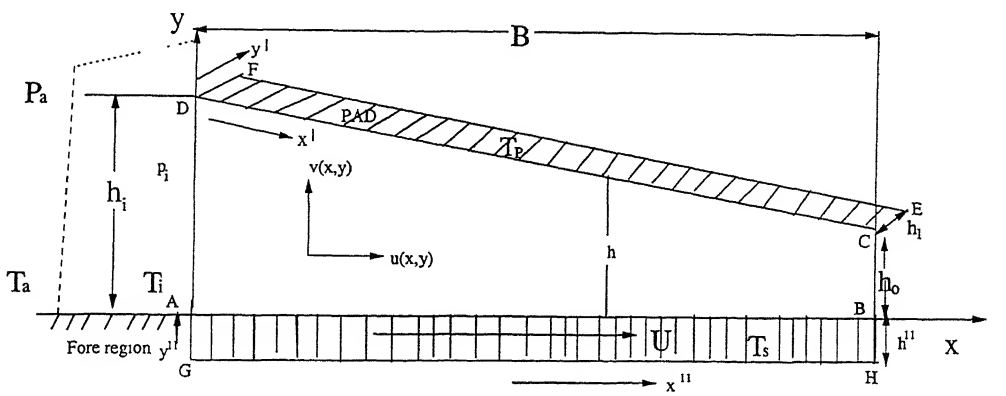

Figure 5.1: Geometry of the slider bearing considering heat conduction in the pad and moving slider

$u^+ = \frac{u}{U}$, $v^+ = \frac{vB}{Uh_o}$, $x^+ = \frac{x}{B}$, $y^+ = \frac{y}{h_o}$

$T^+ = \frac{T}{T_a}$ (subscript "a" indicates ambient condition),

$\mu^+ = \frac{\mu}{\mu_a}$, $\rho^+ = \frac{\rho}{\rho_a}$, $p^+ = \frac{ph_o^2}{\mu_a UB}$ (p is the gage pressure),

$p_i^+ = \frac{p_i h_o^2}{\mu_a UB}$, $h_o^+ = \frac{h_o}{B}$, $h^+ = \frac{h}{h_o}$, $\beta^+ = \beta T_a$,

$\lambda^+ = \lambda T_a$, $P_r E_c = \frac{\mu_a U^2}{kT_a}$, $P_e = \frac{\rho_a U c h_o^2}{kB}$.

$T_p^+ = \frac{T_p}{T_a}$, $T_s^+ = \frac{T_s}{T_a}$,

$x'^+ = \frac{x'}{B}$, $x''^+ = \frac{x'}{B}$, $y'^+ = \frac{y'}{h_1}$, $y''^+ = \frac{y'}{h_{11}}$,

$h_1^+ = \frac{h_1}{B}$. (where h_1 is the thickness of the pad).

$h_{11}^+ = \frac{h_{11}}{B}$. (where h_{11} is the thickness of the slider).

Under the assumptions given in Chapter 3 (section 3.2) and using the above non-dimensional scheme, the standard Naiver-Stokes equations together with the continuity equation reduce to the following form:

$$\frac{\partial p^+}{\partial x^+} = \frac{\partial}{\partial y^+}\left(\mu^+ \frac{\partial u^+}{\partial y^+}\right) \tag{5.1}$$

$$\frac{\partial}{\partial x^+}\left(\rho^+ u^+\right) + \frac{\partial}{\partial y^+}\left(\rho^+ v^+\right) = 0 \tag{5.2}$$

Combining equations (5.1) and (5.2) with the following boundary conditions

$u^+ = 1, \quad v^+ = 0 \quad$ at $y^+ = 0$ and $u^+ = 0, \quad v^+ = 0 \quad$ at $y^+ = h^+$

will lead to the following steady state Generalized Reynolds equation for the pressure distribution.

$$\frac{\partial}{\partial x^+} \left(\frac{{h^+}^3}{6\,\mu^+} \frac{\partial p^+}{\partial x^+} \right) = \frac{\partial h^+}{\partial x^+} \tag{5.3}$$

with the boundary conditions

$$p^+ = p_i^+ \text{ at } x^+ = 0 \text{ and } p^+ = 0 \text{ at } x^+ = 1 \tag{5.4}$$

The energy equation is as follows

$$\rho^+ \left(u^+ \frac{\partial T^+}{\partial x^+} + v^+ \frac{\partial T^+}{\partial y^+} \right) = \frac{1}{P_e} \frac{\partial^2 T^+}{\partial {y^+}^2} + \frac{P_r\, E_c}{P_e} \mu^+ \left(\frac{\partial u^+}{\partial y^+} \right)^2 + \frac{P_r\, E_c}{P_e} u^+ \frac{dp^+}{dx^+} \tag{5.5}$$

where, ρ^+ and μ^+ are given by:

$$\rho^+ = 1 - \lambda^+ \left(T^+ - 1 \right), \quad \mu^+ = \exp \left[-\beta^+ \left(T^+ - 1 \right) \right] \tag{5.6}$$

Equation governing the heat conduction in the pad is

$$(h_1^+)^2 \frac{\partial^2 {T_p}^+}{\partial {x'}^{+2}} + \frac{\partial^2 {T_p}^+}{\partial {y'}^{+2}} = 0 \tag{5.7}$$

And the equation governing the heat conduction in the slider is

$$(h_{11}^+)^2 \frac{\partial^2 {T_s}^+}{\partial {x''}^{+2}} + \frac{\partial^2 {T_s}^+}{\partial {y''}^{+2}} = 0 \tag{5.8}$$

In view of the various industrial applications, the energy equation has been solved under the following different temperature boundary conditions:

- Case1:

  Lubricant boundary conditions:

  $\frac{\partial T^+}{\partial x^+} = 0$, on BC

  $T^+ = T_i^+ = 1.3$, on AD

  Pad boundary conditions:

  $T_p^+ = 1.3$, on DF

$T_p^+ = 1.3$, on CE

$T_p^+ = 1.3$, on EF

Slider boundary conditions:

$T_s^+ = 1.3$, on AG

$T_s^+ = 1.3$, on BH

$T_s^+ = 1.3$, on GH

Interface boundary conditions:

$T^+ = T_p{}^+$ and $k_s \frac{\partial T_p{}^+}{\partial y'^+} = k_f \frac{\partial T^+}{\partial y^+}$, on CD

$T^+ = T_s{}^+ = 1.3$ (or 1.2, or 1.1, or 1.0) and $k'_s \frac{\partial T_s{}^+}{\partial y''^+} = k_f \frac{\partial T^+}{\partial y^+}$, on AB

- Case2:

Lubricant boundary conditions:

$\frac{\partial T^+}{\partial x^+} = 0$, on BC

$T^+ = T_i^+ = 1.3$, on AD

Pad boundary conditions:

$\frac{\partial T_p{}^+}{\partial x'^+} = 0$, on DF

$\frac{\partial T_p{}^+}{\partial x'^+} = 0$, CE

$T_p{}^+ = 1.3$, on EF

Slider boundary conditions:

$\frac{\partial T_s{}^+}{\partial x''^+} = 0$, on AG

$\frac{\partial T_s{}^+}{\partial x''^+} = 0$, BH

$T_s{}^+ = 1.3$, on GH

Interface boundary conditions:

$T^+ = T_p{}^+$ and $k_s \frac{\partial T_p{}^+}{\partial y'^+} = k_f \frac{\partial T^+}{\partial y^+}$, on CD

$T^+ = T_s{}^+ = 1.3$ (or 1.2, or 1.1, or 1.0) and $k'_s \frac{\partial T_s{}^+}{\partial y''^+} = k_f \frac{\partial T^+}{\partial y^+}$, on AB

- Case3:

Lubricant boundary conditions:

$\frac{\partial T^+}{\partial x^+} = 0$, on BC

$T^+ = T_i^+ = 1.3$, on AD

Pad boundary conditions:

$\frac{\partial T_p^+}{\partial x'^+} = 0$, on DF

$\frac{\partial T_p^+}{\partial x'^+} = 0$, on CE

$\frac{\partial T_p^+}{\partial \vec{n}} = 0$, on EF

Slider boundary conditions:

$\frac{\partial T_s^+}{\partial x''^+} = 0$, on AG

$\frac{\partial T_s^+}{\partial x''^+} = 0$, on BH

$\frac{\partial T_s^+}{\partial \vec{n}} = 0$, on GH

Interface boundary conditions:

$T^+ = T_p^+$ and $k_s \frac{\partial T_p^+}{\partial y'^+} = k_f \frac{\partial T^+}{\partial y^+}$, on CD

$T^+ = T_s^+ = 1.3$ (or 1.2 or 1.1 or 1.0) and $k'_s \frac{\partial T_s^+}{\partial y''^+} = k_f \frac{\partial T^+}{\partial y^+}$, on AB

- Case4:

Lubricant boundary conditions:

$\frac{\partial T^+}{\partial x^+} = 0$, on BC

$T^+ = T_i^+ = 1.3$, on AD

Pad boundary conditions:

$\frac{\partial T_p^+}{\partial x'^+} = 0$, on DF

$\frac{\partial T_p^+}{\partial x'^+} = 0$, on CE

$-k_s \frac{\partial T_p^+}{\partial \vec{n}} = -H\ (T_p^+ - 1)$, on EF

Slider boundary conditions:

$\frac{\partial T_s^+}{\partial x''^+} = 0$, on AG

$\frac{\partial T_s^+}{\partial x''^+} = 0$, on BH

$-k'_s \frac{\partial T_s^+}{\partial \vec{n}} = -H\ (T_s^+ - 1)$, on GH

Interface boundary conditions:

$T^+ = T_p^+$ and $k_s \frac{\partial T_p^+}{\partial y'^+} = k_f \frac{\partial T^+}{\partial y^+}$, on CD

$T^+ = T_s^+ = 1.3$ (or 1.2 or 1.1 or 1.0) and $k'_s \frac{\partial T_s^+}{\partial y''^+} = k_f \frac{\partial T^+}{\partial y^+}$, on AB

The load carrying capacity (W^+) and the frictional drag (F^+) have been determined from equations (3.11) and (3.12) respectively.

5.3 Numerical Method

Let Ω the domain of interest be bounded in R^2 with a piecewise smooth boundary Γ. Let (x^+, y^+) denote the vector of spatial coordinate of a generic point in $\bar{\Omega}$ and $\vec{n}$ is the outward unit normal vector drawn at any point (x^+, y^+) on Γ. Now the variational principle $\Pi(p)$ for the Reynolds equation (5.3) in Ω is given by:

$$\Pi(p) = \int_\Omega [\ \frac{h^{+3}}{12\ \mu^+}\ (\ \frac{\partial p^+}{\partial x^+}\ )^2 - h^+\ \frac{\partial p^+}{\partial x^+}\ ]\ d\Omega \tag{5.9}$$

The weighted residual formulation of the energy equation is given by (Reddi [70]).

$$\int_\Omega \tilde{W}_l\ [\ \rho^+(u^+\ \frac{\partial T^+}{\partial x^+} + v^+\ \frac{\partial T^+}{\partial y^+}) - \frac{1}{P_e}\ \frac{\partial^2 T^+}{\partial y^{+2}} - \frac{P_r\ E_c}{P_e}\ \mu^+\ (\ \frac{\partial u^+}{\partial y^+}\ )^2 - \frac{P_r\ E_c}{P_e}\ u^+\ \frac{dp^+}{dx^+}\ ]\ d\Omega \tag{5.10}$$

where, $\tilde{W}_l$ is the modified SUPG weight function. It is to be noted that ρ^+, μ^+ are dependent on T^+ and are defined in equation (5.6). Galerkin formulation for the heat conduction in the pad is given by:

$$\int_{\Omega'}\ [\ (h_1{}^+)^2\ \frac{\partial^2 T_p{}^+}{\partial x'^{+2}} + \frac{\partial^2 T_p{}^+}{\partial y'^{+2}}\ ]\ w_l\ \ d\Omega' = 0 \tag{5.11}$$

And the Galerkin formulation for the heat conduction in the moving slider is

$$\int_{\Omega''}\ [\ (h_{11}^+)^2\ \frac{\partial^2 T_s{}^+}{\partial x''^{+2}} + \frac{\partial^2 T_s{}^+}{\partial y''^{+2}}\ ]\ w_l\ \ d\Omega'' = 0 \tag{5.12}$$

Now to reduce the lubrication problem to one of finite number of unknowns, the solution domain is divided into bilinear rectangular elements and the field variables (pressures,velocities and temperatures) are expressed in terms of approximating trial functions N_i within each element. Now Ω, Ω', Ω'' are discretized into N_e bilinear rectangular elements such that:

$$\cup_{e=1}^{N_e}\ \bar{\Omega}^e = \bar{\Omega} \qquad \cap_{e=1}^{N_e}\ \bar{\Omega}^e = \phi$$

$$\cup_{e=1}^{N_e} \bar{\Omega'}^e = \bar{\Omega'} \qquad \cap_{e=1}^{N_e} \bar{\Omega'}^e = \phi$$

$$\cup_{e=1}^{N_e} \bar{\Omega''}^e = \bar{\Omega''} \qquad \cap_{e=1}^{N_e} \bar{\Omega''}^e = \phi$$

where, Ω^e denotes the interior domain of an element. Let Γ^e be the boundary of Ω^e. The discretized representation of the field variables are given by:

$$u_e^+ \approx \sum_{k=1}^{N_{el}} N_k \, u_k^{+^e}, \qquad v_e^+ \approx \sum_{k=1}^{N_{el}} N_k \, v_k^{+^e}, \qquad p_e^+ \approx \sum_{k=1}^{N_{el}} N_k \, p_k^{+^e},$$

$$T_e^+ \approx \sum_{k=1}^{N_{el}} N_k \, T_k^{+^e}. \qquad T_e^{p^+} \approx \sum_{k=1}^{N_{el}} N_k \, T_k^{p^{+^e}}.$$

where, $N_{el} = 2$ for pressure case and $N_{el} = 4$ for velocities and temperatures. Introducing these elemental discretization details into equations (5.9) - (5.12), we obtain element level representations. The element level representation of equation (5.11) is given by:

$$\int_{\Omega^e} \{ \frac{h^{+3}}{12\,\mu^+} [\frac{\partial}{\partial x^+} (\sum_{j=1}^{N_{el}} p_j^{+^e} N_j^e)]^2 - h^+ \frac{\partial}{\partial x^+} (\sum_{j=1}^{N_{el}} p_j^{+^e} N_j^e) \} \, d\Omega^e = 0 \qquad (5.13)$$

on minimizing the equation with respect to variables p_j^e and on further simplification one would arrive at the following equation.

$$\sum_{j=1}^{N_{el}} \int_{\Omega^e} [\frac{h^{+3}}{6\,\mu^+} \frac{\partial N_j^e}{\partial x^+} \frac{\partial N_i^e}{\partial x^+}] \, p_j^{+^e} d\Omega^e = \int_{\Omega^e} h^+ \frac{\partial N_i^e}{\partial x^+} \, d\Omega^e \qquad (5.14)$$

Now with the SUPG analysis of Brooks and Higher [68] and Grygiel and Tanguy [71] one would obtain the following discretized elemental energy equation.

$$\sum_j \int_{\Omega^e} \{ \tilde{W} \, (1 - \lambda^+ \, (\sum_k N_k^e T_k^{+^e} - 1)) \, [\, (\sum_k u_k^{+^e} N_k^e) \, \frac{\partial N_j^e}{\partial x^+} + (\sum_k v_k^{+^e} N_k^e) \, \frac{\partial N_j^e}{\partial y^+} \,]$$
$$+ \frac{1}{P_e} (\frac{\partial w_i}{\partial y^+} \frac{\partial N_j^e}{\partial y^+}) \} T_j^{+^e} d\Omega^e = \int_{\Omega^e} [\tilde{W} \, \frac{P_r E_c}{P_e} (\exp(-\beta^+ (\sum_k N_k^e T_k^{+^e} - 1))) (\frac{\partial}{\partial y^+} (\sum_k N_k^e u_k^{+^e}))^2$$
$$- (\sum_k N_k^e u_k^{+^e}) \, (\frac{d}{dx^+} (\sum_k N_k^e p_k^{+^e}))] \, d\Omega^e \qquad (5.15)$$

where,

$$\tilde{W}_l = w_i + P_i \quad w_i = N_i \text{ and } P_i = \frac{\tilde{k}\ \hat{u_j}\ w_{i,j}}{\|u\|}$$

And the upwind parameter $\hat{k}$ is calculated using elemental dimensions and elemental velocity (Grygiel and Tanguy [71] and Brooks and Hughes [68]). The discretized elemental level heat conduction equation in the pad is given by:

$$\int_{\Omega'^e} [\ w_i\ \ (h_1^+)^2\ \frac{\partial w_i}{\partial x'^+}\ \frac{\partial N_j{}^e}{\partial x'^+} + \frac{\partial w_i}{\partial y'^+}\ \frac{\partial N_j{}^e}{\partial y'^+}]\ T_{p_j}^{+e}\ d\Omega'^e = 0 \tag{5.16}$$

And the discretized elemental level heat conduction equation in the moving slider is

$$\int_{\Omega''^e} [\ w_i\ \ (h_{11}^+)^2\ \frac{\partial w_i}{\partial x''^+}\ \frac{\partial N_j{}^e}{\partial x''^+} + \frac{\partial w_i}{\partial y''^+}\ \frac{\partial N_j{}^e}{\partial y''^+}]\ T_{s_j}^{+e}\ d\Omega''^e = 0 \tag{5.17}$$

Now based on equations (5.14) - (5.17) the numerical simulations have been carried out on a 30 × 30 finite element mesh system. The results have been obtained to an accuracy of $\epsilon = 5.0 \times 10^{-4}$ i.e

$$(\ \max\ (\ \frac{|\ \gamma_j^{New} - \gamma_j^{Old}\ |}{|\ \gamma_j^{New}\ |}\ )\ ) \leq \epsilon$$

for $i = 1, 2, \cdots, \mathrm{n}, \cdots$. where, γ_i represents any of the field variables $p_j^+, u_j^+, v_j^+, T_j^+$.

5.4 Results and Discussion

The simulations have been carried out on 30 × 30 mesh system. The results have been computed for load carrying capacity, drag force, velocity, pressure and temperature fields. These are presented in the form of computer generated plots and tables on a 30 × 30 mesh system.

The non dimensional load carrying capacity and frictional drag force obtained for k = 0.4, $p_i^+ = 1$, $T_i^+ = T_s^+ = 1.3$ are shown in Table 5.1 for various thermal boundary conditions viz. Case1, Case2, Case3, Case4.

Considering Case4, as a natural heat conduction to the environment, the load carrying capacity at different values of x^+ and for two different inlet temperatures are shown in

Figure 5.2. From this Figure one can notice that for fixed values of x^+, lowering the slider temperature (T_s^+) below the inlet lubricant temperature lead to thermal boosting of the slider bearing performance.

Table 5.1: Comparison of load carrying capacity and frictional drag force at different thermal boundary conditions for $p_i^+ = 1$, $k = 0.4$, $T_i^+ = T_s^+ = 1.3$

Boundary conditions	Case1	Case2	Case3	Case4
W^+	0.7371731	0.7371749	0.7371752	0.7371781
F^+	0.2016197	0.2016298	0.2011301	0.2011315

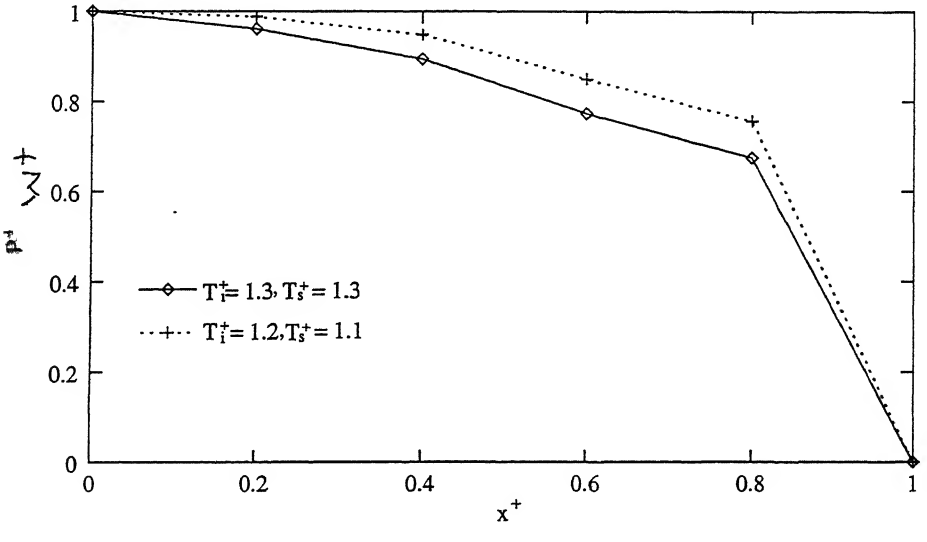

Figure 5.2: Pressure distribution along the sliding direction of the bearing at $k = 0.4$, $p_i^+ = 1$, Case4

In Figure 5.3 pad distribution is shown for different slider temperatures. One can notice that when the non dimensional slider temperature is kept at $T_s^+ = 1.0$ and the inlet lubricant temperature at $T_i^+ = 1.3$, peak pressures are observed at $x^+ = 0.8$ for $p_i^+ = 0$. Both these observations can be attributed to the fall in the average temperature of the lubricant in the domain under consideration, on lowering the slider temperature. From the expression for viscosity μ (T^+), it is clear that for fixed β^+ lowering T^+ leads to higher values for viscosity. Higher the viscosity higher will be the threshold for thermal deformation of the lubricant

and this leads to improved performance of the slider bearing.

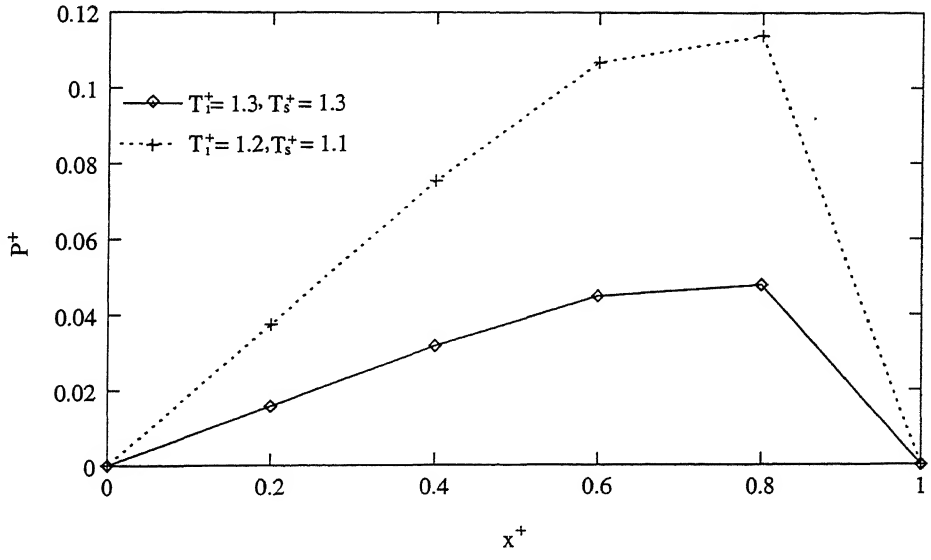

Figure 5.3: Pressure distribution along the sliding direction of the bearing at $k = 0.4$, $p_i^+ = 0$, Case4

The combined effect of thermal boosting and geometric configuration of slider bearing on load carrying capacity and frictional drag are presented in Figure 5.4 and 5.5 respectively for Case4 at $p_i^+ = 1$.

From the plots given in Figure 5.4 and 5.5, it is clear that decreasing either k or T_s^+ or both simultaneously enhances the load carrying capacity but lowers the frictional drag values. Further the combined influence of k and T_s^+ on frictional drag force is clearly seen at all values of k, it is predominantly seen for $0.4 \leq k \leq 0.8$ on load carrying capacity. In the case $k = 0.4$, thermal boosting i.e $T_s^+ = 1.1$, has brought in nearly two fold increase in the load carrying capacity. It may also be interesting to trace the pressures along the sliding direction on the pad for $k = 0.4$ at $p_i^+ = 0$. Hence in Figure 5.6 the corresponding pressures along the pad are presented.

From the Figure 5.6 one may notice that a reduction in the $T_s^+ = 1.2$ does not shift the location of the maximum pressure on the pad significantly. This result is very much in conformity with the standard results for slider bearings (Pinkus and Strenlicht [74]).

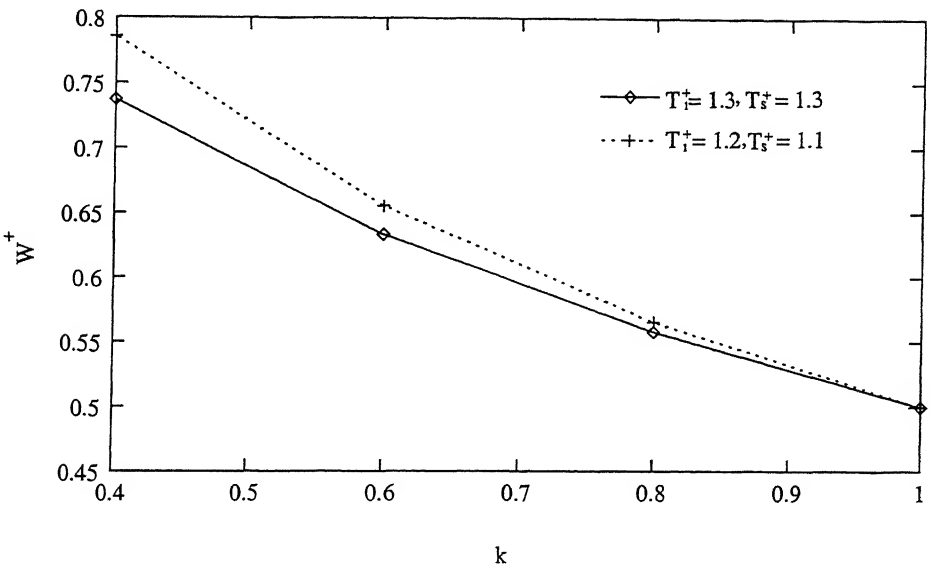

Figure 5.4: Load carrying capacity versus k at $p_i^+ = 1$

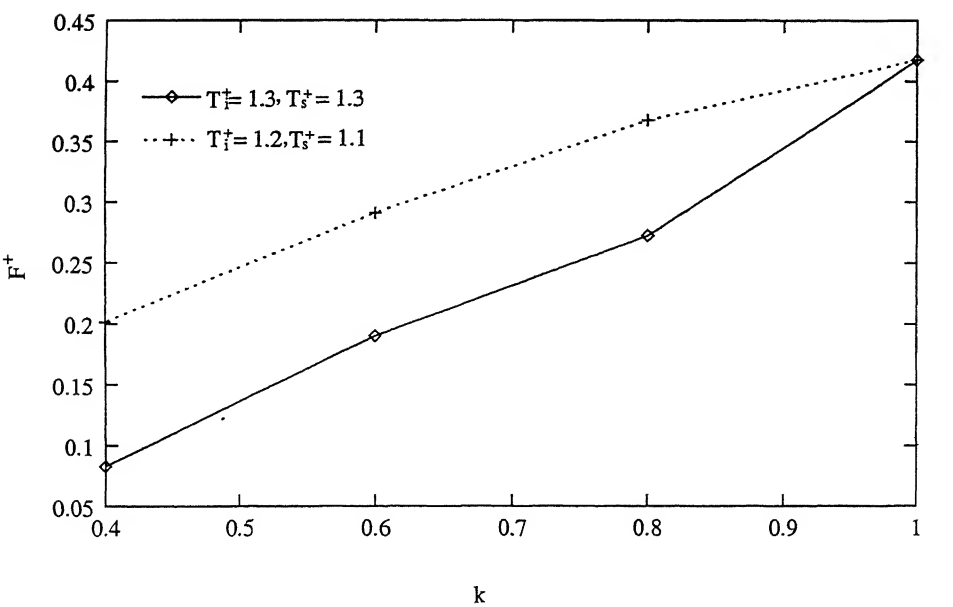

Figure 5.5: Frictional drag force versus k at $p_i^+ = 1$, Case1

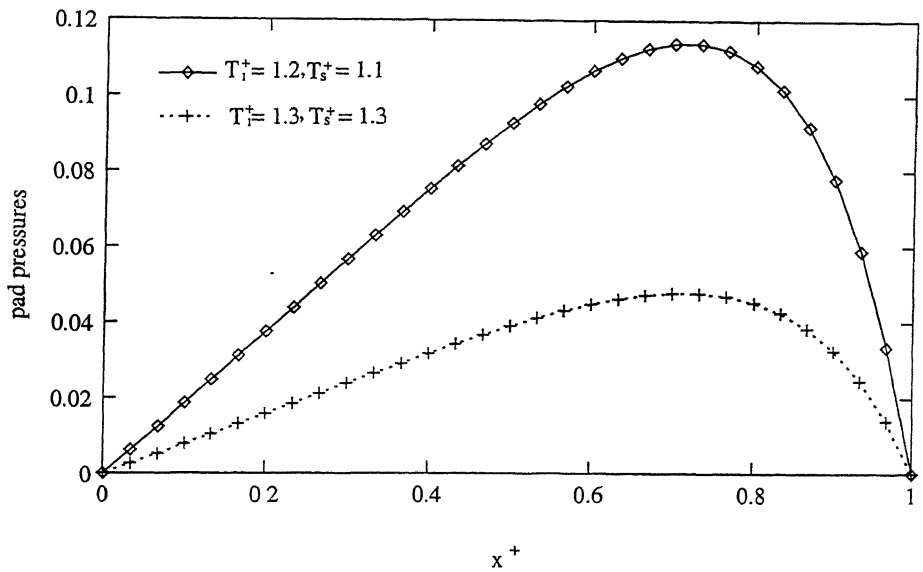

Figure 5.6: Pad pressures along the sliding direction of the bearing at $k = 0.4$, $p_i^+ = 1$

An interesting feature which one may notice in Figure 5.6 is that in the thermal boosting case the pressure peak is more pronounced (around $x^+ = 0.75$ to 0.8).

The influence of solid pad and moving slider with various thermal boundary conditions described by Case1 (pad with isothermal side and top face, slider isothermal side and bottom face), Case2 (Pad with adiabatic sides and top, slider with adiabatic sides and bottom) and Case4 (pad with adiabatic sides and exposed top, slider with adiabatic sides and exposed bottom) on the load carrying capacity and frictional drag force in the fluid film has been analyzed for $T_s^+ = 1.3$, $T_i^+ = 1.3$, $p_i^+ = 1$, $k = 0.4,\ 1$. These results are presented in Tables 5.2 - 5.4. Table 5.2 depicts the results for parallel slider bearing. It is seen that a finite load is generated, due to the assumption of the fore=region pressure. This load remains unaffected by the various thermal boundary conditions. It is observed that even if we reduce the slider temperature below the inlet temperature there is no change in the load carrying capacity (See Tables 5.3 and 5.4), however a slight variation is observed in the frictional drag force.

It is observed that even if we reduce the slider temperature below the inlet temperature there is no change in the load carrying capacity (See Tables 5.3 and 5.4), however a slight variation is observed in the frictional drag force.

Table 5.2: Comparison of load carrying capacity and frictional drag force at different thermal boundary conditions for $p_i^+ = 1,\ k = 1,\ T_i^+ = T_s^+ = 1.3$

Boundary conditions	Case1	Case2	Case3	Case4
W^+	0.4999992	0.4999993	0.5000002	0.4999992
F^+	0.417500	0.4176240	0.40002	03951091

Table 5.3: Comparison of load carrying capacity and frictional drag force at different thermal boundary conditions with $p_i^+ = 1,\ k = 0.4,\ T_i^+ = T_s^+ = 1.3$ for Case1

	$k = 0.4$	$k = 0.6$	$k = 0.8$	$k = 1.0$
W^+	0.785592	0.6554149	0.5655332	0.4999992
f	0.0828 ;9	0.1903 ;62	0.272 ;2 ;	[illegible]

Table 5.4: Comparison of load carrying capacity.and frictional drag force at different thermal boundary conditions with $p_i^+ = 1,\ k = 0.4,\ T_i^+ = 1.2,\ T_s^+ = 1.1$ for Case1

	$k = 0.4$	$k = 0.6$	$k = 0.8$	$k = 1.0$
W^+	0.7855930	0.6554189	0.5655632	0.4999992
F^+	0.0862	0.19312	0.28127	0.44700

To further investigate this, average temperature flux across the slider-lubricant and pad-lubricant are evaluated for the Case4 thermal boundary condition. These interface temperatures at various sliding directions are shown in the Figure 5.7 and 5.8.

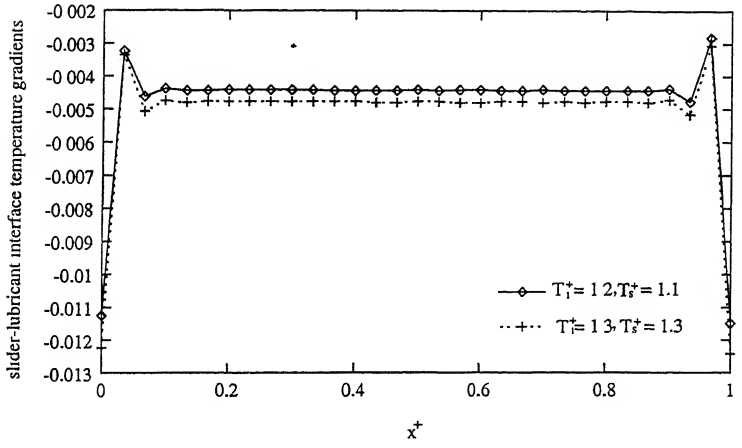

Figure 5.7: Slider-lubricant interface temperature gradients along the sliding direction of the bearing at $k = 0.4$, $p_i^+ = 1$

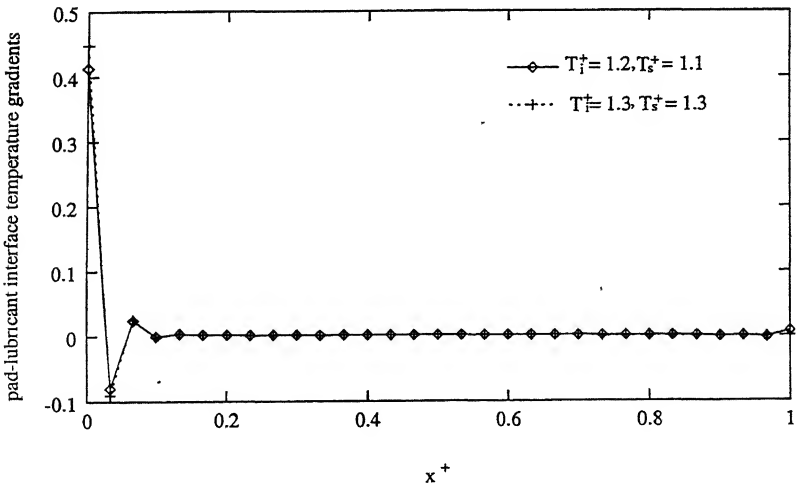

Figure 5.8: Pad-lubricant interface temperature gradients along the sliding direction of the bearing at $k = 0.4$, $p_i^+ = 1$

From Figure 5.7 one can notice that there is a very little variation in slider-lubricant interface temperature gradients, thus the thermal boosting is not sufficient to bring forth any significant changes in the load carrying capacity. Whereas in Figure 5.8 absolutely no changes in the pad-lubricant interface temperature gradients are observed.

To further assess the influence of flux boundary conditions, pad temperatures at various values of x^+ are shown in Figure 5.9. From this Figure one can conclude that although the pad temperatures are slightly high for $T_i^+ = 1.3$, $T_s^+ = 1.3$ compared to the thermal boosting case $T_i^+ = 1.2$, $T_s^+ = 1.1$ for the Case4 at $p_i^+ = 1$, $k = 0.4$, but are not sufficient enough to bring a significant change in load carrying capacity as seen in Tables 5.1 - 5.4.

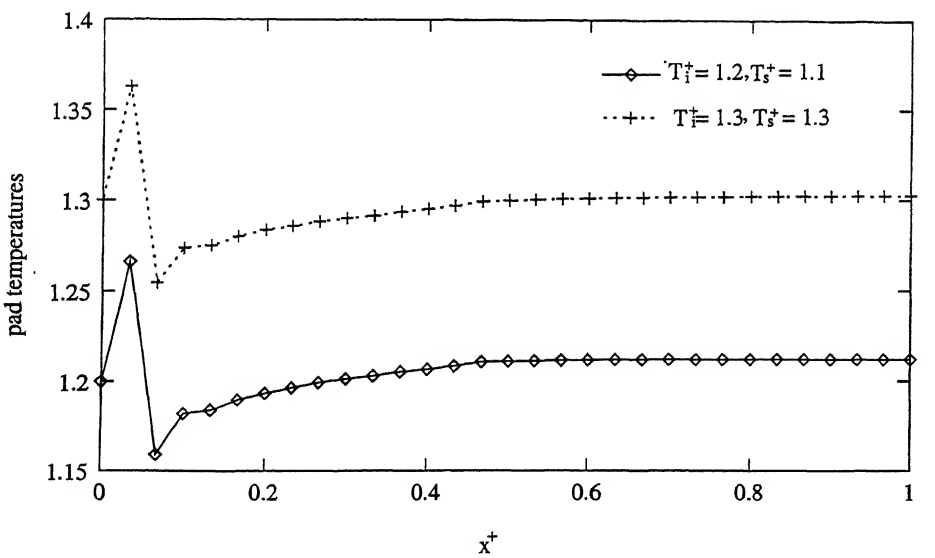

Figure 5.9: Pad temperatures along the sliding direction of the bearing at $k = 0.4, p_i^+ = 1$

In Figure 5.10 the u-velocity contours are plotted at $p_i^+ = 1, k = 0.4, T_i^+ = 1.3, T_s^+ = 1.3$ for Case1 and Case2 respectively. From these Figures we see the manifestation of recirculation zones in region R. These zones can be attributed primarily to the thermal boundary conditions and partly to the geometric configurations of the slider bearings.

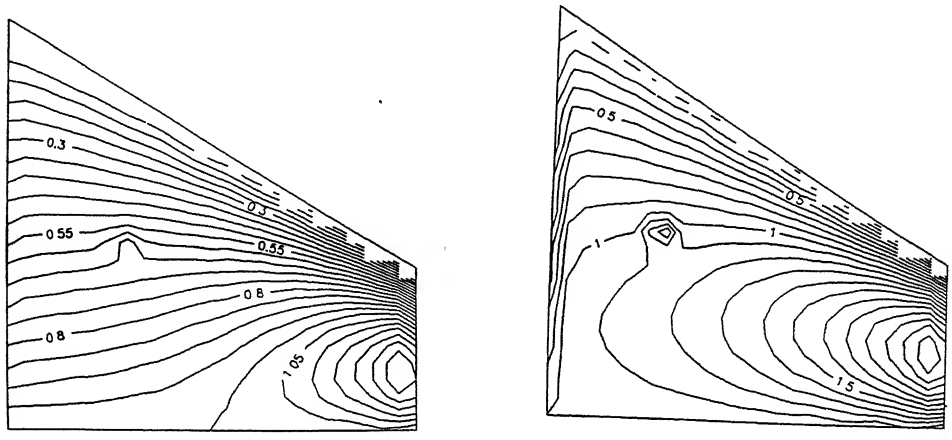

(a) (b)

Figure 5.10: u-velocity contours at $p_i^+ = 1$, $k = 0.4$, $T_i^+ = T_s^+ = 1.3$ for (a) Case1 (b) Case2

5.5 Conclusions

Load carrying capacity and frictional drag of a high speed slider bearing with a solid pad for various thermal boundary conditions in conjunction with thermal boosting for various geometric configurations have been numerically analyzed using FEM. Density and the Viscosity in the mathematical model describing the slider bearing configuration are treated as functions of temperature. SUPG weight functions are found to be effective in precluding the numerical oscillations and in obtaining a convergent solution. Load carrying capacity of slider bearing can be thermally boosted by setting slider at temperatures lower than that of incoming lubricant. Though solid pad and slider conduction with different boundary settings as chosen in this study from application point of view alters the temperature field in the pad and thermal flux across the fluid-solid interface changes marginally and thus the load carrying capacity of the slider bearing remains unaffected. It is to be noted that the isothermal pad employed in the present study have been set at temperature similar to that of inlet flow.

Chapter 6

Thermohydrodynamic Analysis of a Tilted Pad Slider Bearing Considering Fluid Inertia

6.1 Introduction

In the previous Chapters, we have used Reynolds equation which explains the process of hydrodynamic lubrication in both qualitative and quantitative terms. The validity of the equation rests on the physical fact that the height of the fluid film is very small compared to its other physical dimensions. As a consequence all the hydrodynamic variations across the fluid film are negligible and the relevant Reynolds number in the bearings is usually small enough in case of laminar flows for the inertia and the turbulence effects to be neglected. At sufficient large Reynolds number and at high operating speeds and at low viscosity of the lubricant, the inertia force of the lubricant become of the same order of magnitude as the shearing force and the laminar flow gives way in stages to a turbulent state. However, even at moderate Reynolds numbers, for laminar flow of the lubricant, the contribution of the inertia force to the dynamics of bearings remain small. Thus, one visualizes (ref. Pinkus and Sternlich [74]) three broad regimes of the bearing operation: a lower regime of laminar flow in which the viscous forces are dominant (as we have seen in Chapters 3, 4 and 5), a

narrow intermediate regime in which the flow is still laminar but both viscous and inertia forces are significant, and an upper regime in which turbulent conditions prevail. The lower regime is exceptionally well described by Reynolds theory. On the other hand, in the narrow intermediate regime the existing theoretical formulations, like the iteration technique or the average inertia techniques, are applicable for one dimensional incompressible problems only and are not amenable to extensions. Apart from that these techniques cannot be looked upon as parts of a uniformly valid theory connecting the lower two regimes. As a consequence the utility of such scheme is very limited.

In this Chapter, we have investigated the influence of convective inertia, various temperature boundary prescriptions and thermal boosting on bearing characteristics. The equations of mass, momentum and thermal energy conservations with temperature dependent density and viscosity (which brings in extra pseudo compressibility terms into the energy equation) have been solved in a decoupled fashion using the SUPGFEM.

6.2 Governing Equations

$$\frac{\partial}{\partial x^+}\left(\rho^+ u^+\right) + \frac{\partial}{\partial y^+}\left(\rho^+ v^+\right) = 0 \tag{6.1}$$

$$R_e^* \rho^+ \left(u^+ \frac{\partial u^+}{\partial x^+} + v^+ \frac{\partial u^+}{\partial y^+} \right) = - \frac{dp^+}{dx^+} + \frac{\partial}{\partial y^+}\left(\mu^+ \frac{\partial u^+}{\partial y^+}\right) \tag{6.2}$$

$$\rho^+ \left(u^+ \frac{\partial T^+}{\partial x^+} + v^+ \frac{\partial T^+}{\partial y^+} \right) = \frac{1}{P_e} \frac{\partial^2 T^+}{\partial y^{+2}} + \frac{P_r\, E_c}{P_e} \mu^+ \left(\frac{\partial u^+}{\partial y^+} \right)^2 + \frac{P_r\, E_c}{P_e} u^+ \frac{dp^+}{dx^+} \tag{6.3}$$

where, ρ^+, μ^+, h^+, k and R_e^* are given by:

$$\rho^+ = 1 - \lambda^+ \left(T^+ - 1 \right), \quad \mu^+ = \exp\left[-\beta^+ \left(T^+ - 1 \right) \right] \tag{6.4}$$

$$h^+ = 1 - x^+ \left(1 - k \right), \quad k = \frac{h_0}{h_i} \leq 1, \quad R_e^* = \frac{\rho_a U B}{\mu_a} \left(\frac{h_o}{B}\right)^2 \tag{6.5}$$

The boundary conditions on the model are as follows:

$$\text{At inlet}: \quad u^+ = 1 - y^+, \; v^+ = 0, \; p^+ = {p_i}^+ \tag{6.6}$$

$$\text{At outlet}: \quad \frac{\partial u^+}{\partial x^+} = \frac{\partial v^+}{\partial y^+} = {p_i}^+ = 0 \tag{6.7}$$

$$\text{On the pad}: \quad u^+ = v^+ = \frac{\partial p^+}{\partial \vec{n}} = 0 \tag{6.8}$$

$$\text{On the slider}: \quad u^+ = 1, v^+ = \frac{\partial p^+}{\partial \vec{n}} = 0 \tag{6.9}$$

In view of the industrial applications, the energy equation has been solved under the following different temperature boundary conditions:

- Case1: (Isothermal slider and isothermal pad: ISIP or no flux)

  On slider: $T^+(x^+, 0) = {T_s}^+$

  On pad: $T^+(x^+, h^+) = {T_p}^+$

  In the current study, ${T_s}^+ = {T_p}^+ = {T_i}^+$

- Case2: (Isothermal slider and adiabatic pad: ISAP or zero half flux)

  On slider: $T^+(x^+, 0) = {T_s}^+ \; (= {T_i}^+)$

  On pad: $\frac{\partial T^+}{\partial \vec{n}} \; (x^+, h^+) = 0$

- Case3: (Adiabatic slider and Adiabatic pad: ASAP or zero full flux)

  On slider: $\frac{\partial T^+}{\partial n^+} = 0$

  On pad $\frac{\partial T^+}{\partial \vec{n}} = 0$

- Case4: (Isothermal slider and exposed pad: ISEP or non zero half flux)

  On slider: $T^+(x^+, 0) = {T_s}^+ (= {T_i}^+)$

  On pad $k \; \frac{\partial T^+}{\partial \vec{n}} = H \; (T^+ - 1) (= \delta)$

- Case5: (Thermal boosting slider and pad: TBSP)

  (i). ${T_p}^+ = {T_s}^+ > {T_i}^+ \quad (ii). {T_p}^+ > {T_s}^+ > {T_i}^+$

  (iii). ${T_s}^+ > {T_p}^+ > {T_i}^+ \quad (iv). {T_p}^+ = {T_s}^+ < {T_i}^+$

The combination of T_p^+, T_s^+, T_i^+ which enhance the load carrying capacity of a slider bearing constitutes a thermal boosting model. At the inlet/outlet the following boundary conditions

are used:

$$\text{At inlet: } T^+(0, y^+) = T_i{}^+$$
$$\text{At outlet: } \frac{\partial T^+}{\partial x^+} = 0$$

The load carrying capacity (W^+) and the frictional drag force (F^+) have been determined by the following expressions:

$$W^+ = \int_0^1 \hat{p}^+ \; dx^+ \tag{6.10}$$

$$F^+ = \int_0^1 \left(\mu^+ \frac{\partial u^+}{\partial y^+} \right) \quad \text{at } y^+ = 0 \; dx^+ \tag{6.11}$$

where, $\hat{p}^+$, W^+, F^+ are given by:

$$\hat{p}^+ = \frac{1}{h} \int_0^h p(x, y) \, dy, \quad W^+ = \frac{W}{\rho_a \, U^2 \, B}, \quad F^+ = \frac{F h_o}{\mu_a \, U \, B}$$

6.3 Finite Element Formulation & Solution procedure

Let $\Omega \subset \Re^2$ the domain of interest be bounded by a a piecewise smooth curve Γ. Let (x^+, y^+) denote any point in $\bar{\Omega}$ in the cartesian coordinate system and $\vec{n}$ be the outward unit normal drawn at any point (x^+, y^+) on Γ. Substitution for ρ^+, μ^+ and h^+ into equations (6.2) and (6.3) and using equation (6.1) yields the following equations:

$$[1 - \lambda^+(T^+ - 1)] \left(\frac{\partial u^+}{\partial x^+} + \frac{\partial v^+}{\partial y^+}\right) - \lambda^+ \left(u^+ \frac{\partial T^+}{\partial x^+} + v^+ \frac{\partial T^+}{\partial y^+}\right) = 0 \tag{6.12}$$

$$[1 - \lambda^+(T^+ - 1)] \, R_e^* \left(u^+ \frac{\partial u^+}{\partial x^+} + v^+ \frac{\partial v^+}{\partial y^+}\right) = - \frac{dp^+}{dx^+}$$

$$+ \; e^{-\beta^+(T^+ - 1)} \left(\frac{\partial^2 u^+}{\partial y^{+2}} - \beta^+ \frac{\partial T^+}{\partial y^+} \frac{\partial u^+}{\partial y^+}\right) \tag{6.13}$$

$$[1 - \lambda^+(T^+ - 1)] \left(u^+ \frac{\partial u^+}{\partial x^+} + v^+ \frac{\partial v^+}{\partial y^+}\right) = \frac{1}{Pe} \frac{\partial^2 T^+}{\partial y^{+2}}$$

$$+ \; \frac{Ec \; Pr}{Pe} \, e^{-\beta^+(T^+ - 1)} \left(\frac{\partial u^+}{\partial y^+}\right)^2 + \frac{Ec \; Pr}{Pe} \, u^+ \frac{dp^+}{dx^+} \tag{6.14}$$

6.3.1 Petrov-Galerkin Formulation

The Petrov-Galerkin weighted residual formulation of equations (6.12) - (6.14) gives the following equations:

$$\int_\Omega \{[1-\lambda^+(T^+-1)]\,(\frac{\partial u^+}{\partial x^+}+\frac{\partial v^+}{\partial y^+})-\lambda^+\,(u^+\frac{\partial T^+}{\partial x^+}+v^+\frac{\partial T^+}{\partial y^+})\}\,\tilde{W}\,d\Omega=0 \quad (6.15)$$

$$\int_\Omega \{[1-\lambda^+(T^+-1)]\,R_e^*\,(u^+\frac{\partial u^+}{\partial x^+}+v^+\frac{\partial v^+}{\partial y^+})+\frac{dp^+}{dx^+}$$

$$-\,e^{-\beta^+(T^+-1)}\,(\frac{\partial^2 u^+}{\partial y^{+2}}-\beta^+\,\frac{\partial T^+}{\partial y^+}\,\frac{\partial u^+}{\partial y^+})\}\,\tilde{W}\,d\Omega=0 \quad (6.16)$$

$$\int_\Omega \{[1-\lambda^+(T^+-1)]\,(u^+\frac{\partial u^+}{\partial x^+}+v^+\frac{\partial v^+}{\partial y^+})-\frac{1}{Pe}\,\frac{\partial^2 T^+}{\partial y^{+2}}$$

$$-\,\frac{Ec\,Pr}{Pe}\,e^{-\beta^+(T^+-1)}\,(\frac{\partial u^+}{\partial y^+})^2-\frac{Ec\,Pr}{Pe}\,u^+\,\frac{dp^+}{dx^+}\}\tilde{W}\,d\Omega=0 \quad (6.17)$$

Now to reduce the lubrication problem to one of finite number of unknowns, the solution domain is divided into bilinear rectangular elements and the field variables (pressure, velocities and temperature) are expressed in terms of approximating trial functions N_i within each element. The domain now Ω is discretized into N_e bilinear rectangular elements such that:

$$\cup_{e=1}^{N_e}\,\bar{\Omega}^e=\bar{\Omega} \qquad \cap_{e=1}^{N_e}\,\bar{\Omega}^e=\phi$$

where, Ω^e denotes the interior domain of an element. Let Γ^e be the boundary of Ω^e. The discretized representation of the field variables are given by:

$$u_e^+\approx\sum_{k=1}^{N_{el}}N_k\,u_k^{+^e},\qquad v_e^+\approx\sum_{k=1}^{N_{el}}N_k\,v_k^{+^e},\qquad p_e^+\approx\sum_{k=1}^{N_{el}}N_k\,p_k^{+^e},$$

$$T_e^+\approx\sum_{k=1}^{N_{el}}N_k\,T_k^{+^e}.$$

Considering the Petrov-Galerkin weighted residual formulation of equations (6.15) - (6.17) and introducing the above finite element discretizations we obtain the following:

$$\int_{\cup_e \Omega^e} \{[1-\lambda^+(\sum_{k=1}^{N_{el}} N_k{}^e T_k^{+^e} - 1)\,][\frac{\partial}{\partial x^+}(\sum_{k=1}^{N_{el}} N_k{}^e u_k^{+^e}) + \frac{\partial}{\partial y^+}(\sum_{k=1}^{N_{el}} N_k{}^e v_k^{+^e})] - \lambda^+ [(\sum_{i=1}^{N_{el}} u_i^{+^e} N_i^e)(\frac{\partial}{\partial x^+}(\sum_{k=1}^{N_{el}} T_k^{+^e} N_k{}^e)) + (\sum_{i=1}^{N_{el}} v_i^{+^e} N_i^e)(\frac{\partial}{\partial y^+}(\sum_{k=1}^{N_{el}} T_k^{+^e} N_k{}^e))]\} \tilde{W}_l \, d\Omega = 0 \tag{6.18}$$

$$\int_{\cup_e \Omega^e} \{(1-\lambda^+(\sum_{k=1}^{Nel}(T_k^{+^e} N_k) - 1))R_e^*((\sum_{i=1}^{N_{el}} u_i^{+^e} N_i^e)\frac{\partial}{\partial x^+}(\sum_{k=1}^{Nel} u_k^{+^e} N_k^e) + (\sum_{i=1}^{N_{el}} v_i^{+^e} N_i^e)\frac{\partial}{\partial y^+}(\sum_{k=1}^{N_{el}} u_k^{+^e} N_k^e)) + \frac{d}{dx^+}(\sum_{k=1}^{N_{el}} N_k^e p_k^{+^e}) - \exp[-\beta^+(\sum_{i=1}^{N_{el}} T_i^{+^e} N_i^e - 1)](\frac{\partial^2}{\partial y^{+2}}(\sum_{k=1}^{Nel} u_k^{+^e} N_k^e) - \beta^+ \frac{\partial}{\partial y^+}(\sum_{k=1}^{N_{el}} u_k^{+^e} T_k^{+^e}) \frac{\partial}{\partial y^+}(\sum_{j=1}^{N_{el}} N_j^e u_j^{+^e}))\} \tilde{W}_l \, d\Omega = 0 \tag{6.19}$$

$$\int_{\cup_e \Omega^e} \{(1-\lambda^+(\sum_{k=1}^{N_{el}}(T_k^{+^e} N_k) - 1))((\sum_{i=1}^{N_{el}} u_i^{+^e} N_i^e)\frac{\partial}{\partial x^+}(\sum_{k=1}^{N_{el}} T_k^{+^e} N_k^e) + (\sum_{i=1}^{N_{el}} v_i^{+^e} N_i^e)\frac{\partial}{\partial y^+}(\sum_{k=1}^{N_{el}} T_k^{+^e} N_k^e)) - \frac{1}{P_e}\frac{\partial^2}{\partial y^{+2}}(\sum_{k=1}^{N_{el}} T_k^{+^e} N_k^e) - \frac{P_r E_c}{P_e}\exp[(-\beta^+(\sum_{i=1}^{N_{el}} T_i^{+^e} N_i^e - 1))](\frac{\partial}{\partial y^+}(\sum_{k=1}^{N_{el}} N_k^+ u_k^{+^e}))^2 - \frac{P_r E_c}{P_e}(\sum_{i=1}^{N_{el}} N_i^+ u_i^{+^e})\frac{d}{dx^+}(\sum_{k=1}^{N_{el}} N_k^e p_k^{+^e})\} \tilde{W}_l \, d\Omega = 0 \tag{6.20}$$

where the Petrov-Galerkin weight function $\tilde{W}_l$ is defined by:

$$\tilde{W}_l = w_i + P_i, w_l = N_i, P_i = \frac{\tilde{k}\hat{u}_j w_{i,j}}{||u||}$$

The upwind parameter $\tilde{k}$ is calculated using elemental dimensions and elemental velocity (Grygiel and Tanguy [71], Brooks and Hughes [68]). Following the SUPG analysis of Brooks and Hughes [68], equations (6.19) and (6.20) can be cast into the weak form neglecting the inter element jumps arising out of definition of P_i. This is justified as the bilinear elements

employed in the present analysis satisfy the required criteria like non-skewness as mentioned by Brooks and Hughes [68]. For solution evaluation a decoupled approach is taken. From equations (6.18) - (6.20) and boundary conditions the following decoupled equations are obtained for u^+, v^+, and T^+:

(a) Decoupled equation for u^+ obtained from equation (6.16) is the following:

$$\sum_{k=1}^{N_{el}} \int_{\cup_e \Omega^e} \{ [(1-\lambda^+(\sum_{i=1}^{N_{el}} N_i{}^e T_i{}^{+e^{(n-1)}} - 1))\, R_e^* \,((\sum_{i=1}^{N_{el}} N_i{}^e u_i{}^{+e^{(n-1)}})\ \frac{\partial}{\partial x^+} N_k{}^e + (\sum_{i=1}^{N_{el}} N_i{}^e v_i{}^{+e^{(n-1)}})\ \frac{\partial}{\partial y^+} N_k{}^e)$$

$$+\ \beta^+ \exp\,[-\beta^+ (\sum_{i=1}^{N_{el}} T_i{}^{+e^{(n-1)}} N_i{}^e - 1)]\ \frac{\partial}{\partial y^+} (\sum_{j=1}^{N_{el}} N_j{}^e T_j{}^{+e^{(n-1)}})\ \frac{\partial}{\partial y^+} N_k{}^e\ ]\ \tilde{W}_l$$

$$-\ \exp\,[-\beta^+ (\sum_{i=1}^{N_{el}} T_i{}^{+e^{(n-1)}} N_i{}^e - 1)]\ \frac{\partial N_k{}^e}{\partial y^+}\ \frac{\partial \tilde{W}_l}{\partial y^+} \}\ u_k{}^{+e^{(n)}}\ d\Omega =$$

$$-\ \int_{\cup_e \Omega^e} (\sum_{i=1}^{N_{el}} \frac{dN_i{}^e}{dx^+}\ p_i{}^{+e^{(n)^*}})\ \tilde{W}_l\ d\Omega$$

$$-\ \int_\Gamma \tilde{W}_l \exp\,[-\beta^+ (\sum_{i=1}^{N_{el}} T_i{}^{+e^{(n-1)}} N_i{}^e - 1)]\ \frac{\partial u^+}{\partial \tilde{n}}\ d\Gamma \qquad (6.21)$$

In view of the boundary conditions on u^+, the last term in equation (6.21) can be safely omitted without any loss of generality. In the above expression the superscripts (n-1) and (n) denote the values of the variables at the previous and current iterations and (n*) denotes the n level field variable values available at the time of the current calculation.

(b) Equation for v^+ obtained from equation (6.18) is the following:

$$\sum_{k=1}^{N_{el}} \int_{\cup_e \Omega^e} \{ (1-\lambda^+(\sum_{i=1}^{N_{el}} N_i{}^e T_i{}^{+e^{(n-1)}} - 1))\ \frac{\partial}{\partial y^+} N_k^e - \lambda^+\ N_k{}^e\ \frac{\partial}{\partial y^+} (\sum_{i=1}^{N_{el}} N_i{}^e T_i{}^{+e^{(n-1)}}) \}\ \tilde{W}_l\ v_k^{e(n)}\ d\Omega$$

$$= -\ \int_{\cup_e \Omega^e} \{ (1-\lambda^+(\sum_{j=1}^{N_{el}} N_j{}^e T_j{}^{+e} - 1))\ \frac{\partial}{\partial x^+} (\sum_{i=1}^{N_{el}} N_i{}^e u_i{}^{+e^{(n)^*}})$$

$$-\ \lambda^+ [\ (\sum_{i=1}^{Nel} u_i{}^{+e^{(n)^*}}\ N_i{}^e)\ (\frac{\partial}{\partial x^+} (\sum_{k=1}^{N_{el}} T_k{}^{+e^{(n-1)}}\ N_k{}^e)\ ]\} \tilde{W}_l\ d\Omega \qquad (6.22)$$

(c) Equation for T^+ obtained from equation (6.20) is the following:

$$\sum_{k=1}^{N_{el}} \int_{\cup_e \Omega^e} \{ (1-\lambda^+(\sum_{i=1}^{N_{el}} N_i{}^e T_i{}^{+e(n-1)} - 1)) ((\sum_{i=1}^{N_{el}} N_i{}^e u_i{}^{+e(n^*)}) \frac{\partial}{\partial x^+} N_k{}^e + (\sum_{j=1}^{N_{el}} N_j{}^e v_j{}^{+e(n^*)}) \frac{\partial}{\partial y^+} N_k{}^e) \tilde{W}_l + \frac{1}{P_e} \frac{\partial}{\partial y^+} N_k{}^e \frac{\partial}{\partial y^+} \tilde{W}_l \} T_k{}^{+e(n)} \, d\Omega$$

$$= \int_{\cup_e \Omega^e} \{ \frac{P_r E_c}{Pe} \exp[-\beta^+ (\sum_{i=1}^{N_{el}} T_i{}^{+e(n-1)} N_i{}^e - 1)] (\frac{\partial}{\partial y^+} (\sum_{j=1}^{N_{el}} N_j{}^e u_j{}^{+e(n^*)}))^2 + \frac{P_r E_c}{P_e} (\sum_{i=1}^{N_{el}} N_i{}^e u_i{}^{+e(n^*)}) \frac{d}{dx^+} (\sum_{j=1}^{N_{el}} N_j{}^e p_j{}^{+e(n^*)}) \} \tilde{W}_l \, d\Omega - \int_\Gamma \frac{1}{P_e} \frac{\partial T}{\partial \bar{n}} \tilde{W}_l \, d\Gamma \tag{6.23}$$

Again in view of thermal boundary conditions excepting for the Case3 (ISEP) the boundary term on the right hand side of equation (6.21) may be omitted without any loss of generality.

(d) Pressure p^+ is obtained from the momentum equation (6.19) which is analogous to Poisson equation for pressure from momentum equations. Equation for p^+ obtained from equation (6.19) is as follows:

$$\sum_{k=1}^{N_{el}} \int_{\cup_e \Omega^e} \{N_k{}^e \tilde{W}_l\} \, p_k{}^{+e(n)} \, d\Omega$$

$$= - \int_{\cup_e \Omega^e} \{ (1-\lambda^+(\sum_{i=1}^{N_{el}} N_i{}^e T_i{}^{+e(n-1)} - 1)) R_e^* \tilde{W}_l ((\sum_{j=1}^{N_{el}} N_j{}^e u_j{}^{+e(n-1)}) \frac{\partial}{\partial x^+} (\sum_{i=1}^{N_{el}} N_i{}^e u_i{}^{+e(n-1)}) + (\sum_{j=1}^{N_{el}} N_j{}^e v_j{}^{+e(n-1)}) \frac{\partial}{\partial y^+} N_k{}^e (\sum_{i=1}^{N_{el}} N_i{}^e u_i{}^{+e(n-1)})) + \exp[-\beta^+ (\sum_{i=1}^{N_{el}} T_i{}^{+e(n-1)} N_i{}^e - 1)] (\frac{\partial}{\partial y^+} (\sum_{j=1}^{N_{el}} N_j{}^e u_j{}^{+e(n-1)}) \frac{\partial \tilde{W}_l}{\partial y^+} + \beta^+ \frac{\partial}{\partial y^+} (\sum_{i=1}^{N_{el}} N_i{}^e T_i{}^{+e(n-1)}) \tilde{W}_l \frac{\partial}{\partial y^+} (\sum_{j=1}^{N_{el}} N_j{}^e u_j{}^{+e(n-1)})) \} \, d\Omega - \int_\Gamma \exp[-\beta^+ (\sum_{i=1}^{N_{el}} T_i{}^{+e(n-1)} N_i{}^e - 1)] (\frac{\partial u}{\partial \bar{n}}) \, d\Gamma \tag{6.24}$$

Here again the boundary term on the right hand side of equation (6.24) may be safely omitted without any loss of generality. It must be mentioned that just to trigger the numerical calculations, pressures are initially obtained from the variational principle (Reddi [70]) for

Generalized Reynolds equation (Kumar et al. [73]). Now based on equations (6.21) - (6.24) the field variables (u^+, v^+, p^+, T^+) are calculated in a decoupled fashion according to the following algorithm:

6.3.2 Algorithm

- Step: 0, Initialization:

  (a) Carry out boundary settings for (u^+, v^+, T^+, p^+).

  (b) Set initial lubricant temperature to inlet lubricant temperature.

- Step: 1, If i = 1 (first iteration) then Evaluate p^+ minimizing the variational principle for Generalized Reynolds equation (Kumar et al. [73]). i.e.

$$\delta\Pi(p) = \int_\Omega [\frac{h^{+3}}{12\mu^+} (\frac{\partial p^+}{\partial x^+})^2 - h^+ \frac{dp^+}{dx^+}] \, d\Omega \tag{6.25}$$

  else

  Evaluate $p^{+(i)}$ based on equation (6.24) using $u^{+(i-1)}$, $v^{+(i-1)}$, $T^{+(i-1)}$.

- Step: 2, If i = 1 (first iteration) then

  Evaluate $u^{+(1)}$ using $p^{+(1)}$ from the direct integration of linearized x-momentum equation i.e.

$$\frac{\partial}{\partial y^+} (\mu^+ \frac{\partial u^+}{\partial y^+}) = \frac{dp^+}{dx^+} \tag{6.26}$$

  else

  Evaluate evaluate $u^{+(i)}$ using $u^{+(i-1)}$, $v^{+(i-1)}$, $T^{+(i-1)}$.

- Step: 3, If i = 1 (first iteration) then

  Evaluate $v^{+(1)}$ directly from the continuity equation treating ρ^+ to be a constant and using $u^{+(1^*)}$.

  else

  Evaluate $v^{+(i)}$ based on equation (6.22) using $u^{+(1^*)}$, $T^{+(i^*)}$.

The convex parabolic pressure profiles corresponding to $(p_i^+, p_o^+) = (0, 0)$ clearly indicate the pressure generation in the slider bearings for zero inlet pressure. It can be easily observed that the increase in the tilt of the pad significantly enhance the pad pressures and shifts the location of peak pad pressure occurrence closer to the outlet. These observations are very much in tune with the earlier studies (Pinkus and Strenlicht [74]). To study the effect of non zero inlet pressure, simulations are carried out maintaining (p_i^+, p_o^+) at $(1, 0)$ and fixing $T_i^+ = T_p^+ = T_s^+ = 1.3$ for $k = 0.4, 0.6, 0.8, 1.0$. Pad pressures along the sliding direction are shown in Figure 6.2.

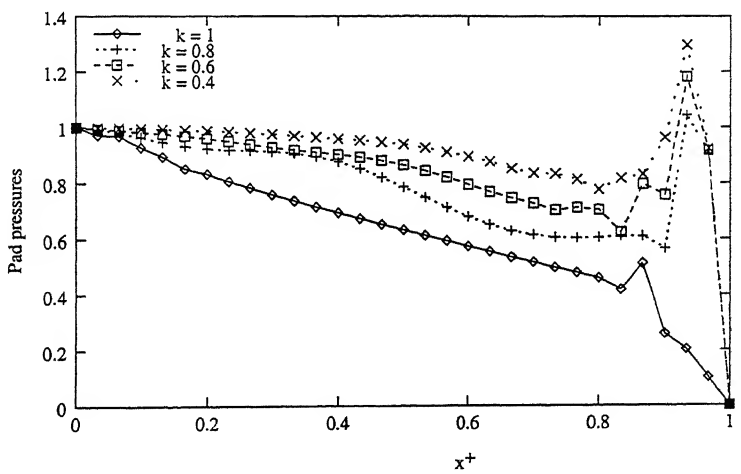

Figure 6.2: Pressures along the pad for $p_i^+ = 1, T_i^+ = T_p^+ = T_s^+ = 1.3$

Again the pad pressure increase with the tilt in the pad and the peak pad pressures are noticed closer to the outlet. For $k = 0.4, 0.6, 0.8$ it is to be noted that the peak pressures seen near the outlet are higher than the prescribed inlet pressure. These observations are compatible with several experimental findings Pinkus [31] and indicate the possibilities of enhancing load carrying capacity of slider bearings by considering fore-region pressure and necessitates further investigations on the influence of fore-region pressure. Hence simulations are carried out for $p_i^+ = 2.5, 5, 10$ fixing $T_i^+ = T_p^+ = T_s^+ = 1.3$ for $k = 0.4, 0.6, 0.8, 1.0$. In Figure 6.3 pressure distribution on the pad in sliding direction for $k = 0.4$ and $p_i^+ = 0, 1, 2.5, 5, 10$ are presented.

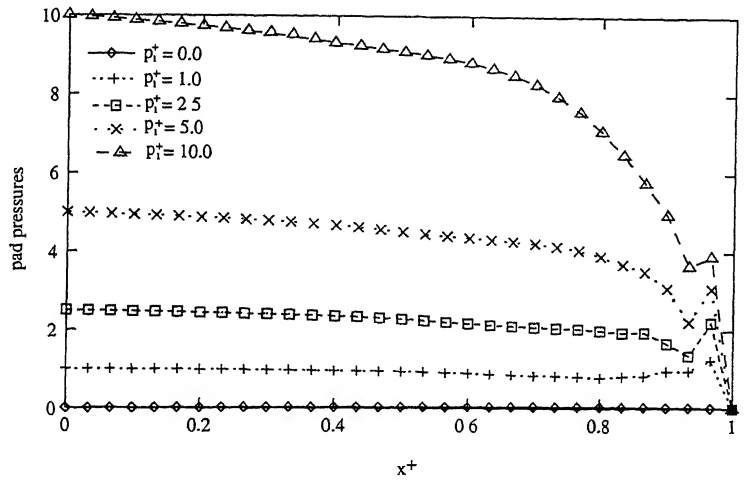

Figure 6.3: Pad pressures $k = 0.4, T_i^+ = T_p^+ = T_s^+ = 1.3$ for various values of p_i^+

Clearly an increase in the inlet lubricant pressure increases the pad pressures which in turn leads to an enhanced load carrying capacity. The load carrying capacity of the slider bearing corresponding to the above settings are evaluated and are presented in Figure 6.4.

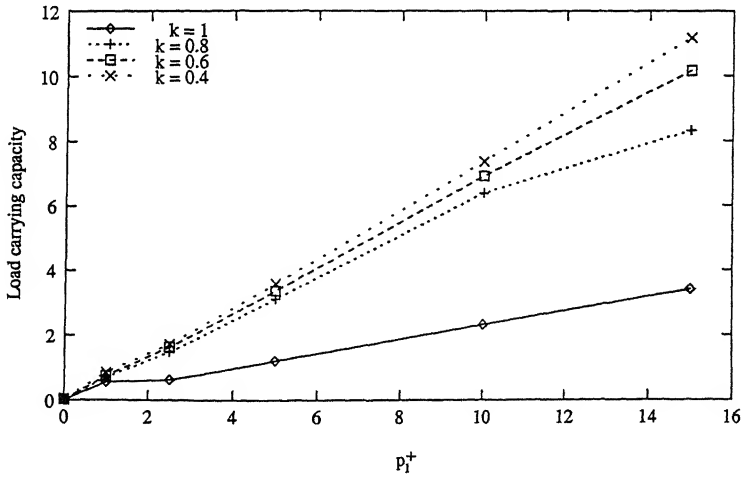

Figure 6.4: Influence of various inlet pressures on load carrying capacity for $T_i^+ = T_p^+ = T_s^+ = 1.3$ for various values of k

From this Figure 6.4 it may be noted that the load carrying capacity of slider bearing can be enhanced either by increasing the tilt of the pad (k) or by the consideration of fore-region pressure (p_i^+). Clearly the combined influence of k and p_i^+ on the load generation is

greater than their segregated influences.

The frictional drag coefficient associated with above setting are evaluated and presented in Figure 6.5.

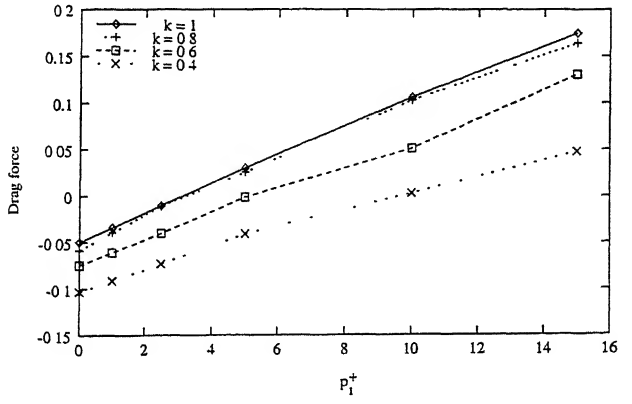

Figure 6.5: Influence of various inlet pressures on frictional drag force for $T_i^+ = T_p^+ = T_s^+ = 1.3$ for various values of k

It is amply clear that the frictional drag reduces with the tilt in pad and increases with the increasing p_i^+. This may be attributed to the acceleration in the flow brought in by fore-region pressures or by the geometric effect of the slider bearing. All of the above investigations pertain to the ISIP settings. It is essential to investigate the influence of other boundary settings as defined under cases ISAP, ISEP and ASAP on load generation and frictional drag. The load carrying capacity and the frictional drag associated with the slider bearing for these various boundary settings are evaluated and presented in Tables 6.1 and 6.2.

Here the computations have been done for $(p_i^+, p_o^+) = (0,0), (1,0)$. T_s^+, T_p^+, T_i^+ are fixed at 1.3, whenever applicable and on ad-hoc out flux of magnitude 0.2 is considered for ISEP (non zero half flux) case. From Table 6.1 one can notice that the consideration of fore-region pressures brings in a significant enhancement in load carrying capacity for all boundary settings. Further the boundary settings corresponding to the case ISEP (non zero half flux) lead to relatively higher load carrying capacity of the slider bearing.

Table 6.1: Load capacity at various settings for $T_i^+ = T_p^+ = T_s^+ = 1.3$

$p_i^+ = 0$	W^+	W^+	W^+	W^+
Cases	ISIP	ISAP	ASAP	ISEP
k = 1	0.0003775	0.00037653	0.0037654	0.000399943
k = 0.8	0.007463	0.007456	0.007455	0.0094824
k = 0.6	0.0188987	0.01889406	0.0188956	0.019489
k = 0.4	0.04600167	0.0460329	0.0460306816	0.04702043
$p_i^+ = 1$	W^+	W^+	W^+	W^+
k = 1	0.559023	0.5590082	0.5590084	0.5751408
k = 0.8	0.69404	0.69621	0.69622	0.698157
k = 0.6	0.741607726	0.74160432	0.741603315	0.7423247
k = 0.4	0.8276344	0.82726675	0.8272555	0.8539077

Table 6.2: Frictional drag force at various settings for $T_s^+ = T_p^+ = T_s^+ = 1.3$

$p_i^+ = 0$	F^+	F^+	F^+	F^+
Cases	ISIP	ISAP	ASAP	ISEP
k = 1	-0.049685374	-0.049685359	-0.0496150441	-0.049724504
k = 0.8	-0.058889322	-0.058889363	-0.0587618388	-0.0588530414
k = 0.6	-0.0746395215	-0.074275121	-0.074275121	-0.0746286213
k = 0.4	-0.103227668	-0.103228159	-0.102606408	-0.103196517
$p_i^+ = 1$	F^+	F^+	F^+	F^+
k = 1	-0.03409398	-0.0340939611	-0.034287925	-0.0341370404
k = 0.8	-0.0394585505	-0.039458595	-0.038821835	-0.0392912589
k = 0.6	-0.0609837808	-0.060953608	-0.0614150167	-0.060973309
k = 0.4	-0.0913590118	-0.0913589522	-0.0907316506	-0.0913887247

The load carrying capacity of slider bearing do not change or differ marginally for ISEP, ISAP and ASAP boundary settings. Recall that the viscosity and the density of the lubricant given by equation (6.4) are sensitive to the temperature. From the expression for the viscosity it is clear that for fixed values of β^+ smaller the value of $(T^+ - 1)$ larger will be ρ^+. Generally, lubricants with larger viscosity and density will have higher threshold for thermal expansion and can lead to relatively larger load carrying capacity. So the lubricant temperature fields associated with the ISEP, ISIP, ISAP and ASAP boundary settings can explain the observed behavior of the load carrying capacity of slider bearings as one moves from ISIP (Case 1) settings to ISEP (Case 4) settings. Hence in Figures 6.6 and 6.7 lubricant

temperature field associated with ISIP, ISAP, ASAP and ISEP boundary settings for $k = 0.4$, and $p_i^+ = 0, 1$ are presented respectively. In these simulations T_s^+, T_p^+, T_i^+ are fixed at 1.3 wherever applicable and the non-zero out flux for ISEP case is fixed at an ad hoc value of -0.2.

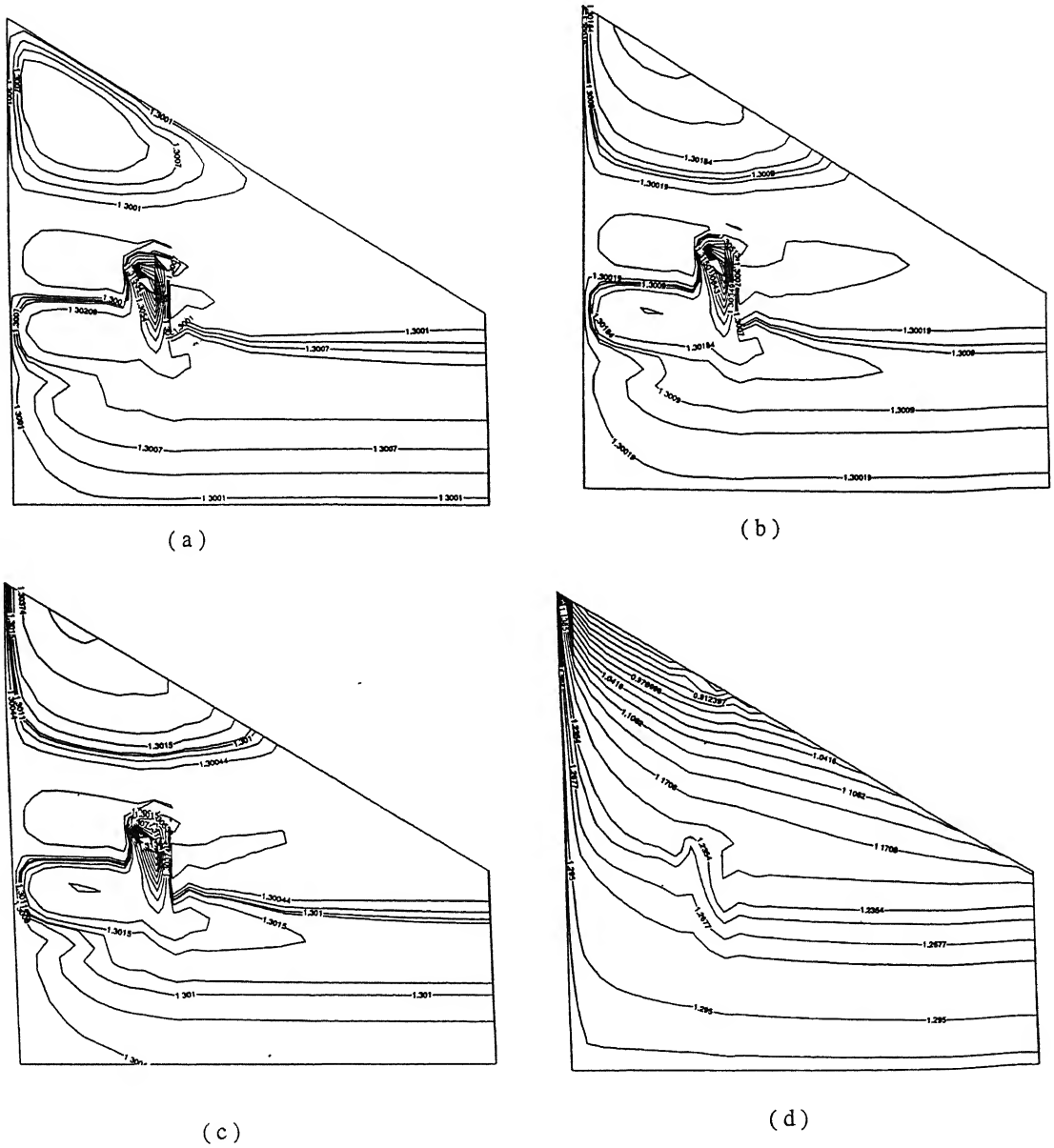

Figure 6.6: Iso-temperature lines for $p_i^+ = 0, k = 0.4, T_i^+ = T_p^+ = T_s^+ = 1.3$: (a) Case1 (b) Case2 (c) Case3 and (d) Case4

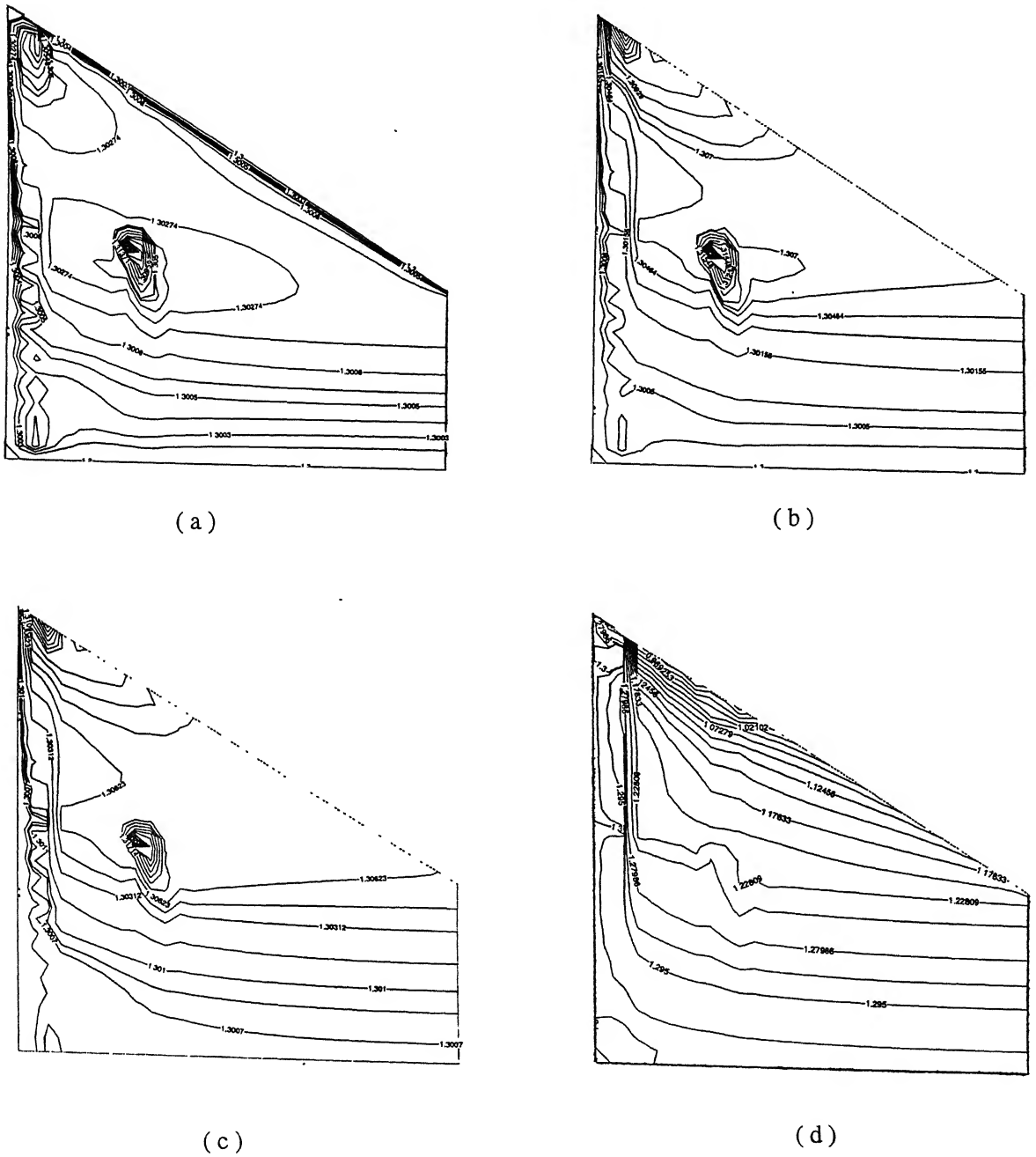

Figure 6.7: Iso-temperature lines for $p_i^+ = 1, k = 0.4, T_i^+ = T_p^+ = T_s^+ = 1.3$: (a) Case1 (b) Case2 (c) Case3 and (d) Case4

From the temperature fields as seen in Figures 6.6 and 6.7 one can notice that the average temperature of the lubricant for ISIP, ISAP, ASAP cases is above 1.3. Whereas for ISEP it is around 1.2. Further from the Figures 6.6 and 6.7 corresponding to ISIP, ISAP and ASAP cases, hot temperature zones where the temperatures rises above 1.3 are noticed in the regions $0.2 \leq x \leq 0.4$, $0.3 \leq y \leq 0.6$ and $0 \leq x \leq 0.5$, $0.7 \leq y \leq 1.0$. But in Figures 6.6 (d) and 6.7 (d) corresponding to ISEP boundary settings no such hot spots are noticed. Higher temperatures lead to lower effective viscosity and density. Consequently one gets a lower load carrying capacity of the slider bearing associated with the ISEP, ISIP, ISAP boundary settings. The temperature distribution in the Figures 6.6 and 6.7 suggests that ISEP boundary settings can lead to better performance of slider bearing. To ensure that these conclusions and reasoning independent of k, isotherms for $k = 1$ at $p_i^+ = 0, 1$ for the boundary settings ISIP, ISAP, ASAP and ISEP are presented in Figures 6.8 and 6.9 respectively. Again observations similar to those found in Figures 6.6, 6.7 are noticed. The circular isotherms found in the above plots indicate the possibility of recirculation zones in the interior region of flow field.

To further investigate these recirculation zones the iso-u velocities or streamlines (as v-velocities are negligible) for $k = 0.8, 0.4$ at $p_i^+ = 0, 1$ respectively are presented in Figures 6.10 and 6.11. From these Figures it may be seen that for all the four boundary settings and both at $p_i^+ = 0, 1$ circular contours indicating recirculation zones are noticed in the region $0.2 \leq x \leq 0.4$, $0.3 \leq y \leq 0.6$. Exactly this is the region of high temperature zone or hot spot in the corresponding lubricant temperature field. The combined influence of geometric parameter k and the consideration of fore-region pressure on the flow field is clearly visible as the laminar boundary aligned streamline flow seen at $p_i^+ = 0$ for $k = 0.8$ changes to a gushing flow at $p_i^+ = 1$ for $k = 0.4$. This also suggests that for high speed lubrication one can not rely on conventional models based on linearized velocity calculations.

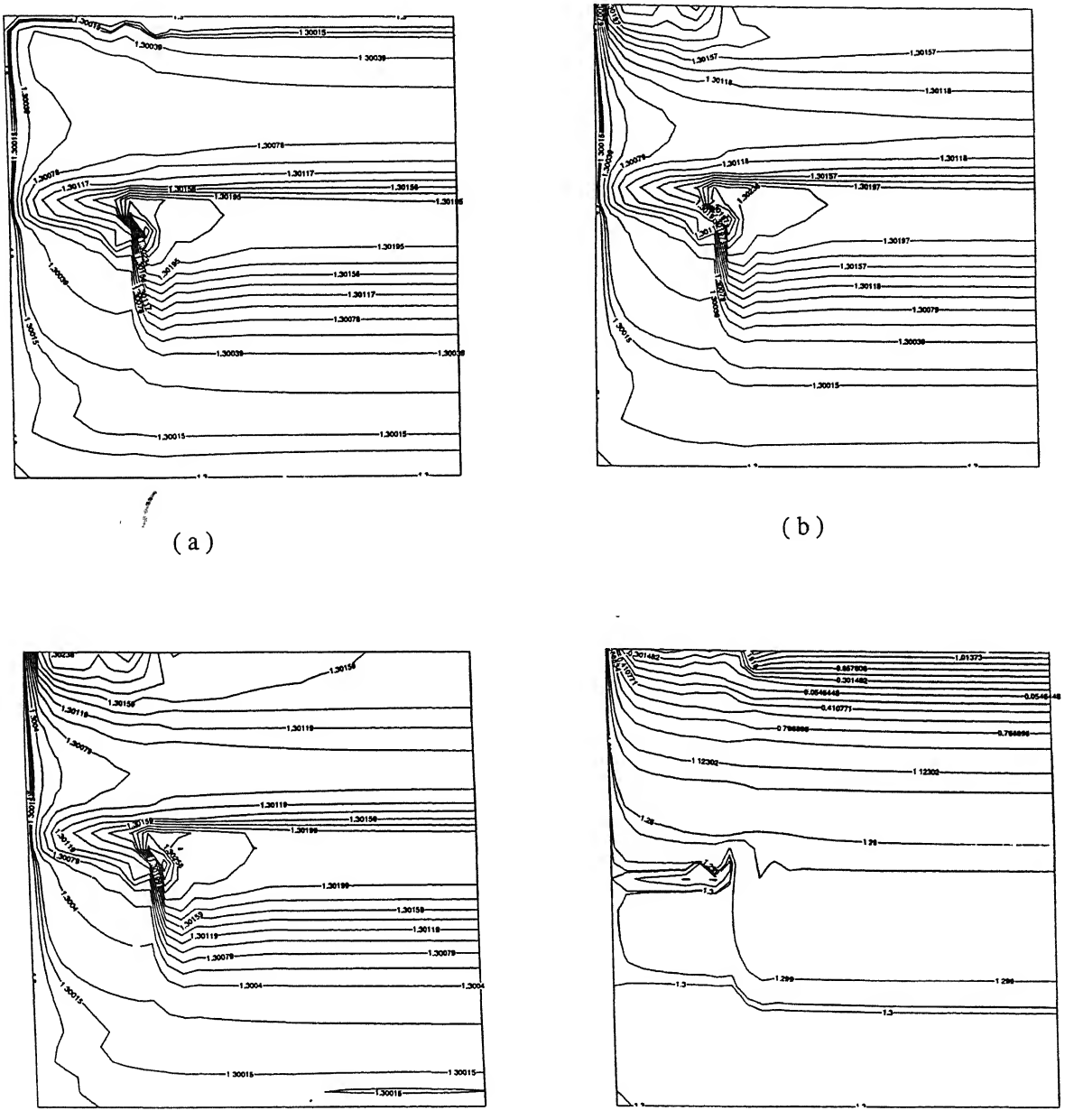

Figure 6.8: Iso-temperature lines for $p_i^+ = 0, k = 1.0, T_i^+ = T_p^+ = T_s^+ = 1.3$: (a) Case1 (b) Case2 (c) Case3 and (d) Case4

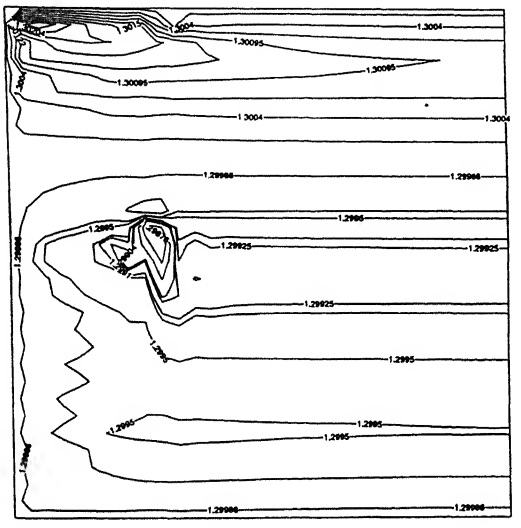

(a)

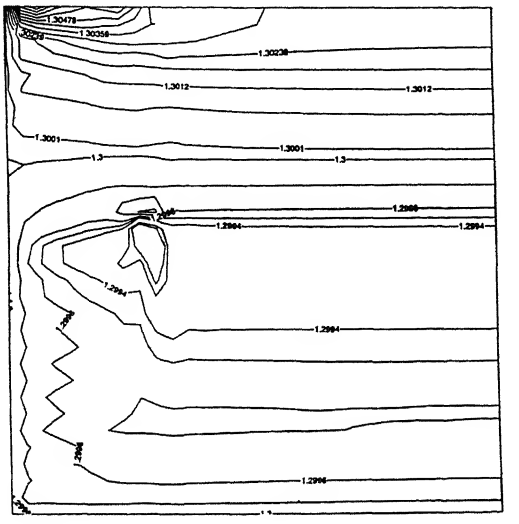

(b)

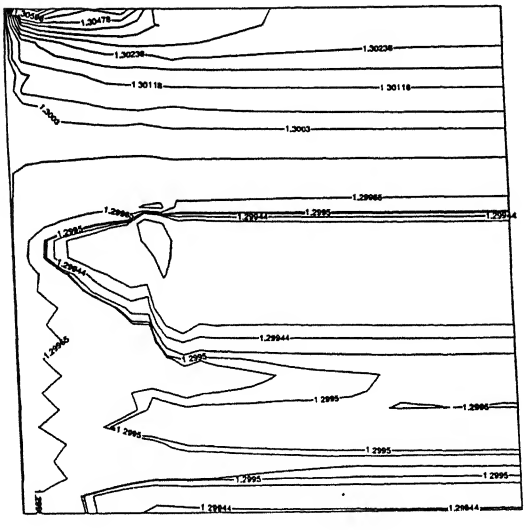

(c)

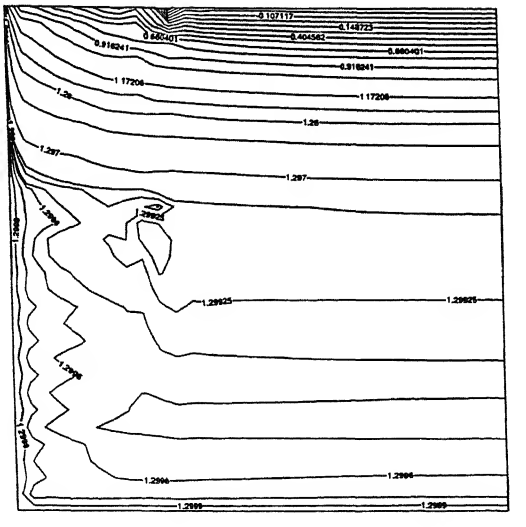

(d)

Figure 6.9: Iso-temperature lines for $p_i^+ = 1, k = 1.0, T_i^+ = T_p^+ = T_s^+ = 1.3$: (a) Case1 (b) Case2 (c) Case3 and (d) Case4

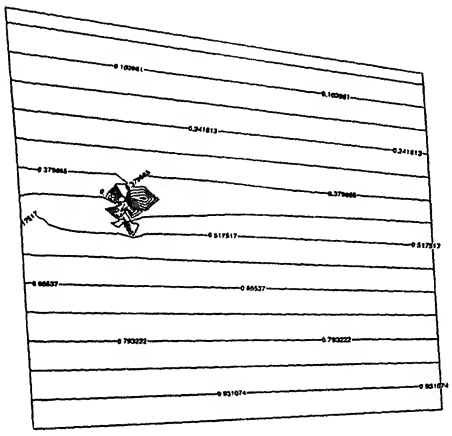

(a)

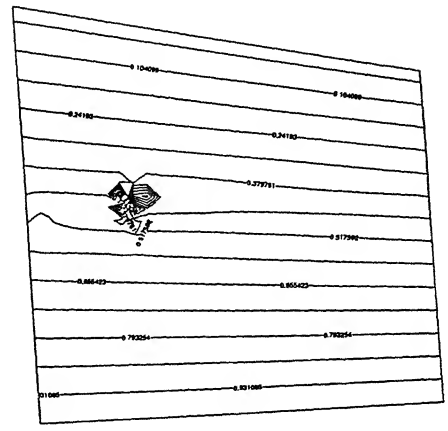

(b)

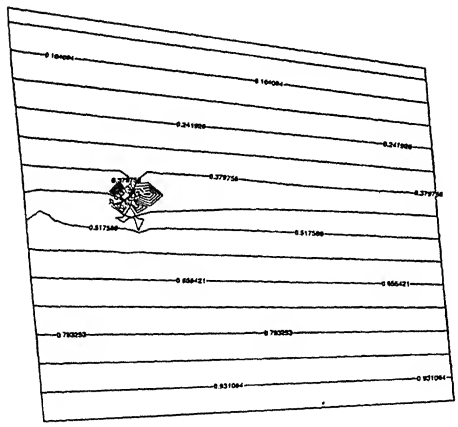

(c)

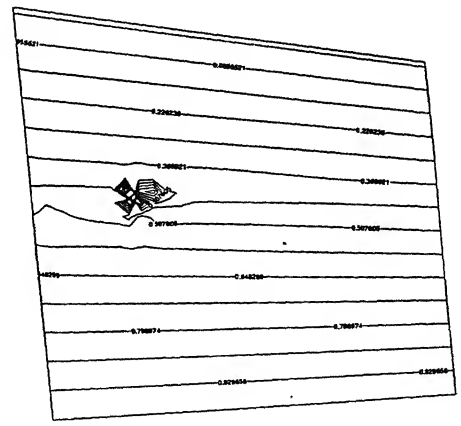

(d)

Figure 6.10: Iso-u velocities for $T_i^+ = T_s^+ = T_p^+ = 1.3, p_i^+ = 0, k = 0.8$: (a) Case1 (b) Case2 (c) Case3 and (d) Case4

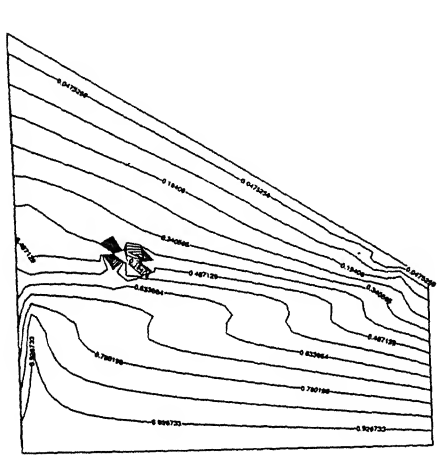

(a)

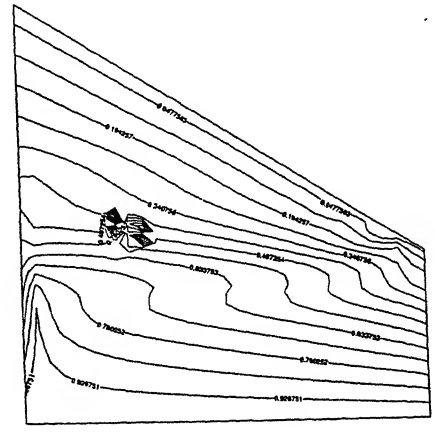

(b)

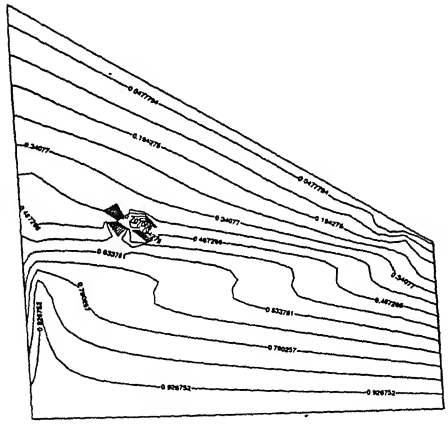

(c)

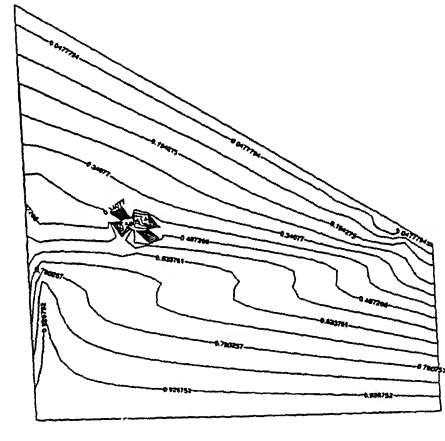

(d)

Figure 6.11: Iso-u velocities for $T_i^+ = T_s^+ = T_p^+ = 1.3, p_i^+ = 1, k = 0.4$: (a) Case1 (b) Case2 (c) Case3 and (d) Case4

The frictional drag coefficient associated with ISIP, ISAP, ASAP and ISEP boundary settings for $k = 0.4, 0.6, 0.8, 1.0$ at $p_i^+ = 0, 1$ (as seen in Table 6.2) depict only a marginal variation. Recall that the frictional drag co-efficient is evaluated using equation (6.11) and viscosity μ^+ is temperature dependent. Now a look at the flow field and temperature field in the immediate vicinity of $y^+ = 0$, where frictional drag co-efficient is calculated, show hardly any variation, as one moves from ISIP setting to ISEP settings and hence the marginal differences in the frictional co-efficient.

For high speed slider bearings inclusion of inertia effects, as in the present case, has been recommended by several researchers (Rodkiewicz and Sinha [58]). To understand the influence of inertia effects on load carrying capacity a comparison of load carrying capacity obtained in the current simulation wherein inertial effects have been considered with the earlier simulations devoid of inertial effects is made in Table 6.3.

Table 6.3: Comparison of load capacity with and without fluid inertia

$p_i^+ = 0$				
k	1	0.8	0.6	0.4
W^+ (without inertia)	0.000000464727	0.004307854	0.012646012	0.03063336
W^+ (with inertia)	0.00003774193	0.006632	0.0188987	0.04600167
$p_i^+ = 1$				
W^+ (without inertia)	0.4999	0.5580224	0.63334724	0.7378243
W^+ (with inertia)	0.559023	0.5702698	0.6403325	0.8539077

It is interesting to note that consideration of inertial effects enhance the load carrying capacity of high speed slider bearings for all values of k and p_i^+.

The influence of thermo viscosity parameter (β^+) on the load generation in high speed slider bearing lubrication has been analyzed at different fore-region pressures for various slider bearing geometries. Plots in Figure 6.12 depict the dependency of load carrying capacity on β^+ for $p_i^+ = 0, 0.5, 1$. For small fore-region pressure load generation in high

speed slider bearings decrease with increasing β^+ but at high inlet pressures this reduction in load generation becomes marginal. This may be explained directly from the expression for μ^+ given in equation (6.4). It can be noted that for fixed $T^+, \mu^+(T^+)$ increases with decreasing β^+, and thus the effective viscosity of the lubricant increases and will lead to higher load carrying capacity.

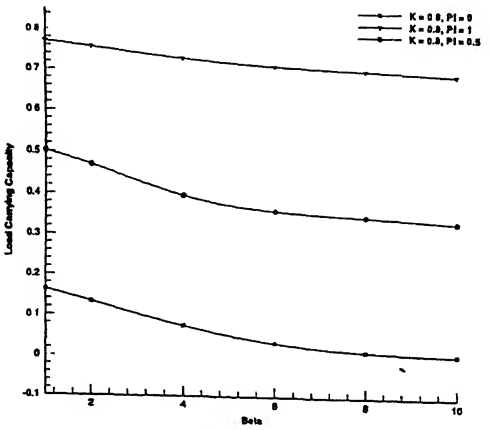

Figure 6.12: Comparison of load carrying capacity with β^+ at $T_i^+ = T_p^+ = T_s^+ = 1.3$ for various values of k and p_i^+

Now to find the thermal boosting boundary settings for slider bearing simulations have been carried out at $p_i^+ = 1$, fixing (a) $T_s^+ = T_p^+ = 1.3, T_i^+ = 1.2$ (b) $T_i^+ = T_s^+ = 1.3, T_p^+ = 1.2$ (c) $T_s^+ = T_p^+ = 1.2, T_i^+ = 1.3$ (d) $T_i^+ = T_s^+ = T_p^+ = 1.3$ and are shown in Table 6.4.

Table 6.4: Load capacity at various settings for $p_i^+ = 1, k = 0.4$

T_i^+	T_s^+	T_p^+	W^+
1.3	1.2	1.3	0.795805991
1.3	1.3	1.3	0.85390777
1.3	1.3	1.2	0.956600515
1.3	1.2	1.2	0.887764513

From the Table 6.4 we see that the thermal settings under (b) and (c) can boost load carrying capacity of high speed slider bearings. Maintaining either pad at lower temperature

or both pad and slider at lower temperatures than the incoming lubricant thermally boost the load carrying capacity of the slider bearing. To obtain a causative picture of this thermal boosting of load generation, temperature fields in the form of isotherms associated with the above settings are presented in Figures 6.13 and 6.14. From the temperature distribution seen in these Figures, the net average lubricant temperatures associated with the above cases (a), (b), (c) are in the order $T_{(a)} > T_{(b)} > T_{(c)} > 1$. Now by the reasoning presented earlier i.e. based on $\mu^+(T^+)$ the trend observed in the load carrying capacity gets justified. It may be noted that the pad is stationary and it is reasonable to find that maintaining it at lower temperature leads to increased load generation.

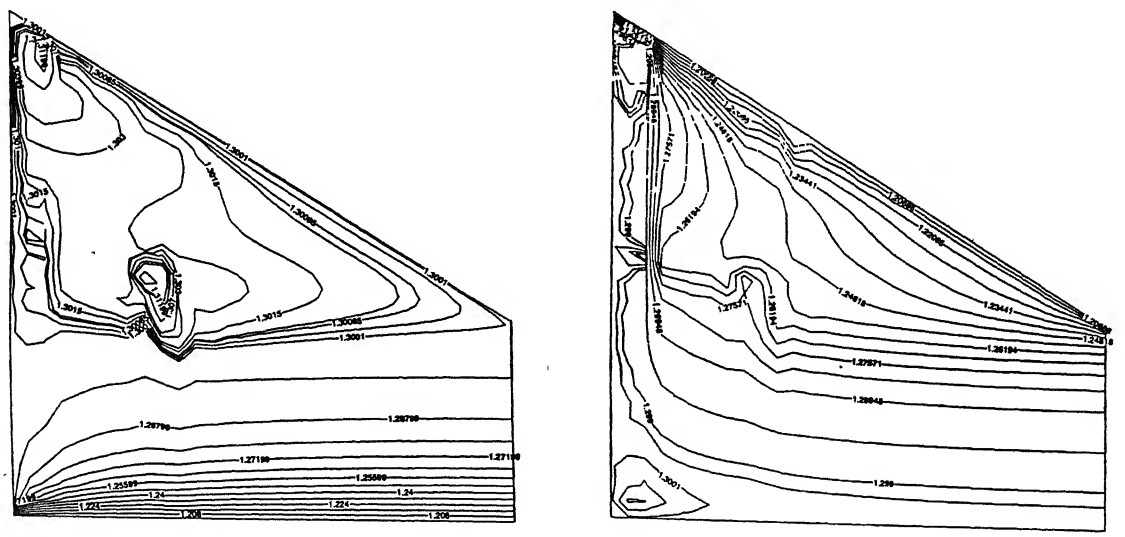

(a) (b)

Figure 6.13: Iso-temperature lines for $T_i^+ = 1.3, k = 0.4, p_i^+ = 1$, Case1: (a) $T_p^+ = 1.3$, $T_s^+ = 1.2$ (b) $T_p^+ = 1.2, T_s^+ = 1.3$

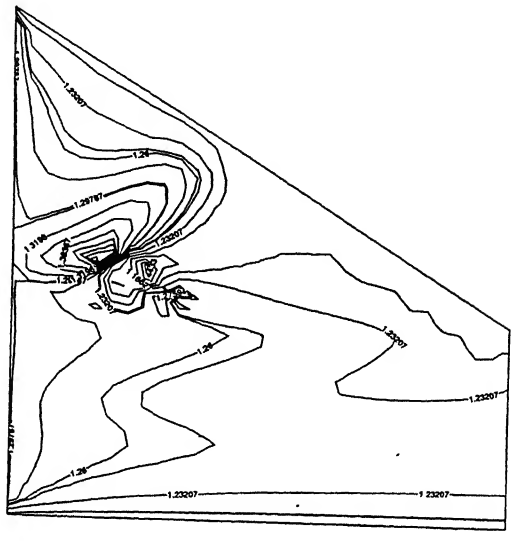

Figure 6.14: Iso-temperature lines for $T_i^+ = 1.3, k = 0.4, p_i^+ = 1$, Case1: $T_s^+ = T_p^+ = 1.2$

6.5 Conclusions

The thermal effects and inertia effects on bearing characteristics in slider bearings have been analyzed. An orderly analysis identifying the influence of various factors viz. inlet pressure, inlet lubricant temperature, thermal boosting, slider bearing geometry on load carrying capacity and frictional drag force have been provided. The Figures and Tables depicted in this Chapter reveal that the consideration of inlet pressure or thermal boosting or both will enhance the load carrying capacity of a slider bearing with a reduction in frictional drag force. Further, it has been observed that consideration of fluid inertia will enhance the effective load carrying capacity of a slider bearing.

Chapter 7

Thermohydrodynamic Analysis of a Tilted Pad Slider Bearing Considering Fluid Inertia and Heat Conduction in the Pad

7.1 Introduction

It has already been mentioned in Chapter 4 and also in Chapter 6 , that for lubrication under high loads and high speeds, large amount of heat may be generated. Heat created in the lubricant film has a profound effect on bearing characteristics. Thus, an analysis, aimed at accurately predicting the bearing performance must consider not only the conservation equations of mass, momentum in the fluid film, but also the conservation equation of thermal energy in the fluid as well as conduction in the stationary pad.

Studying the nature of thermal effects and heat conduction in the stationary pad, Strenlicht [75] performed a restricted adiabatic analysis of a sector-shaped thrust bearing. His results showed that temperature variations in the direction perpendicular to the direction of sliding are not always negligible.

Although studies up to 1957 did not allow for temperature variations across the film,

they did demonstrate that accurate prediction of bearing performance is seldom possible if fluid-film property variations are neglected. Zienkiewicz [42] was the first to formulate a numerical scheme for simultaneously solving the conservation equations in the fluid film with temperature variations across the film. Zienkiewicz's and later follow-up results of Hunter and Zienkiewicz [12] convincingly indicate that viscosity variation with temperature is far more important than density variation.

In a pair of papers, Dowson and Hudson [44] performed a thermohydrodynamic analysis of parallel and inclined slider bearings of infinite length. Their results dramatically show the negligible effect of density changes and the dominant effect of viscosity changes due to temperature gradients across the film.

Hahn and Kettleborough [45] analytically approached the "Fogg Paradox" (ref. Fogg [36] by considering thermal distortion and viscosity variations along and across the film. They have presented an analysis for heat conduction and thermal gradients in one-dimensional slider bearings having a general film shape.

In this Chapter, we have analyzed the slider bearing performance by considering the governing equations of mass, momentum and energy in the lubricant film and the conduction equation in the solid pad, using the SUPG Finite Element Method.

7.2 Governing Equations and Solution Procedure

$$\frac{\partial}{\partial x^+}\left(\rho^+ u^+\right) + \frac{\partial}{\partial y^+}\left(\rho^+ v^+\right) = 0 \tag{7.1}$$

$$R_e^* \rho^+ \left(u^+ \frac{\partial u^+}{\partial x^+} + v^+ \frac{\partial u^+}{\partial y^+}\right) = -\frac{dp^+}{dx^+} + \frac{\partial}{\partial y^+}\left(\mu^+ \frac{\partial u^+}{\partial y^+}\right) \tag{7.2}$$

$$\rho^+ \left(u^+ \frac{\partial T^+}{\partial x^+} + v^+ \frac{\partial T^+}{\partial y^+}\right) = \frac{1}{P_e} \frac{\partial^2 T^+}{\partial y^{+2}} + \frac{P_r\, E_c}{P_e} \mu^+ \left(\frac{\partial u^+}{\partial y^+}\right)^2 + \frac{P_r\, E_c}{P_e} u^+ \frac{dp^+}{dx^+} \tag{7.3}$$

where, ρ^+, μ^+, h^+, k and R_e^* are given by:

$$\rho^+ = 1 - \lambda^+ \, (\, T^+ - 1 \,), \quad \mu^+ = \exp \, [\, -\beta^+ \, (\, T^+ - 1 \,) \,] \tag{7.4}$$

$$h^+ = 1 - x^+ \, (\, 1 - k \,), \quad k = \frac{h_0}{h_i} \leq 1, \quad R_e^* = \frac{\rho_a U B}{\mu_a} (\frac{h_o}{B})^2 \tag{7.5}$$

The equation governing heat conduction in the stationary pad is:

$$[\, (h_1^+)^2 \, \frac{\partial^2 T_p{}^+}{\partial x'^{+2}} + \frac{\partial^2 T_p{}^+}{\partial y'^{+2}} \,] \, = 0 \tag{7.6}$$

Now using the Petrov-Galerkin finite element discretization for the above equations, we obtain the following equations.

$$\int_\Omega \, \{[1 - \lambda^+(T^+ - 1)] \, (\frac{\partial u^+}{\partial x^+} + \frac{\partial v^+}{\partial y^+}) - \lambda^+ \, (u^+ \frac{\partial T^+}{\partial x^+} + v^+ \frac{\partial T^+}{\partial y^+})\} \, \tilde{W} \, d\Omega = 0 \tag{7.7}$$

$$\int_\Omega \, \{[1 - \lambda^+(T^+ - 1)] \, R_e^* \, (u^+ \frac{\partial u^+}{\partial x^+} + v^+ \frac{\partial v^+}{\partial y^+}) + \frac{dp^+}{dx^+}$$

$$- \, e^{-\beta^+(T^+ - 1)} \, (\frac{\partial^2 u^+}{\partial y^{+2}} - \beta^+ \, \frac{\partial T^+}{\partial y^+} \, \frac{\partial u^+}{\partial y^+})\} \, \tilde{W} \, d\Omega \, = \, 0 \tag{7.8}$$

$$\int_\Omega \, \{[1 - \lambda^+(T^+ - 1)] \, (u^+ \frac{\partial u^+}{\partial x^+} + v^+ \frac{\partial v^+}{\partial y^+}) - \frac{1}{Pe} \, \frac{\partial^2 T^+}{\partial y^{+2}}$$

$$- \, \frac{Ec \, Pr}{Pe} \, e^{-\beta^+(T^+ - 1)} \, (\frac{\partial u^+}{\partial y^+})^2 - \frac{Ec \, Pr}{Pe} \, u^+ \, \frac{dp^+}{dx^+} \, \} \tilde{W} \, d\Omega = 0 \tag{7.9}$$

And the Galerkin finite element discretization for heat conduction equation is as follows:

$$\int_{\Omega'} \, [\, w_i \, (h_1^+)^2 \, \frac{\partial w_i}{\partial x'^+} \, \frac{\partial N_j^e}{\partial x'^+} + \frac{\partial w_i}{\partial y'^+} \, \frac{\partial N_j^e}{\partial y'^+}] \, T_{p_j}^{+e} \, d\Omega' = 0 \tag{7.10}$$

Equations (7.7)-(7.10) are solved iteratively (for details see Chapter 6) under the following temperature boundary conditions (see Figure 3.1), to yield the field variables viz. u^+, v^+, p^+, T^+.

- Case1:

  Lubricant boundary conditions:

  $T^+ = T_s^+ = 1.3, \quad$ on AB

$\frac{\partial T^+}{\partial x^+} = 0$, on BC

$T^+ = T_i^+ = 1.3$, on AD

Pad boundary conditions:

$T_p^+ = 1.3,,$ on DF

$T_p^+ = 1.3,,$ on CE

$T_p^+ = 1.3,,$ on EF

Interface boundary conditions:

$T^+ = {T_p}^+$ and $k_s \frac{\partial {T_p}^+}{\partial {y'}^+} = k_f \frac{\partial T^+}{\partial y^+}$, on CD

- Case2:

Lubricant boundary conditions:

$T^+ = T_s^+ = 1.3$, on AB

$\frac{\partial T^+}{\partial x^+} = 0$, on BC

$T^+ = T_i^+ = 1.3$, on AD

Pad boundary conditions:

$\frac{\partial {T_p}^+}{\partial {x'}^+} = 0$, on DF

$\frac{\partial {T_p}^+}{\partial {x'}^+} = 0$, CE

${T_p}^+ = 1.3$, on EF

Interface boundary conditions:

$T^+ = {T_p}^+$ and $k_s \frac{\partial {T_p}^+}{\partial {y'}^+} = k_f \frac{\partial T^+}{\partial y^+}$, on CD

- Case3:

Lubricant boundary conditions:

$T^+ = T_s^+ = 1.3$, on AB

$\frac{\partial T^+}{\partial x^+} = 0$, on BC

$T^+ = T_i^+ = 1.3$, on AD

Pad boundary conditions:

$\frac{\partial {T_p}^+}{\partial {x'}^+} = 0$, on DF

$\frac{\partial {T_p}^+}{\partial {x'}^+} = 0$, on CE

$\frac{\partial {T_p}^+}{\partial \bar{n}} = 0$, on EF

Interface boundary conditions:

$T^+ = {T_p}^+$ and $k_s \frac{\partial {T_p}^+}{\partial {y'}^+} = k_f \frac{\partial T^+}{\partial y^+}$, on CD

- Case4:

Lubricant boundary conditions:

$T^+ = T_s^+ = 1.3$, on AB

$\frac{\partial T^+}{\partial x^+} = 0$, on BC

$T^+ = T_i^+ = 1.3$, on AD

Pad boundary conditions:

$\frac{\partial {T_p}^+}{\partial {x'}^+} = 0$, on DF

$\frac{\partial {T_p}^+}{\partial {x'}^+} = 0$, on CE

$-k_s \frac{\partial {T_p}^+}{\partial \bar{n}} = -H\ ({T_p}^+ - 1)$, on EF

Interface boundary conditions:

$T^+ = {T_p}^+$ and $k_s \frac{\partial {T_p}^+}{\partial {y'}^+} = k_f \frac{\partial T^+}{\partial y^+}$, on CD

7.3 Results and Discussion

The simulations have been carried out on 30 × 30 grid system. The results have been presented for load carrying capacity in the form of tables for various boundary settings.

The load carrying capacity for the setting $T_i^+ = T_p^+ = T_s^+ = 1.3, p_i^+ = 1$ have been compared with the results obtained for a linearized velocities model (Chapter 4) and are shown in Table 7.1. Inclusion of inertia results in an enhancement of load capacity for all values of k.

In Table 7.2, comparison of load carrying capacity with conduction in the pad (Chapter 7) and with no heat conduction in the pad (Chapter 6) have been made for various slider bearing geometries with the setting $T_i^+ = T_p^+ = T_s^+ = 1.3, p_i^+ = 1$ Case4 boundary condition.

Table 7.1: Comparison of load capacity with inertia and without inertia forces for $p_i^+ = 1$, Case4

Cases	k = 0.4	k = 0.6	k = 0.8	k = 1.0
W^+, without inertia (linearized model)	0.7378243	0.633222824	0.55832	0.49989
W^+, with inertia (nonlinear model)	0.855990	0.7502945	0.69157	0.57481

Table 7.2: Comparison of load capacity with conduction and without conduction in the pad for $p_i^+ = 1$, Case4

Cases	k = 0.4	k = 0.6	k = 0.8	k = 1.0
W^+ with conduction	0.855990	0.7502945	0.691857	0.57481
W^+without conduction	0.8539077	0.7423247	0.698157	0.575108

From Table 7.2, It is observed that the load carrying capacity associated without conduction in the pad are marginally higher for the cases $k = 1, 0.8$, whereas for the case $k = 0.6, 0.4$, these are lower. It shows that as the tilt of the pad increases the load carrying capacity decreases for the case with conduction in compared with the case without conduction. Similar observations were made for the linearized model (Chapters 3, 4). Inclusion of the inertia forces and heat conduction in the pad supports the pressure generation when the tilt is raised from $k = 0.6$ to 0.8.

In Table 7.3, the load carrying capacity for various boundary conditions at various values of k for the setting $T_i^+ = T_p^+ = T_s^+ = 1.3, p_i^+ = 1$ are shown. From Table 7.3, one can observe that Case4 boundary condition has higher values of load carrying capacity for various values of k as compared with the other Cases. This is due to the fact that the temperature of the lubricant decreases when we allow the pad conduction to the environment. Also, it is observed that for parallel slider case (k = 1) there are negligible variations in the computed load carrying capacity for all the temperature boundary conditions. This could be due to no change in the temperature gradients as we have seen in Chapter 5.

Table 7.3: Comparison of load capacity for various boundary conditions at $p_i^+ = 1, T_i^+ = T_p^+ = T_s^+ = 1.3$

Cases	k = 0.4	k = 0.8	k = 0.6	k = 1.0
W^+, Case1	0.8350990	0.735544	0.6947003	0.559120
W^+, Case2	0.824330	0.725974	0.6947007	0.559001
W^+, Case3	0.8251006	0.725946	0.690537	0.559008
W^+, Case4	0.855990	0.7502945	0.691857	0.575481

7.4 Conclusions

Load carrying capacity of a high speed slider bearing with conduction in the stationary pad for various thermal boundary conditions for various geometric configurations have been numerically analyzed using FEM. Density and the Viscosity in the mathematical model describing the slider bearing configuration are treated as functions of temperature. Though solid pads with different boundary settings as chosen in this study from application point of view alters the temperature field in the pad the thermal flux across the fluid-solid interface changes marginally and thus there is a little change in the load carrying capacity of the slider bearing.

Bibliography

[1] Tower. B, "First report on friction experiments," *Proc. Inst. Mech. Eng.*, Vol. 34, pp. 632–666, 1883.

[2] Petroff. N. P, "Friction in machines and the effect of the lubricant (roman)," *Inzh. Zh. St. Petersburg*, Vol. 1, pp. 71–140, 1883.

[3] Petroff. N. P, "Friction in machines and the effect of the lubricant (roman)," *Inzh. Zh. St. Petersburg*, Vol. 2, pp. 227–279, 1883.

[4] Petroff. N. P, "Friction in machines and the effect of the lubricant (roman)," *Inzh. Zh. St. Petersburg*, Vol. 3, pp. 377–436, 1883.

[5] Petroff. N. P, "Friction in machines and the effect of the lubricant (roman)," *Inzh. Zh. St. Petersburg*, Vol. 4, pp. 535–564, 1883.

[6] Tower. B, "Second report on friction experiments (experimets on the oil pressure in a bearing," *Proc. Inst. Mech. Eng.*, pp. 58–70, 1885.

[7] Reynolds. O, "On the theory of lubrication and its application to mr. beachamp tower's experiments including an experimental determination of the viscosity of olive oil," *Phi. Trans. Roy. Soc. of London (series: A)*, Vol. 117, pp. 137, 1886.

[8] Martin. H.M, "Lubrication of gear teeth," *Engineering (London)*, Vol. 102, pp. 119–121, 1916.

[9] Christopherson. D.G, "A new mathamatical method for the solution if film lubrication problems," *Proc. Inst. Mech. Engg.*, Vol. 146, pp. 126–135, April 1942.

[10] Cameron. A and Wood. W.L, "Parallel surface thrust bearing," *ASLE, Trans.*, Vol. 1, pp. 254–258, 1958.

[11] Cope. W.F, "The hydrodynamic theory of lubrication," *Proc. of Royal Soc. of London*, Vol. 197, pp. 201, 1949.

[12] Hunter. W and Zienkiewicz. O.C, "Effects of temperature variation across the lubricant film in the theory of hydrodynamic lubrication," *Jl. Mech. Engg. Sci.*, Vol. 2, No. 1, pp. 52–58, 1960.

[13] Dowson. D, "A generalized Reynolds equation for fluid film lubrication," *Int. Jl. Mech. Sci.*, Vol. 4, pp. 159–170, 1962.

[14] Huebner. K.H, "Application of finite element method to thermohydrodynamic lubrication," *Int. Jl. for Num. Meth. in Engg*, Vol. 8, pp. 139–165, 1974.

[15] Ezzat. H and Rohde. S, "A study of the thermohydrodynamic perfromance of finite slider bearings," *Trans. ASME, Jl. Lub. Tech.*, Vol. 75, No. 5, pp. 298–307, 1973.

[16] Khonsari. M. M, "A review of thermal effects in hydrodynamic bearings. part i: Slider/thrust bearings, part ii: Journal bearings," *ASLE, Trans.*, Vol. 30, pp. 19–33, 1987.

[17] Gethin. D.T, "An application of the finite element method to the thermohydrodynamic analysis of a thin film cylindrical bore bearings running at high sliding speed," *Trans. ASME, Jl. Lub. Tech.*, Vol. 109, pp. 283–290, 1987.

[18] Gero. L.R and Ettles. C.M, "A three dimensional thermohydrodynamic finite element scheme for fluid film bearings," *STLE, Tribology Trans.*, Vol. 31, No. 2, pp. 182–191, 1987.

[19] Schumack. M.R, "Application of the pseudo spectral method to thermohydrodynamic lubrication," *Int. J. for Num. Meth. in Fluids*, Vol. 23, pp. 1145–1161, 1996.

[20] Myllerup. C. M and Hamrock. B.J, "Local effects in thin film lubrication," *Presented and published in the 19th Leeds-Lyon Symposium on Tribology*, 1992.

[21] Tichy. J.A, "A study of the effect of fluid inertia and end leakage in the finite squeeze film damper," *Trans. ASME, Jl. of Tribology*, Vol. 109, pp. 54–59, 1987.

[22] Talmage. G and Carpino. M, "A pseudo spectral finite difference analysis of an infinitely wide slider bearing with thermal and inertial effcets," *STLE, Tribology Trans.*, Vol. 40, No. 2, pp. 251–258, 1997.

[23] Prasad. D Singh. P and Sinha. P, "Thermal and inertia effects in hydrodynamic lubrication of rollers by a power law fluid considering cavitation," *Trans. ASME, Jl. of Tribology*, Vol. 115, pp. 319–326, 1993.

[24] Gross. W.A, "Fluid film lubrication," 1980, Addison Wisley publishers.

[25] Haupert. L and Hamrock. B.J, "First approach for calculating film thickness and pressures in ehd lubricated contacts at high loads," *Trans. ASME, Jl. of Tribology*, Vol. 108, pp. 411, 1986.

[26] Hamrock. B.J and Dowson. D, "Isothermal elastohydrodynamic lubrication of point contacts: part i," *Trans. ASME, Jl. of Tribology*, Vol. 98, pp. 223–229, 1976.

[27] Hamrock. B.J and Dowson. D, "Isothermal elastohydrodynamic lubrication of point contacts: part ii," *Trans. ASME, Jl. of Tribology*, Vol. 98, pp. 375–383, 1976.

[28] Hamrock. B.J and Dowson. D, "Isothermal elastohydrodynamic lubrication of point contacts: part iii," *Trans. ASME, Jl. of Tribology*, Vol. 99, pp. 264–276, 1977.

[29] Ghosh. K and Hamrock. B.J, "Thermal fluid lubrication of line contacts," *ASLE*, Vol. 28, pp. 159–171, 1985.

[30] Venkateswarlu. K and Rodkiewicz. C.M, "On the thrust bearing characteristics in turbulent flow," *Trans. ASME, Jl. Lub. Tech*, Vol. 103, pp. 450, 1981.

[31] Pinkus. O, "Thermal aspects of fluid film tribology, asme press, newyork," 1990.

[32] Shukla. J.B and Isa. M, "Thermal effects in squeeze films and externally pressurized bearings with power law lubricants," *Wear*, Vol. 51, pp. 237, 1987.

[33] Hirst. W and Moore. A.J, "Non-newtonian behavior in elastohydrodynamic lubrication," *Proc. Roy. Soc. of London*, Vol. 33, pp. 101–113, 1974.

[34] Caldewell. D. H and Babbitt. H. E, ," *Trans. Amer. Instt. Chem. Engrs.*, Vol. 37, pp. 237, 1941.

[35] Sheu. S and Wilson. W. R. D, "Viscoplastic lubrication of asperities," *Jour. Lub. Tech.*, Vol. 104, No. 4, pp. 568–574, 1982.

[36] Fogg. A, "Fluid film lubrication of parallel thrust surfaces," *Proc. Inst. of Mech. Engrs.*, Vol. 155, pp. 49–53, 1946.

[37] Rodkiewicz. C.M Kim. K.W and Kennedy. J.S, "On the significance of the inlet pressure build-up in the design of tilted pad bearings," *Trans. ASME, Jl. of Tribology*, Vol. 122, No. 1, pp. 17–22, 1990.

[38] Osterle. F Charnes. A and Saibel. E, "On the solution of the Reynolds equation for slider bearing lubrication - vi, the parallel-surface slider bearing without side leakage," *Trans. ASME, Jl. of Tribology*, pp. 1133–1136, 1953.

[39] Lewicki. W, "Theory of hydrodynamic lubrication in parallel sliding," *Engineer, London*, Vol. 200, pp. 939–941, 1955.

[40] Hagg. A.C, "Heat effects in lubricating films," *Trans. ASME, Jl. of Applied Mechanics*, pp. A–72, June 1944.

[41] Tipei. N and Nica. Al, "On the field of temperature in lubricating films," *Trans. ASME, Jl. of Tribology*, p. 482, 1967.

[42] Zienkiewicz. O.C, "Temperature distribution within lubricating films between parallel bearing surfaces and its effect on the pressures developed," *Conf. on Lubrication and Wear, Paper No: 7, Inst. Mech. eng, London*, 1957.

[43] Cameron. A, "The viscosity wedge," *Trans. ASME, Jl. of Tribology*, Vol. 1, pp. 248–253, 1958.

[44] Dowson. D and Hudson. J.D, "Thermo hydrodynamic analysis of the infinite slider bearings: Part i, the inclined plane slider bearing," *Jl. of Mech. Engrs. Lubrication and Wear Convention, Paper 4*, 1963.

[45] Hahn. E.J and Kettleborough. C.F, "Solution for the pressure and temperature in an infinite slider bearing of arbitrary profile," *Trans. ASME, Jl. Lub. Tech*, p. 445, 1967.

[46] Hahn. E.J and Kettleborough. C.F, "Thermal effects in slider bearings," *Proc. of the Inst. of Mech. Engg.*, Vol. 183, pp. 1, 1968.

[47] Lebeck. A.O, "Parallel slider load support in the mixed friction regime, part i - the experiamental data," *Trans. ASME, Jl. of Tribology*, Vol. 109, pp. 189–195, 1987.

[48] Lebeck. A.O, "Parallel slider load support in the mixed friction regime, part ii - evaluation of the mechanism," *Trans. ASME, Jl. of Tribology*, Vol. 109, pp. 196–205, 1987.

[49] Rohde. S.M and Kong. O.P, "A thermohydrodynamic analysis of finite slider bearing," *Trans. ASME, Jl. Lub. Tech*, pp. 450–460, 1975.

[50] Hill. D.L Bhaskarone. E. A and Andres. L.S, ," *Trans. ASME, Jl. Lub. Tech*, Vol. 117, pp. 498–505, 1995.

[51] Artiles. A Walowit. J and Shapiro. W, ," *Advances in Computer Aided Bearing Design ASME Publication, G00220.*, pp. 25–52, 1982.

[52] Yang. P and Rodkiewicz. C.M, "On the numerical analysis to the thermohydrodynamic lubrication of a tilted pad inclusive of side leakage," *Trans. ASME, Jl. of Tribology*, Vol. 40, No. 2, pp. 259–266, 1997.

[53] Hashimoto. H and Wada. S, "The effect of fluid inertia forces in parallel circular squeeze film bearings lubricated with pseudo-plasic fluids," *Trans. ASME, Jl. of Tribology*, Vol. 108, pp. 282, 1986.

[54] Elkouch. A.F, "Fluid ineria effects in non-newtonian squeeze film," *Trans. ASME, Jl. of Tribology*, Vol. 98, pp. 409–411, 1976.

[55] Dowson. D Smith. E. H and Taylor. C.M, "An experimental study of hydrodynamic film rupture in a steadily loaded non-conformal contacts," *Jl. of Mech. Engg. Sci.*, Vol. 22, pp. 71–78, 1980.

[56] You. H.I and Lu. S, "Inertia effects in hydrodynamic lubrication with film rupture," *Trans. ASME, Jl. of Tribology*, Vol. 109, pp. 86, 1987.

[57] Zhang. J.X and Rodkiewicz. C.M, "On the design of thrust bearings using a cfd technique," *STLE, Tribology Trans.*, Vol. 40, No. 3, pp. 403–412, 1997.

[58] Rodkiewicz. C.M and Sinha. P, "On the lubrication theory: A mechanism responsible for generation of the parallel bearing load capacity," *Trans. ASME, Jl. Lub. Tech*, Vol. 115, pp. 584–590, 1993.

[59] Courant. R, "Variational methods for the solution of problems of equilibrium and vibrations," *Bull. American Math. Sci.*, Vol. 49, 1943.

[60] Euler. L, "Methods inveniendi lineas curvas maximi minimine proprietate gaudentes, m. bousquet lausanne and geneva," .

[61] Weinberger. H. F, "Upper and lower bounds for eigen values by finite difference methods," *Comm. in Pure Math.*, Vol. 9, 1956.

[62] Weinberger. H.F, "Lower bounds for higher eigen values by finite diffecrence method," *Pacific Jl. Math.*, Vol. 8, 1958.

[63] Poly. G, "Sur une interpretation de la methode des differences finies qui peit fournir des bornes superieueres n inferieures," *C.R. Acad. Sci.*, Vol. 235, 1952.

[64] Poly. G, "Studies presented to richard von mises," *Acad. Press, Newyork*, 1954.

[65] Hersch. J, "Equations differentielles et functions de celllules," *C.R. Acad. Sci.*, Vol. 240, 1955.

[66] Zienkiewicz. O.C and Cheng. Y.K, "Finite elements in the solution of field problmes," *Engineer*, Vol. 220, 1965..

[67] Zienkiewicz. O.C, "The finite element method in engineering science," *McGra-Hill Book Company, London*, 1971.

[68] Brooks. A.N and Hughes. T.J.R, "Streamline upwind/petrov-galerkin formulations for convection dominated flows with particulat emphasis on the incompressible navier-

stokes equations," *Computer Meth. in Appl. Mech. and Engg*, Vol. 32, pp. 199–259, 1982.

[69] Young. J, "The thermal wedge in hydrodynamic lubrication," *Engineerinh Jl.*, Vol. 45, No. 3, pp. 46–54, 1962.

[70] Reddi. M.M, "Finite element solution of the incompressible lubrication problem, series: f," *Trans. ASME, Jl. Lub. Tech*, Vol. 91, No. 3, pp. 524–531, July 1969.

[71] Jean-Michel Grygiel and Tanguy Philippe, "Finite element solution for advection dominated thermal flows," *Comp. Meth. in Appl. Mech. and Engg.*, Vol. 93, pp. 277–289, 1991.

[72] Khonsari. M.M and Wang. S.H, "Notes on transient thd effects in a lubricating film," *STLE, Tribology Trans.*, pp. 177–183, 1992.

[73] Kumar. B.V.R Rao. P.S and Sinha. P, "Streamline upwind petrov galerkin finite element analysis of thermal effects on load carrying capacity in slider bearings," *International Journal of Numerical Heat Transfer: Part: A Applications (to appear)*, 2000.

[74] Pinkus. O and Sternlicht. B, "Theory of hydrodynamic lubrication," *McGra-Hill, Newyork*, 1961.

[75] Strenlicht. B, "Energy and Reynolds considerations in thrust bearing analysis," *Conf. on Lubrication and Wear, IME Publ., London*, 1957.

Publications

1. B.V.R. Kumar, P.S. Rao and P. Sinha, " Streamline Upwind Petrov-Galerkin Finite Element Analysis of Thermal Effects on Load Carrying Capacity in Slider Bearings," Accepted for publication in the Internatinal Journal of Numerical Heat Transfer: Part A. Applications.

2. P.S. Rao, B.V.R. Kumar and P. Sinha, " A Thermohydrodynamic Analysis of a Tilted Pad Slider Bearing with Heat Conduction in the Pad and Slider", Accepted for publication in the 55^{th} STLE Annual Meeting proceedings".

3. B.V.R. Kumar, P.S. Rao and P. Sinha, " A Numerical Study of Performance of a Slider Bearing with Heat Conduction in the Pad", (Submitted for publication in the Journal: "Finite Elements in Analysis and Design".